



## AEDC HIGH-TEMPERATURE TESTING CAPABILITIES

M. H. Trimble, R. T. Smith, and R. K. Matthews  
ARO, Inc., a Sverdrup Corporation Company

ARNOLD ENGINEERING DEVELOPMENT CENTER  
AIR FORCE SYSTEMS COMMAND  
ARNOLD AIR FORCE STATION, TENNESSEE 37389

April 1978

Final Report for Period December 1976 - May 1977

Approved for public release; distribution unlimited.

Prepared for

ARNOLD ENGINEERING DEVELOPMENT CENTER/DO  
ARNOLD AIR FORCE STATION, TENNESSEE 37389

## NOTICES

When U. S. Government drawings, specifications, or other data are used for any purpose other than a definitely related Government procurement operation, the Government thereby incurs no responsibility nor any obligation whatsoever, and the fact that the Government may have formulated, furnished, or in any way supplied the said drawings, specifications, or other data, is not to be regarded by implication or otherwise, or in any manner licensing the holder or any other person or corporation, or conveying any rights or permission to manufacture, use, or sell any patented invention that may in any way be related thereto.

Qualified users may obtain copies of this report from the Defense Documentation Center.

References to named commercial products in this report are not to be considered in any sense as an indorsement of the product by the United States Air Force or the Government.

This report has been reviewed by the Information Office (OI) and is releasable to the National Technical Information Service (NTIS). At NTIS, it will be available to the general public, including foreign nations.

## APPROVAL STATEMENT

This report has been reviewed and approved.

FOR THE COMMANDER



CHAUNCEY D. SMITH, JR, Lt Colonel, USAF  
Director of Test Operations  
Deputy for Operations



# UNCLASSIFIED

## 20. ABSTRACT (Continued)

planning purposes, a potential user should contact AEDC for an evaluation of requirements, selection of the most suitable facility, scheduling, and costs.

## PREFACE

The work reported herein was conducted by the Arnold Engineering Development Center (AEDC), Air Force Systems Command (AFSC), under Program Element 65807F. The results were obtained by ARO, Inc., AEDC Division (a Sverdrup Corporation Company), operating contractor for the AEDC, AFSC, Arnold Air Force Station, Tennessee. The manuscript was submitted for publication on December 19, 1977.

Testing of equipment and materials at elevated temperatures requires facilities with special features and capabilities. This report summarizes the AEDC high-temperature facilities testing capability, discussing both the present and future capabilities of existing test units. Adequate information is included to define the thermal, pressure, velocity, and geometrical boundaries. These parameters are indicative of a capability; however, for test planning purposes, a potential user should contact AEDC for an evaluation of requirements, selection of the most suitable facility, scheduling, and costs.

If additional information is desired, contact

Arnold Engineering Development Center  
Deputy for Operations (DO)  
Arnold Air Force Station, Tennessee 37389

Phone 615-455-2611, Extension 7621  
or Autovon 882-1520, Extension 7621.

**CONTENTS**

**1.0 INTRODUCTION**

**2.0 AERODYNAMIC AND PROPULSION TEST UNIT (APTU)**

**3.0 HYPERSONIC WIND TUNNELS (B) AND (C)**

**4.0 HYPERBALLISTIC RANGE (G)**

**5.0 HIGH-ENTHALPY ABLATION TEST (HEAT) FACILITY**

**6.0 DUST EROSION TUNNEL (DET)**

## 1.0 INTRODUCTION

## 1.0 INTRODUCTION

Technological trends in aircraft, missiles, and space vehicles appear to be advancing into an era of increasing importance on lightweight/high-temperature structures. The NASA/Air Force approach on the National Hypersonic Research Facility (NHRF), formally the X-24C program, which utilizes a lightweight aluminum structure covered with high-temperature ceramics appears to be a natural follow-on for military aircraft where high thrust-to-weight ratios for both maneuverability and payload are of increasing importance. As the aerodynamic bodies for efficient hypervelocity flight are developed, it will be necessary to provide compatible propulsion systems, and it follows that, as the prime vehicle or carrier increases in speed, there will have to be a similar increase in missile and reentry vehicle performance. This increase in performance results in increasing testing requirements in the area of ablation, particle erosion, and ablation/erosion of nosetips. From this simple assessment it can readily be projected that high-enthalpy testing will increase dramatically over the next 10 to 15 years. The behavior of ceramics and other high-temperature materials in a properly simulated flight environment will be of extreme importance to designers of both aerodynamic structures and advanced propulsion systems because of the high cost and human risks encountered with failure.

Testing of equipment and materials at elevated temperatures has for the past 20 to 30 years been of continuing and increasing interest on both military and space programs. The testing techniques have for the most part, by necessity, been tailored to existing capabilities with neither time nor resources available for carefully planned new facilities. As an outgrowth of this approach, a variety of testing capabilities has emerged, which can adequately meet selected requirements. The purpose of this report is to summarize the present and, in some cases, the projected capabilities of the AEDC test units which can provide the environment to meet high-temperature material and component test requirements. The test units included are:

1. Aerodynamic Propulsion Test Unit (APTU)
2. Hypersonic Wind Tunnels (B) and (C)
3. Hyperballistic Range (G)
4. High-Enthalpy Ablation Test (HEAT) Facility
5. Dust Erosion Tunnel (DET)

A specific introduction is included in the follow-on sections for each test unit. There are other tunnels, such as Tunnel F, which are not included because of the limited run time of a few milliseconds. However, Tunnel F can be used as a tool for determining heat-transfer coefficients.

To summarize the full range of capabilities for these facilities is difficult because of the large number of variables encountered. However, a partial comparison of these test unit capabilities is presented in Fig. 1.1.

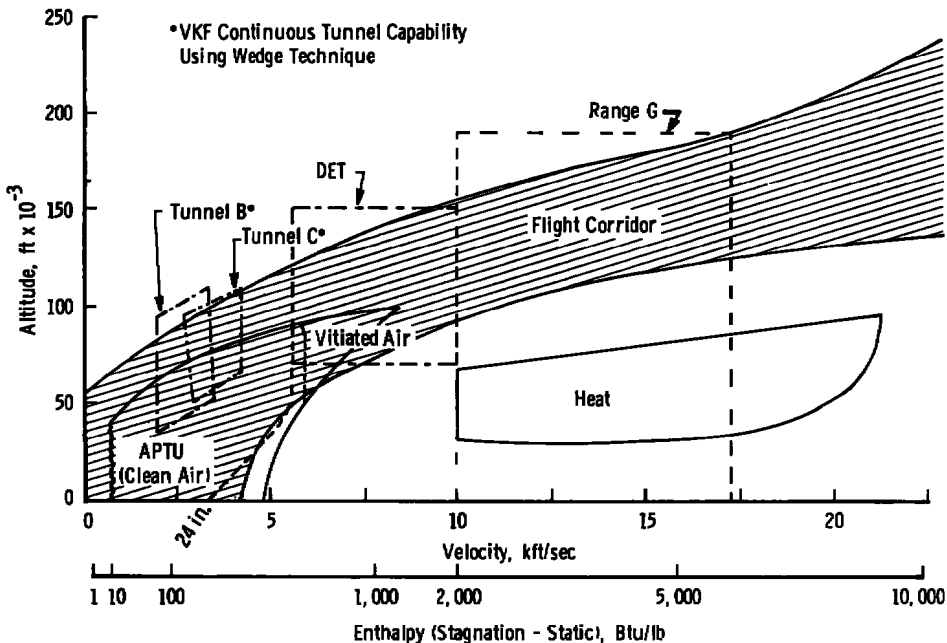


Figure 1.1 Capabilities of AEDC high-temperature facilities.

In general, when the velocity is in the 10,000- to 20,000-ft/sec range (Range G and HEAT), the model will be rather small (0.5- to 2.5-in. diameter). For the lower velocities (below about 7,000 ft/sec), larger models (up to 4 ft<sup>2</sup> maximum-cross-sectional area) can be used. Descriptions of the individual test units, which are described in detail herein, should be referred to for specific information of interest on model sizing (or test airstream size), run duration, discrete tunnel Mach numbers available, etc.

The ideal facilities would have the following capabilities:

1. Large enough to test full-scale hardware,

2. Stagnation temperature and local density levels duplicating those of flight, and
3. Run times long enough to provide component wall temperatures equal to those in flight.

These capabilities are extremely difficult to attain, and, as noted in this report, there are several facilities that address various aspects of these requirements. The selection of which facility is best suited for a particular test is strongly dependent on the size of the test article and the specific requirement of each individual test. Table 1.1 will aid the potential user in selecting facilities which may be compatible with his specific test requirement. This table lists examples of the types of equipment or materials testing which can be performed and the facilities which should be considered.

**Table 1.1 Facility Selection Information**

Class of Vehicle	Facility				
	APTU	Tunnels B and C	Range G	HEAT	DET
<b><u>Reentry Vehicles</u></b>					
Full-Scale Vehicle	1	---	---	---	---
Full-Scale Nose Cone	1	---	1	1	2
Sample of Thermal Protection System	1	2	2	2	2
Full-Scale Control Surface	1	1	---	---	1
Thermal Response of Internal Components	1	1	---	1	1
Particle Erosion Test	---	---	2	---	2
Ablation/Erosion Test	---	---	2	1	---
<b><u>Missiles</u></b>					
Full-Scale Vehicle	2	1	---	---	---
Full-Scale Inrdome or Radome	1	2	---	---	---
Full-Scale Control Surface	1	1	---	---	---
Sample of Above Materials	1	1	2	2	2
Thermal Response of Internal Components	1	2	---	1	1
Propulsion System (Full Scale)	2	---	---	---	---
Propulsion System Nozzle Materials	1	1	1	1	1
<b><u>Space Shuttle</u></b>					
Samples of Thermal Protection System	1	2	2	---	1
Components Including Protection System	1	2	---	---	---
Propulsion System Materials	1	1	---	---	---
<b><u>Aircraft and/or Stores</u></b>					
Sample of Materials	1	1	---	---	1
Thermal Response of Components	1	2	---	---	1

1. Facility should be considered for testing.
2. Facility has conducted similar test.

**2.0 AERODYNAMIC AND PROPULSION TEST UNIT (APTU)**

<b>2.1</b>	<b>Types of Testing</b>	<b>13</b>
<b>2.2</b>	<b>Facility Performance</b>	<b>14</b>
<b>2.3</b>	<b>Facility Description</b>	<b>17</b>
<b>2.4</b>	<b>Future Capabilities</b>	<b>24</b>

## 2.0 AERODYNAMIC AND PROPULSION TEST UNIT (APTU)

The Aerodynamic and Propulsion Test Unit (APTU) was planned and assembled at AEDC to meet future Air Force and Navy requirements primarily in the ramjet missile category. Facilities such as the Ordnance Aerophysics Laboratory (OAL) and the Little Mountain Facility (LMF) provided, in part, capabilities to meet these requirements. For cost effective reasons, these facilities were closed, and the usable equipment from these facilities was brought to AEDC and integrated into the APTU facility.

The facility is comprised of a 22,200-ft<sup>3</sup> high-pressure air storage reservoir, and 87,000,000-Btu pebble bed storage heater, a 16-ft-diam test cell, and an air ejector exhaust system to increase the altitude capability. Most of the piping, valves, free-jet nozzles, consummable systems (nitrogen, propane), controllers, hydraulic system, etc., were also surplus equipment.

Initial operation of the facility was in 1973. Since that time, testing has involved facility shakedown, two ramjet programs, and an aerial cannon/fuel tank investigation. Since the facility has several features which are state-of-the-art in nature and require development of sophisticated engineering approaches and operational procedures, the facility shakedown program is a continuing process which must be developed as new operating regions are encountered.

Operation of the facility is based on a simple concept of storing energy (both high-pressure air and heater thermal energy) over a period of time (hours) and then utilizing these energy sources in controlled quantities to produce the desired test conditions for a time period of up to several minutes. Considerations in the operation of the APTU include refractory thermal shock, thermal stress in high-temperature components, and flow dynamics encountered in mixing processes. The following sections will develop more fully the APTU operating performance and describe the various facility components and associated limitations.

### 2.1 TYPES OF TESTING

The APTU has the potential capability of accomplishing several types of tests. Typical types of tests include:

1. Free-jet propulsion system development and qualification tests,
2. Direct-connect propulsion system component development tests,
3. True temperature aerodynamic tests, and
4. High-temperature materials tests.

Initial planning for APTU considered provisions for Items 1 and 2 test capability in support of ramjet test programs. Two such programs, the Air Force Multi-Purpose Missile and the Navy IRR-SSM, have been conducted in APTU. The latter two types of testing, which were also recognized initially and in which user interest has been expressed, include development of such items as missile radomes, insulating materials for research vehicles, and full-scale missile inlets. One aerodynamic-type test, which has been conducted in APTU, was an aircraft fuel tank vulnerability test.

A unique capability of the facility is the ability to establish and control for selected periods of time a series of conditions (combinations of pre-selected pressures and temperatures). This has been demonstrated for up to 10 different altitude conditions at a fixed Mach number. Controlled transient conditions can also be provided. Mission trajectories or duty cycles can be simulated for direct-connect testing but must currently be limited to a fixed supersonic Mach number for free-jet testing.

Subsonic test conditions have been demonstrated where stream pressure, temperature, and cell pressure were computer controlled to maintain test conditions. Original planning did not include the subsonic region; however, the lower temperature and pressure region was easily integrated into the APTU operating envelope by procedural and control system changes.

## 2.2 FACILITY PERFORMANCE

The range of planned facility performance capability in terms of an altitude/Mach number envelope in the supersonic regime is shown in Fig. 2.1. Currently, hardware development and operational checkout have been limited to the performance region identified for the low-pressure mixer (maximum stagnation conditions 300 psia at 1,850°R). Expansion of the "developed" portion of the facility operating range will be accomplished as required to support user test requirements.

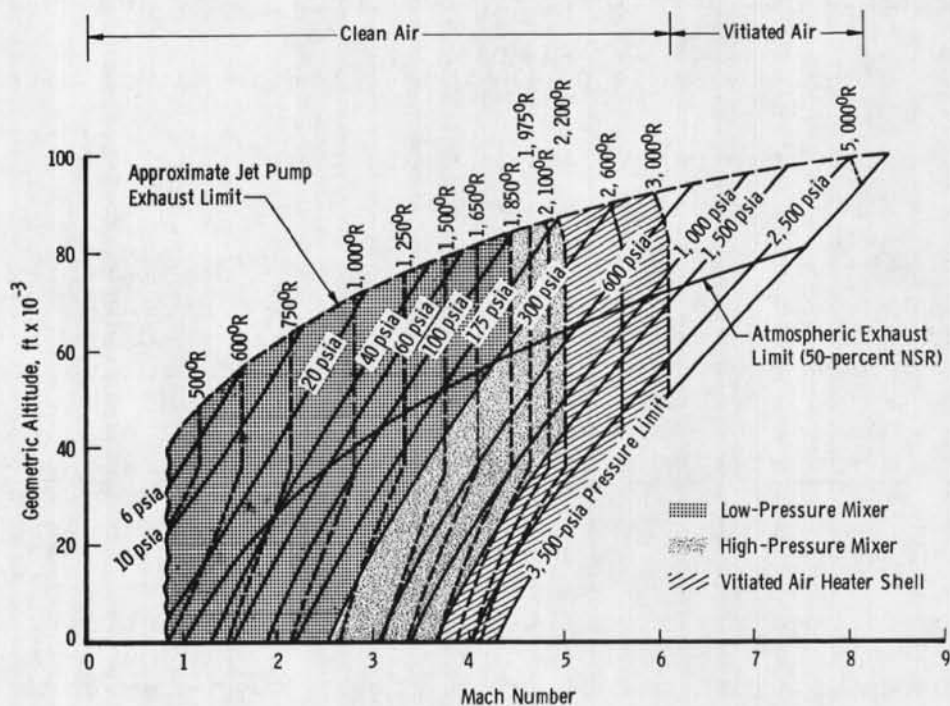


Figure 2.1 APTU test envelope capability.

The APTU, because it is a blowdown-type facility with limited storage of thermal energy and high-pressure air, has a limited run time capability at any specific test condition. In the free-jet test mode, the factors which influence run time are altitude, Mach number, and the desired free-stream test diameter. Estimated available steady-state test time as a function of these three variables is shown in Fig. 2.2. At test altitudes below the 50-percent normal shock recovery limit, altitude simulation is accomplished via the engine exhaust diffuser. As test altitudes increase above the 50-percent normal shock recovery (NSR) limit, diffuser pumping augmentation with the annular air ejector is required. Hence, for a given Mach number, the available test time is seen to increase with altitude until the 50-percent NSR limit is reached at which point further increases in altitude will cause test time to decrease because of air consumption by the annular air ejector.

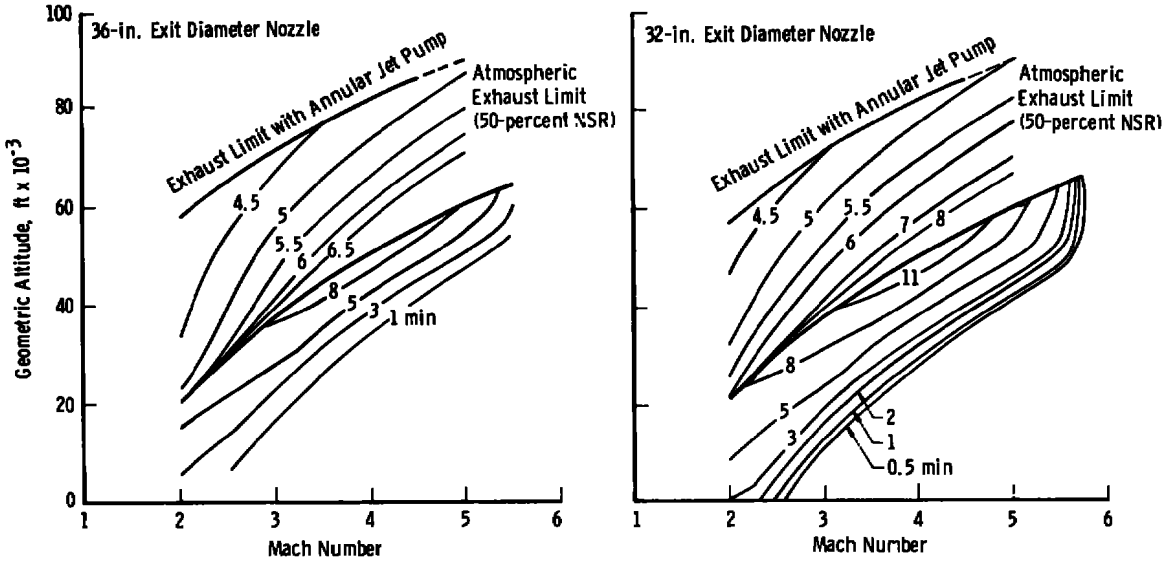


Figure 2.2 Estimated facility run times for the free-jet configuration.

Figure 2.3 relates the maximum mass flow-temperature capability of the facility for direct-connect testing, materials testing, and other forms of high-enthalpy testing not directly related to a specific altitude/Mach number point. Lines of constant estimated facility run time, exclusive of air ejector requirements, are shown in this figure. Any vacuum simulation required above that available via the exhaust diffuser will decrease the run times shown in Fig. 2.3.

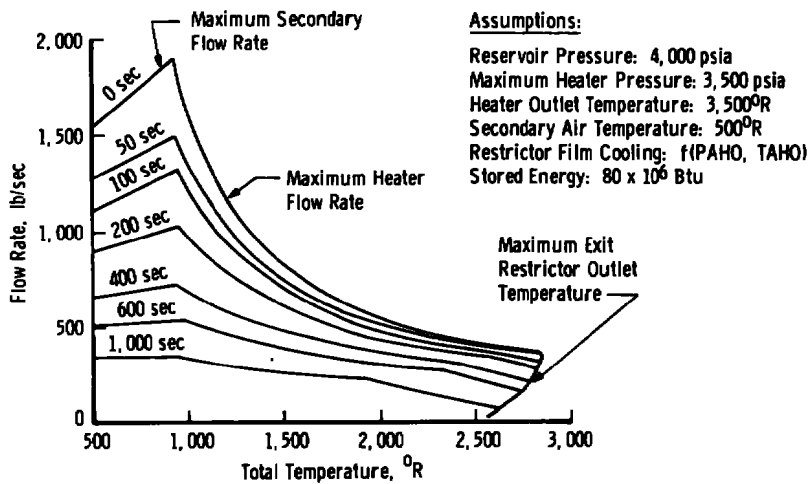


Figure 2.3 APTU maximum mass flow/temperature capability.

## 2.3 FACILITY DESCRIPTION

The APTU is an intermittent (blowdown) type, true temperature test facility. Major components of the facility are schematically depicted in Fig. 2.4. An artist's conception of this facility is shown in Fig. 2.5. Functionally, the facility produces a high-energy test airstream over a wide range of stagnation conditions by blending (in the facility air mixer) varying quantities of heated air, which has passed through the stored energy heater, with air directly from the storage reservoir. The test airstream is accelerated to the desired test Mach number, typically using an axisymmetric free-jet nozzle, and is directed on the test article. A diffuser/air ejector system is used to capture and discharge the test airstream and test article exhaust gases to atmosphere. Altitude simulation is provided by the pumping action of the diffuser/ejector system. The facility blowdown operation is fully automated, and the primary data recording system is a high-speed digital data acquisition system.

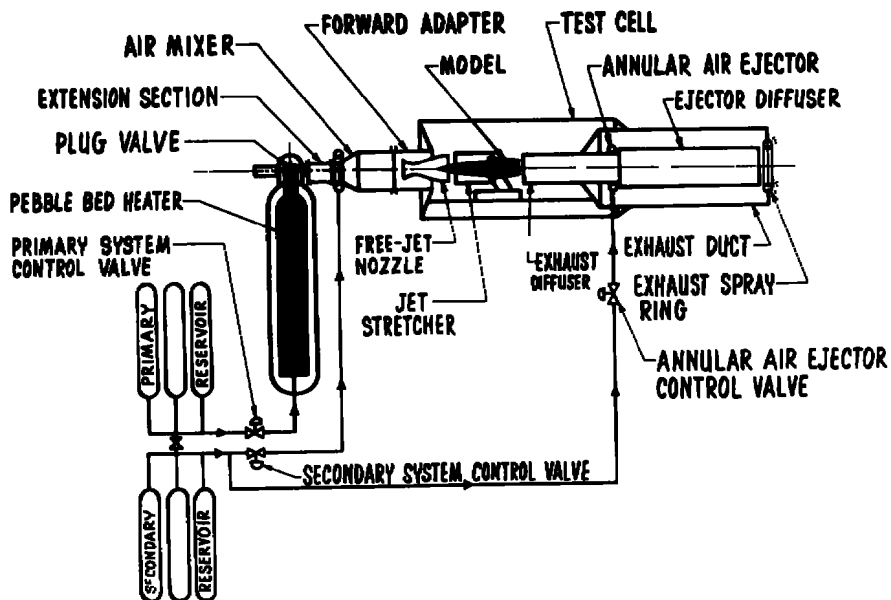


Figure 2.4 APTU facility schematic.

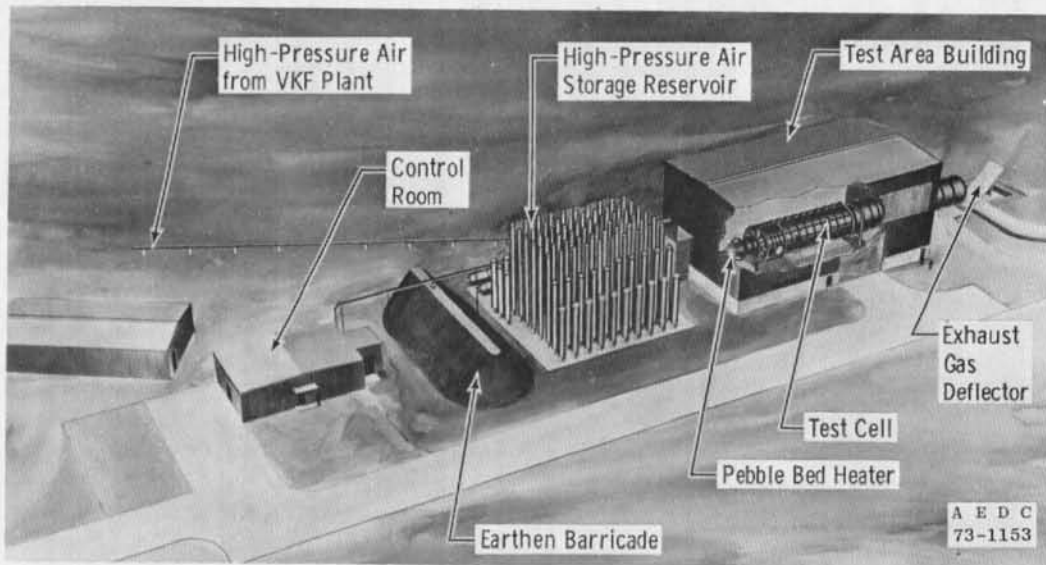


Figure 2.5 APTU (artist's conception).

### 2.3.1 High-Pressure Air Storage System

The high-pressure air storage reservoir has a storage volume of 22,200 ft<sup>3</sup>, and approximately 450,000 lb of compressed air may be stored at 4,000 psia. The reservoir is composed of 95 pressure vessels with a valving arrangement which will permit the system to be used as a single storage system or divided into two independent storage systems. Two air supply systems are utilized: a primary system which supplies high-pressure air through the stored energy heater to the air mixer and a secondary system which supplies high-pressure air directly to the mixer and the air ejector. Airflow through each supply circuit is controlled by hydraulically operated control valves. The air storage reservoir is charged by the VKF compressor system at flow rates up to 87 lb/sec at 4,000 psia.

### 2.3.2 Pebble Bed Heater

The thermal energy storage system is a regeneratively charged pebble bed heater. The energy storage matrix is a bed 86 in. in diameter and 24 ft high containing 140,000 lb of 3/4-in.-diam, high-density alumina (AL<sub>2</sub>O<sub>3</sub>) pebbles (Fig. 2.6). The storage matrix is contained by an insulated heater vessel which is approximately 11 ft in diameter and 45 ft long. The maximum heater temperature and flow rate are approximately 3,500°R and 300 lb/sec, respectively. A propane-fired burner is used to charge the heater to the

desired temperature. The heater outlet is closed by means of a hydraulically operated plug valve to allow prepressurization of the heater vessel prior to testing (Fig. 2.7). This is accomplished by the plug valve seating in the heater exit restrictor nozzle. Maximum design working pressure of the heater vessel is 5,000 psia.

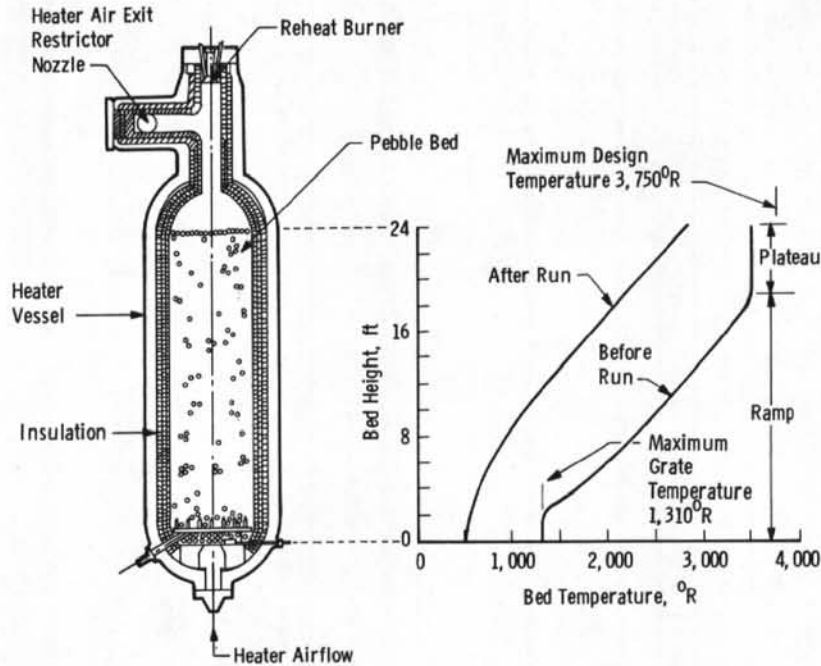


Figure 2.6 Pebble bed heater schematic and operation.

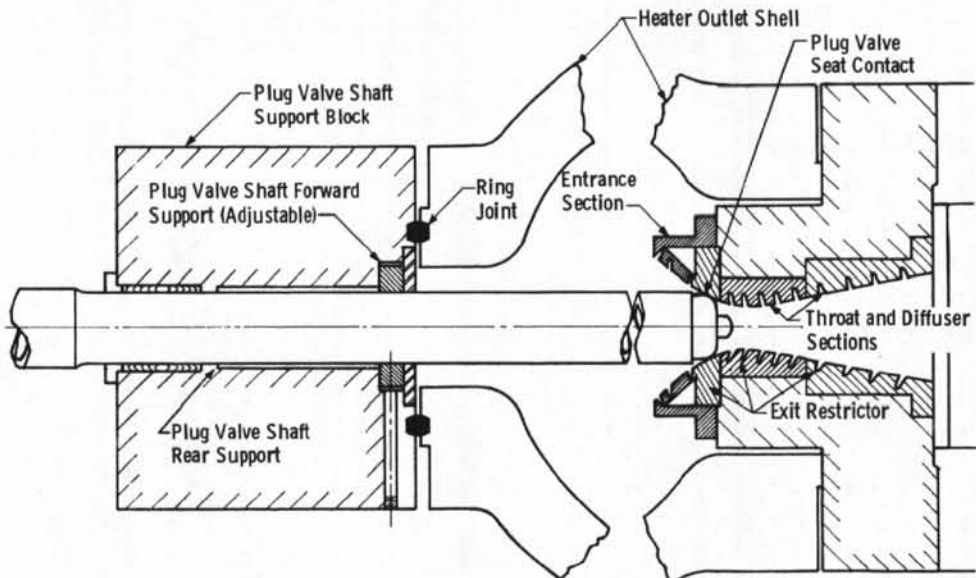


Figure 2.7 Plug valve/exit restrictor assembly.

### 2.3.3 Air Mixer

An air mixer (Fig. 2.8) is utilized to blend high-energy primary air from the stored energy heater and cooler secondary air bypassing the heater. The secondary air is injected into the hot stream through 8 radial jets inclined upstream at a 60-deg angle relative to the mixer centerline. Primary and secondary air valves are modulated to produce the desired stagnation pressure and temperature in the mixed test airstream upstream of the nozzle entrance. As indicated in Fig. 2.1, different mixer hardware is required for the higher stagnation conditions. The status of the different hardware is summarized in Table 2.1. The mixer includes hardware, as shown in Fig. 2.8, to uniformly distribute the flow and dampen turbulence in the mixer. The mixer test airstream turbulence level has been established for the low-pressure air mixer and is presented in Fig. 2.9.

Table 2.1 Status of APTU Air

	Vessel Fabricated	Forward Adapter	TPS*	Core Breaker	Screen
Low-Pressure Air Mixer (300 psi and 2, 200°R)	Yes	Yes	Yes	Yes	Yes
High-Pressure Air Mixer (1, 500 psi and 2, 200°R)	Yes	No	No	No	No
High-Pressure Air Mixer No. 2 (3, 500 psi and 3, 000°R)	No	No	No	No	No
Vitiation Air Heater (5, 000 psi and 5, 460°R)	Yes	No	Yes	No	---

\* TPS: Thermal Protection System

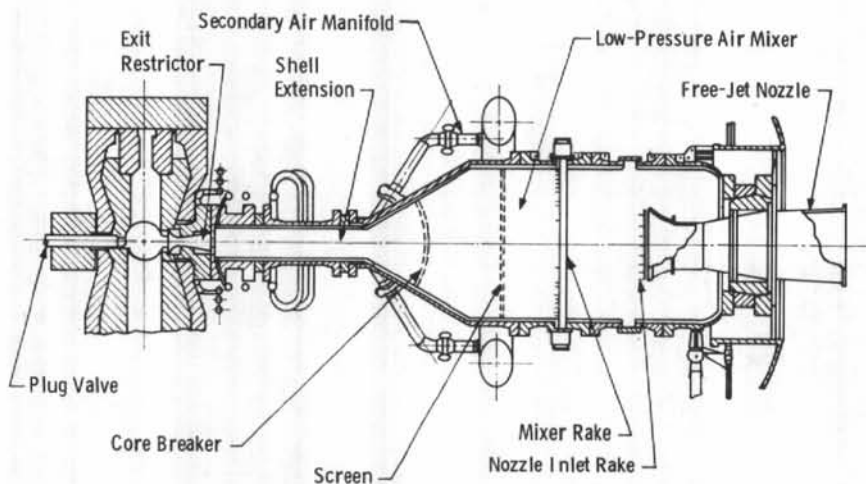
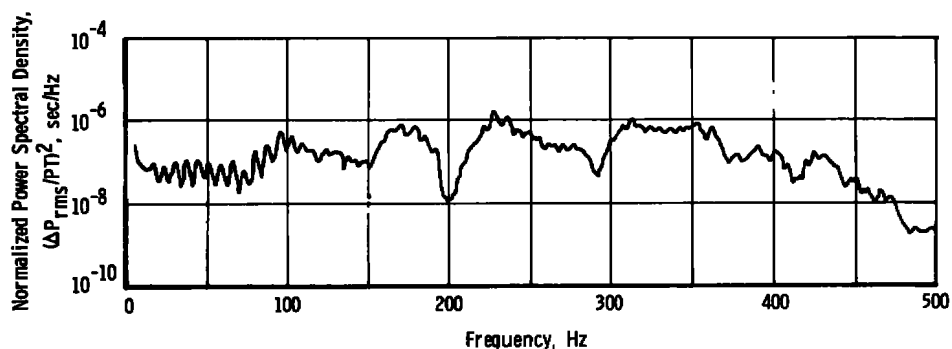


Figure 2.8 APTU low-pressure air mixer.



**Figure 2.9** Typical frequency spectrum at nozzle inlet with low-pressure air mixer configuration.

### 2.3.4 Test Cell

The test cell, which is 16 ft in diameter and about 42 ft long, encloses the test article setup. Either a free-jet or direct-connect test hardware setup is utilized depending on test requirements. A typical free-jet setup is shown in Fig. 2.5, which reflects use of an axisymmetric free-jet nozzle and a jet stretcher to extend the region of flow simulation. Different free-jet nozzles are used for each desired Mach number. Table 2.2 lists the free-jet nozzles currently available in APTU. The test article mounting hardware has a 10-deg angular adjustment capability. Total test article angle of attack depends on the installation configuration. Access into the test cell is provided by a 15- by 34-ft equipment hatch and a personnel door as indicated in Fig. 2.10. Mounted in the test cell are diffuser ducting, a force-measuring system, optical ports for the facility shadowgraph system, a CO<sub>2</sub> fire extinguishing manifold system, and a cooling-water supply. Connector ports are provided in the test cell for lighting, instrumentation leads, and electrical power.

### 2.3.5 Diffuser/Ejector Assembly

A diffuser/ejector assembly captures the test airstream, discharges the flow to atmosphere through a cooling-water spray, and produces altitude simulation in the test cell (Fig. 2.5). The assembly consists of a 4-ft-diam test cell diffuser, an annular air ejector, and a 5-ft-diam ejector diffuser. The combined assembly can provide free-jet altitude simulation, depending on Mach number and test configuration, up to 100,000 ft. The desired test cell pressure is controlled by modulating the airflow to the ejector. Other facility systems include a GN<sub>2</sub> supply system, a liquid storage CO<sub>2</sub> system, a fuel system, and a pyrophoric igniter system.

**Table 2.2 Available Free-Jet Nozzles**

Group I		Group II		Group III		Group IV	
Mach Number	Exit Diameter, in.						
3.00	10.0	1.00	27.3	1.50	30.0	2.50	49.3
3.50	10.0	1.30	28.0	1.90	32.9	3.00	43.6
3.80	10.0	1.90	25.3	2.00	32.0	3.50	43.6
		2.02	24.8	2.20	32.0	5.17	41.6°
		2.20	23.5	2.20	32.5	6.05	42.1°
		2.20	29.5	2.35	32.5	7.25	42.7°
		2.35	22.7	2.44	32.0		
		2.35	27.0	2.50	32.5		
		2.35	28.6	2.50	34.6		
		2.44	24.0	2.55	36.0		
		2.50	22.3	2.70	32.5		
		2.50	28.8	2.72	32.0		
		2.70	24.4	3.00	32.8		
		2.70	26.2	3.50	32.0		
		2.70	27.9	3.50	32.8		
		2.72	24.8	4.10	38.1		
		3.00	21.6	5.00	32.0		
		3.00	27.0				
		3.04	24.8				
		3.41	24.8				
		3.85	24.8				
		4.10	24.8				
		4.38	24.8				

\* NASA/Lewis Nozzles

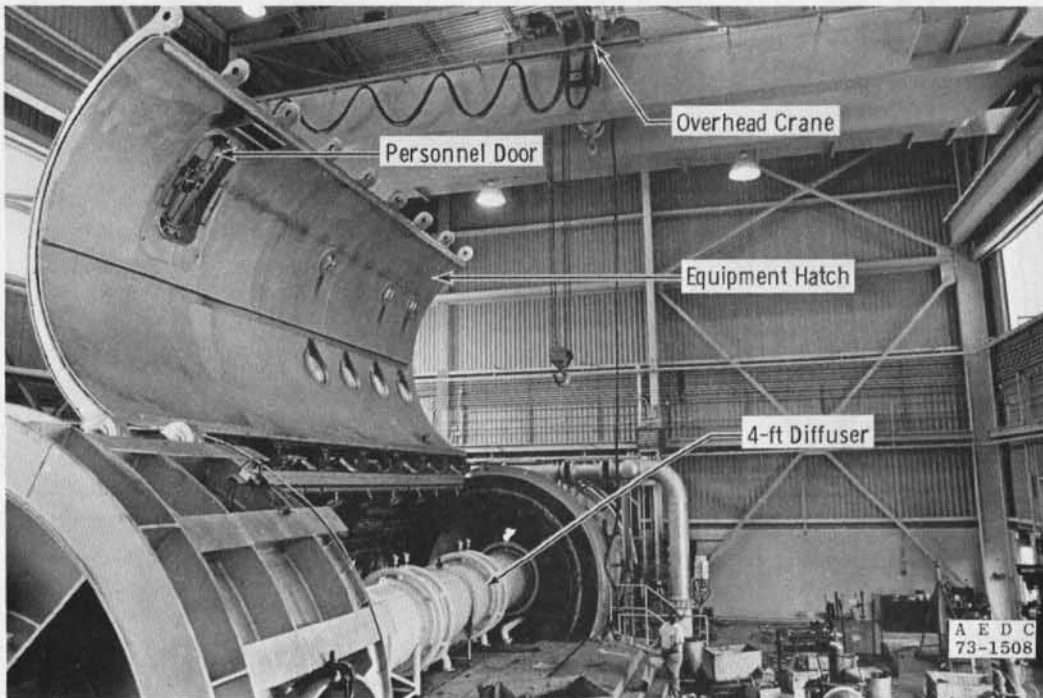


**Figure 2.10 APTU test cell.**

### 2.3.6 Control System

The facility blowdown operation is controlled by a pre-programmed, automatic digital process control system shown block diagrammed in Fig. 2.11. The system is fully automatic, and the control actions include (1) process controls for facility and test article systems, (2) sequencing of on/off items, (3) parameter limit checking and monitoring of events for safety purposes, and (4) integration of actions into a cohesive operating system. Facility and test article operations are monitored in the control room using analog meters, cathode-scope digital display of parameters from digital data acquisition system, and closed-circuit television with video record/playback capability.

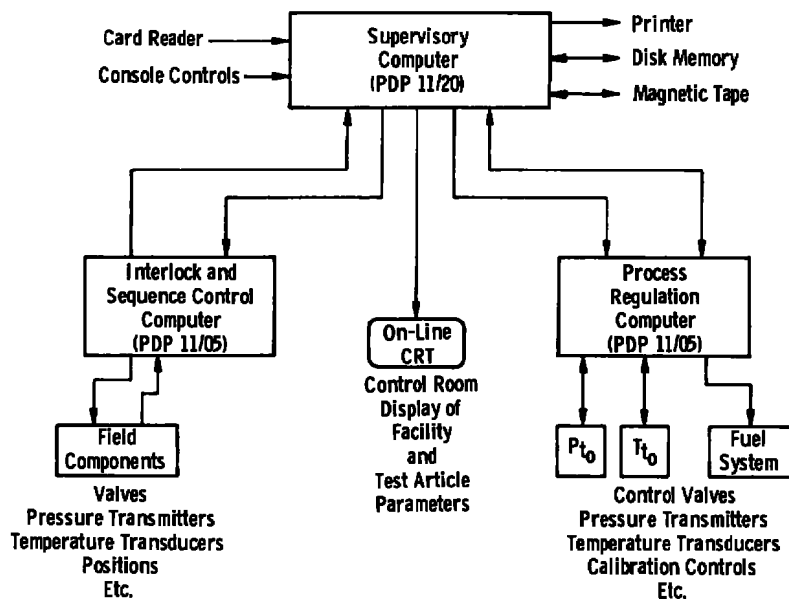


Figure 2.11 Controls system block diagram.

### 2.3.7 Data Acquisition Systems

The basic data recording system is a digital data acquisition system. The system has the capability to record both steady-state and dynamic data, sample each data channel sequentially at nominal rates from 3 to 10,000 samples/sec, and record each data sample for 352 data channels on magnetic tape in digital form. Dynamic data can also be recorded in analog form on magnetic tape with a 40-KHz response wideband frequency-modulated record electronics system. The facility is also equipped with a shadowgraph system which can be displayed on closed-circuit television in the control room and recorded on motion-picture film.

## 2.4 FUTURE CAPABILITIES

Future potential capabilities in the APTU include longer run times, higher test airstream stagnation temperatures, higher test airstream mass flow rates, and increased simulated altitude capability. Options available to extend facility capabilities in these areas include the following:

1. Expansion and partition of the high-pressure air storage reservoir system to provide longer test times,
2. Modification of the material and configuration of the heat storage media in the stored energy (clean air) heater to permit higher test airstream stagnation temperatures and/or mass flow rates,
3. Installation of a vitiation heater to provide airstream stagnation temperatures above that of the stored energy heater capability and to function as a backup system for the stored energy heater, and
4. Connection of the APTU to the ETF plant exhaust machinery and/or installation of auxiliary ejector pumping systems as a means to improve the APTU simulated altitude capability.

The above items are discussed in subsequent sections. It is important to note, however, that whereas the above would provide for better utilization of the basic facility systems, additional facility hardware (heater exit restrictor, modified thermal protection systems, air mixers, demineralized cooling-water system, etc.) would be required to utilize the extended capabilities.

### 2.4.1 High-Pressure Air Reservoir Expansion and Volume Distribution

The existing high-pressure air storage reservoir volume (22,200 ft<sup>3</sup>) can be utilized either as one reservoir or be partitioned into a reservoir system of approximately 40-percent primary (Fig. 2.5) and 60-percent secondary by closing a single isolation valve. Studies have shown that facility run times can be optimized for most free-jet conditions with the 32- and 36-in. exit diameter nozzles by using the existing reservoir volume distribution plus two additional volume distributions, specifically 20- and 60-percent primary volumes. Typical increase in facility run time resulting from different reservoir volume distributions are shown in Figs. 2.12 and 2.13 as a function of Mach number and altitude, respectively. Increasing the air storage volume to 57,000 ft<sup>3</sup> from the existing 22,200-ft<sup>3</sup> capacity is feasible using existing surplus vessels.

Such an increase would extend facility run times by a ratio that is a function of the Mach number/altitude test condition. Typical gains in run time for storage volume increases to 35,000 and 57,000 ft<sup>3</sup> are shown in Fig. 2.14.

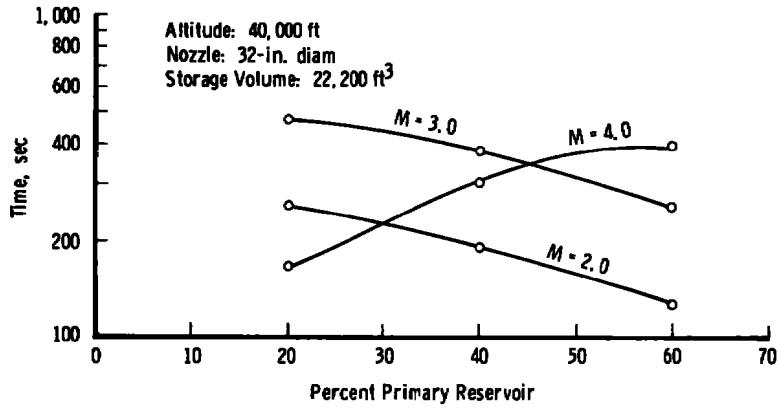


Figure 2.12 Facility run time versus reservoir volume distribution for different Mach numbers.

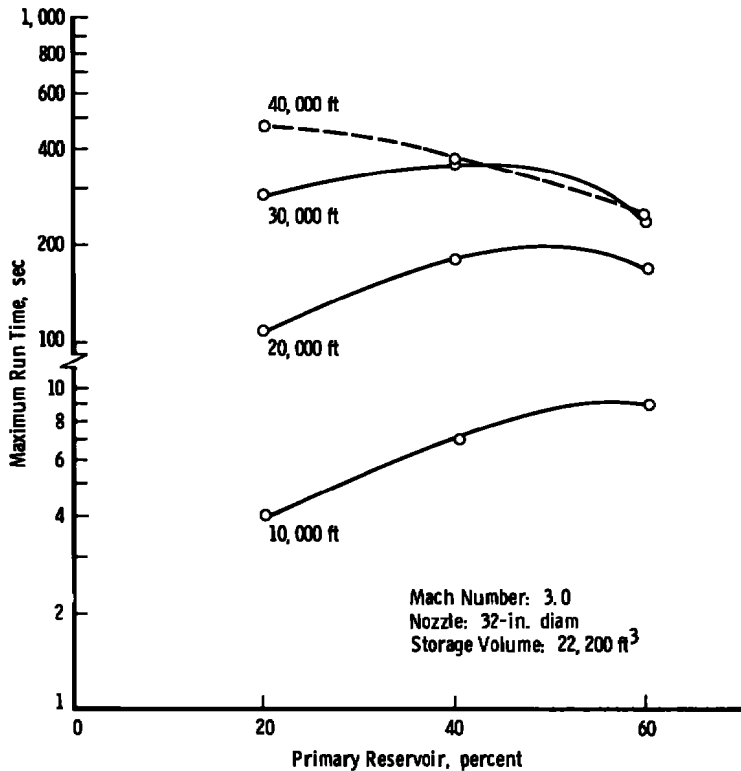


Figure 2.13 Facility run time versus reservoir volume distribution for different altitudes.

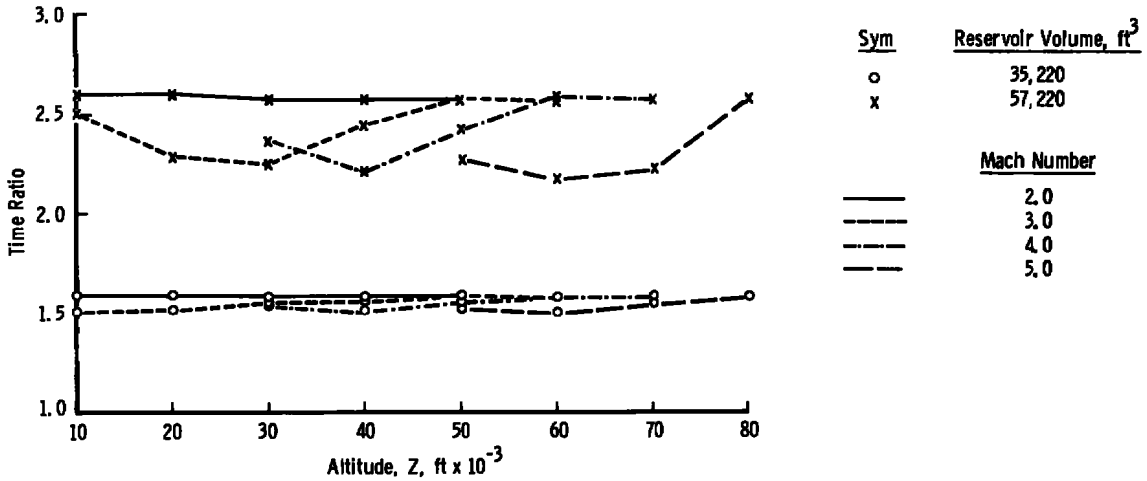


Figure 2.14 Reservoir volume comparisons (performance).

2.4.2 Storage Heater Modifications

The storage heater modification would reconfigure the heater storage media of alumina pebbles to a cored brick bed of either alumina or a mixture of alumina (lower half of the bed) and yttria stabilized zirconia (upper half of the bed). The cored brick configuration would permit maximum mass flows through the heater to over four times the maximum permissible through the pebble bed. Also, the combination alumina/zirconia bed would permit a maximum heater temperature of 4,500°R compared with 3,500°R for an alumina bed. Estimated facility performance utilizing the three different heater beds is shown in Fig. 2.15. In this figure, the one-minute total facility run time lines are plotted for each type bed for direct comparison.

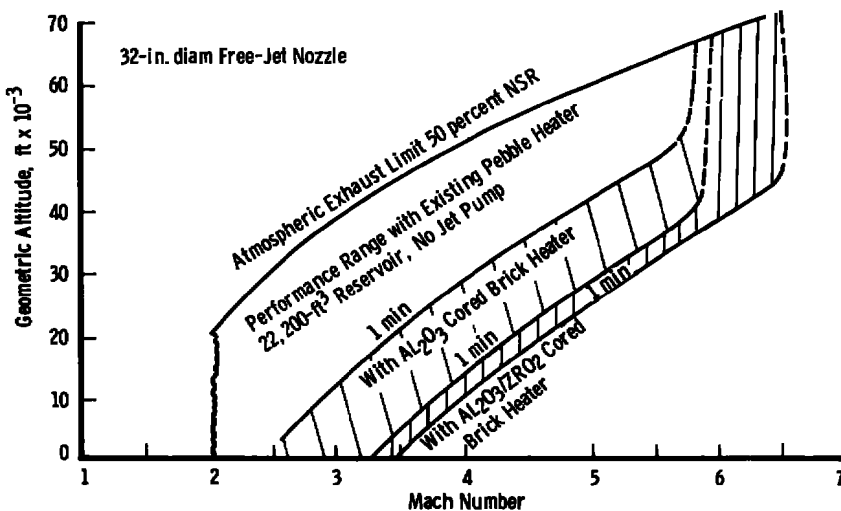


Figure 2.15 Estimated APTU performance with three different storage heater matrices.

### 2.4.3 Vitiation Heater Installation

The maximum clean air temperature from the alumina pebble bed stored energy heater is about 3,000°R. Above this level, direct instream (vitiating) heating, with oxygen replenishment, is required to raise the test airstream temperature up to 5,000°R. This region of potential improvement of the APTU facility performance map is shown in Fig. 2.1. This capability can be provided by a vitiation heater installation in series with the stored energy heater. In addition, a properly sized vitiation system separate from the stored energy could duplicate the facility performance capability of the stored energy heater and thereby serve as a backup heater system in case of refractory problem.

### 2.4.4 Facility Exhaust Pumping

Currently, exhaust jet pump augmentation is required for high-altitude simulation. However, this augmentation is obtained by using large quantities of air from the high-pressure air storage system, thus depleting the air available for the test airstream and reducing facility run times. An exhaust system independent from the high-pressure air storage system could not only produce higher simulated altitudes but also extend facility run times. Connections of the APTU to the ETF exhaust machinery and/or use of other ejector systems would provide this additional capability.

**3.0 HYPERSONIC WIND TUNNELS (B) AND (C)**

**3.1 Facility Performance . . . . . 31**  
**3.2 Facility Description . . . . . 32**  
**3.3 Types of Materials Tests . . . . . 37**  
**3.4 Future Capabilities . . . . . 48**



### 3.0 HYPERSONIC WIND TUNNELS (B) AND (C)

Tests of hypersonic vehicle heat shield materials have been conducted for many years in arc heaters and range facilities. Sled tracks have also been extensively used for materials testing. These types of facilities have the capability of producing high enthalpy levels; however, there can be certain disadvantages, such as small test core, short run times, contaminated flow, excess vibration, low productivity, and high cost. On the other hand, continuous-flow wind tunnels are not capable of providing the required enthalpy levels and, therefore, are generally not used for materials testing. However, in the supersonic Mach number range, the enthalpy levels are significantly lower, and recent experience has shown that there is a need for materials testing in this flight regime.

Within the past two years, a new testing technique has been developed at the Arnold Center. This new technique utilizes the large continuous-flow hypersonic Tunnels B and C to duplicate supersonic flight conditions. Normally, these facilities are used to simulate hypersonic flow on scaled models of aerospace vehicles; however, for materials testing, true pressure, temperature, and Mach number are required. To provide this environment a large wedge is used to reduce the local Mach number to the desired supersonic level, and the tunnel stagnation conditions are adjusted to produce the local pressure and temperature that duplicate the desired local flow conditions for a given situation.

#### 3.1 FACILITY PERFORMANCE

Performance and calibration data are presented in Tables 3.1, 3.2, and 3.3. The calibration data show flow uniformity at Mach numbers 6, 8, and 10.

Table 3.1 Performance of Tunnels B and C

Tunnel	Nominal Mach Number	$P_0$ , psia		$T_0$ , °F	$q_{\infty}$ , psia		$Re/ft \times 10^{-6}$	
		Min.	Max.	Max.	Min.	Max.	Min.	Max.
B	6	20	270*	390***	0.3	4.1	0.3	4.7
B	8	50	850**	890	0.3	3.8	0.3	3.7
C	10	200	2000	1450****	0.3	3.0	0.3	2.4

\*Maximum for short duration 300 psia

\*\*Maximum for short duration 900 psia

\*\*\*Up to 890°F can be supplied at low stagnation pressures

\*\*\*\*Maximum of 1,800°F at maximum  $P_0$  of 1,200 psia (available, but nonstandard)

$P_0$	Stagnation Pressure	$q_{\infty}$	Free-stream dynamic pressure
$T_0$	Stagnation temperature	Re	Free-stream Reynolds number

**Table 3.2 Open-Circuit Operating Conditions**

Tunnel B			Tunnel C		
Mach Number	$p_0$ , psia	Re/ft x $10^{-6}$	Mach Number	$p_0$ , psia	Re/ft x $10^{-6}$
6	25	0.5	10	300	0.4
6	60	1.1	10	525	0.7
6	175	3.1	10	700	0.9
8	125	0.7	10	975	1.3
8	250	1.3	10	1725	2.1
8	850	3.7			

 $p_0$  Stagnation Pressure

Re Free-stream Reynolds number

**Table 3.3 Flow Calibration for Tunnels B and C**

Mach Number		Re/ft x $10^{-6}$	Test Core Diameter, in.*
Average	Standard Deviation		
5.88	±0.02	0.6	38
5.91	±0.01	1.0	39
5.95	±0.01	4.7	39
7.85	±0.01	0.3	33
7.95	±0.01	1.0	34
8.00	±0.01	3.7	34
9.88**	±0.02	0.4	26
9.98**	±0.02	1.0	27
10.13**	±0.02	2.4	29

\*Data obtained throughout test core from station -16 to +20 in.

\*\*Mach numbers are obtained at each test condition with a retractable probe.

During tests which have material ablation or injection of foreign gases into the airstream, the tunnels are operated in an open-circuit mode. In this mode, atmospheric pressure must be attained at some stage of plant compression resulting in the test conditions being limited to those listed in Table 3.2.

### 3.2 FACILITY DESCRIPTION

The 50-in. hypersonic tunnels are Tunnel B (Figs. 3.1 and 3.2) for Mach 6 and 8 and Tunnel C (Figs. 3.3 and 3.4) for Mach 10. Both tunnels are closed circuit with axisymmetric contoured nozzles and operate continually over a range of pressure levels with air supplied by the main compressor system. Stagnation temperatures sufficient to avoid liquefaction in the test section are obtained through the use of a natural-gas-fired combustion heater in combination with the compressor heat of compression at Mach 6 and 8 and in

combination with electric resistance heaters at Mach 10. Each entire tunnel (throat, nozzle, test section, and diffuser) is cooled by integral, external water jackets. Both tunnels have identical test sections equipped with model injection systems.

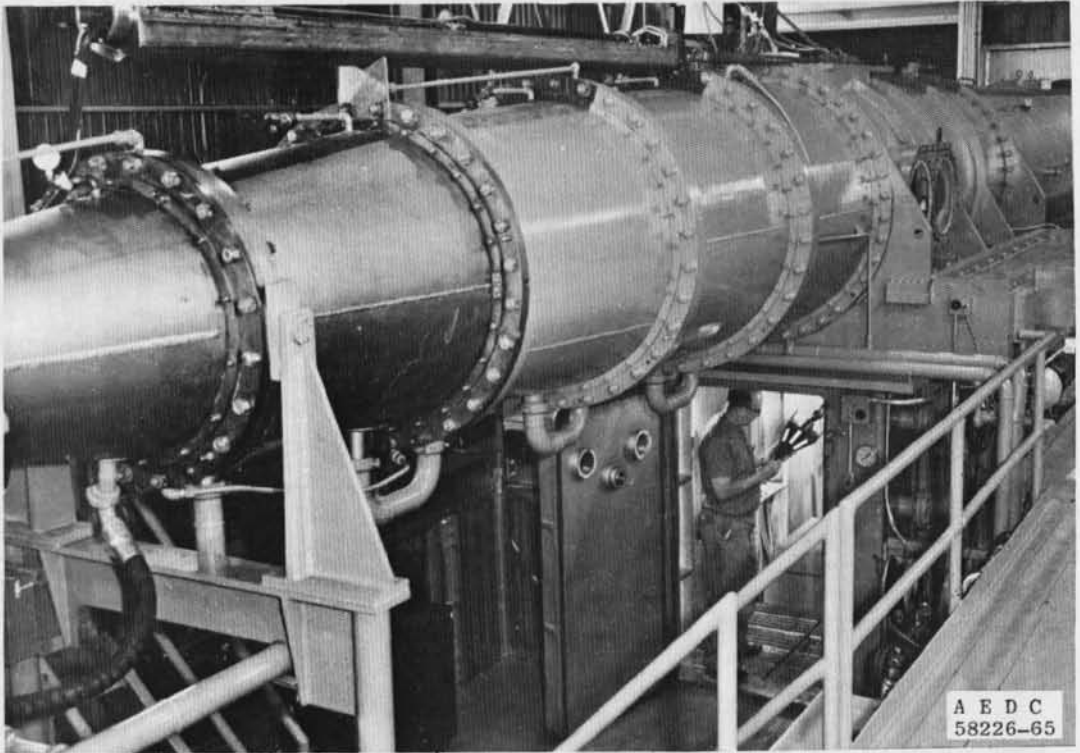


Figure 3.1 Tunnel B.

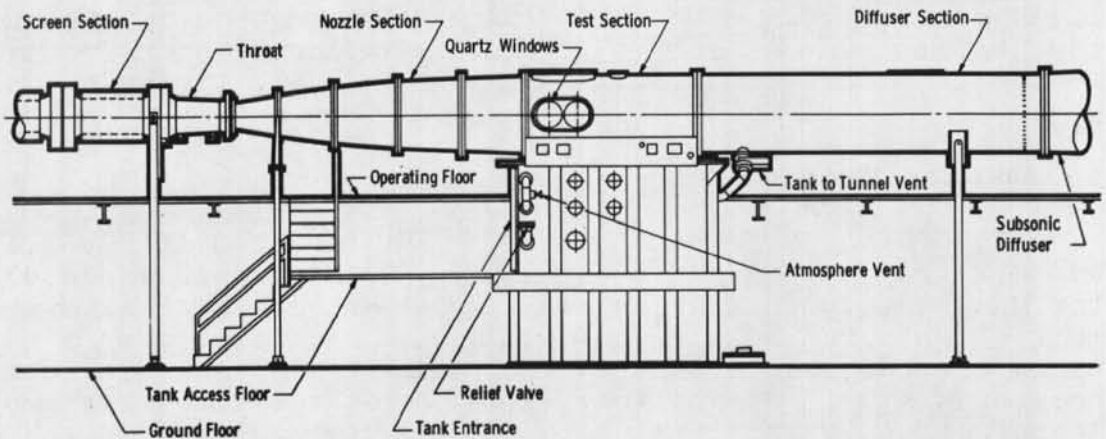


Figure 3.2 Tunnel B assembly.

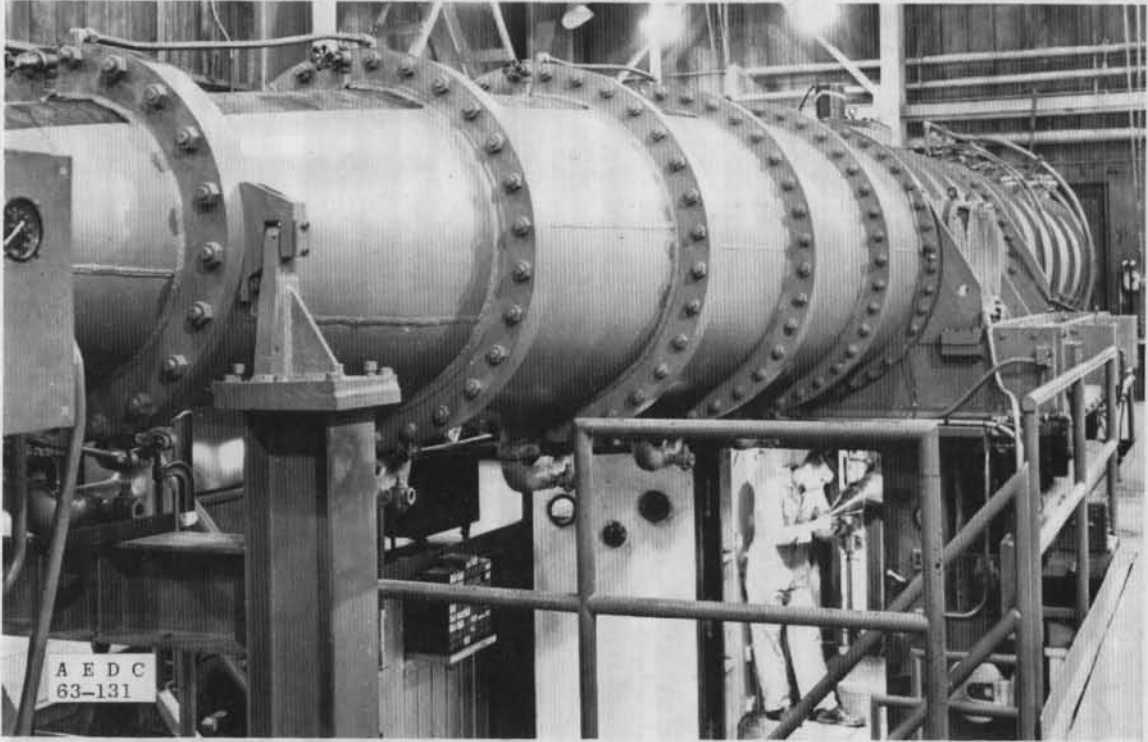


Figure 3.3 Tunnel C.

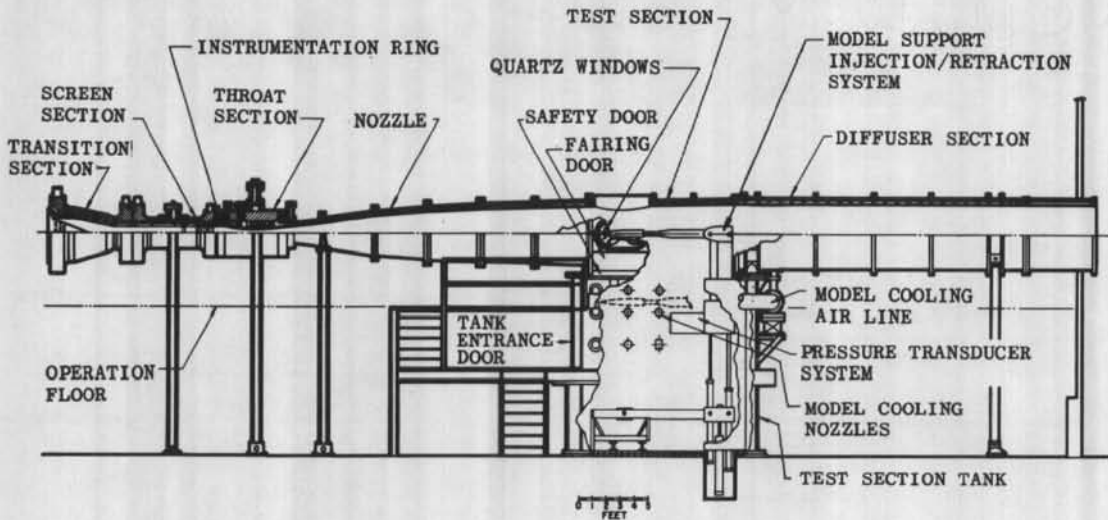


Figure 3.4 Tunnel C assembly.

### 3.2.1 Test Section and Tank

Directly below each test section is a test section tank (Fig. 3.5) into which the model and its support can be

retracted. When the model and support are retracted, the test section can be sealed from its tank so that the tunnel can remain running while the tank is vented to atmospheric pressure in order that personnel may enter the tank to make modifications to the model or its support system. After the desired modifications are made and the tank entrance door is closed, the tank is vented to the test section pressure, the doors between the tank and test section are opened, and the model is injected into the airstream to obtain the desired data. Upon completion of the data acquisition, the model is retracted, and the cycle is completed. The injection system is also used for materials tests in which the model is cooled in the retracted position, set at the desired attitude, and injected into the airstream to obtain the time history of the sample. The minimum injection time is about two seconds, and the maximum acceleration or deceleration is about one g. The model is exposed to the airstream approximately 0.9 sec prior to the injection stroke limit with the model in the test position.

Each test section is equipped with six fused quartz windows. The two on either side are used for the shadowgraph or schlieren system, and the two on top are used for either photographic purposes or overhead test support and boundary-layer survey equipment. The viewing area of each window is about 17.25 in. in diameter. Two additional 12-in.-diam window ports are provided in each test section for auxiliary lighting and photographic purposes. These windows are located on top,  $\pm 45$  deg off vertical axis, and near downstream edges of the large viewing windows.

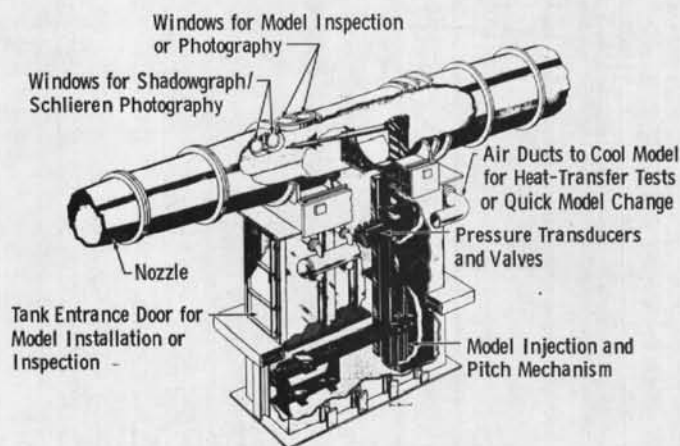


Figure 3.5 Tunnel C test section tank.

### 3.2.2 Model Support

Models are generally supported from the rear by stings which attach to the roll mechanism on top of the single-ended support strut. The support system will accommodate a vertical load of 1,500 lb or a horizontal load of 1,000 lb applied at the nominal center of model rotation. The relationship of the model support and the windows is shown in Fig. 3.6. In either the retracted or injected position, the model can be rolled  $\pm 180$  deg and pitched through a range of 30 deg when the center-of-model rotation is within the rearward 10 in. of its travel. The center-of-model rotation can be moved so that the region of interest on the model remains within the viewing area of the windows. At the most forward position of the center-of-model rotation, the angle-of-attack range is limited to about 24 deg. Straight and bent water-cooled stings are available for supporting the models. One series of split bent stings has prebends of 3, 12, 30, 39, and 48 deg which can be interchanged without disconnecting the model instrumentation. Combinations of angle of attack and angle of sideslip can be obtained by rolling the model-sting arrangement. Details pertaining to attachment of models to available stings will be furnished upon request.

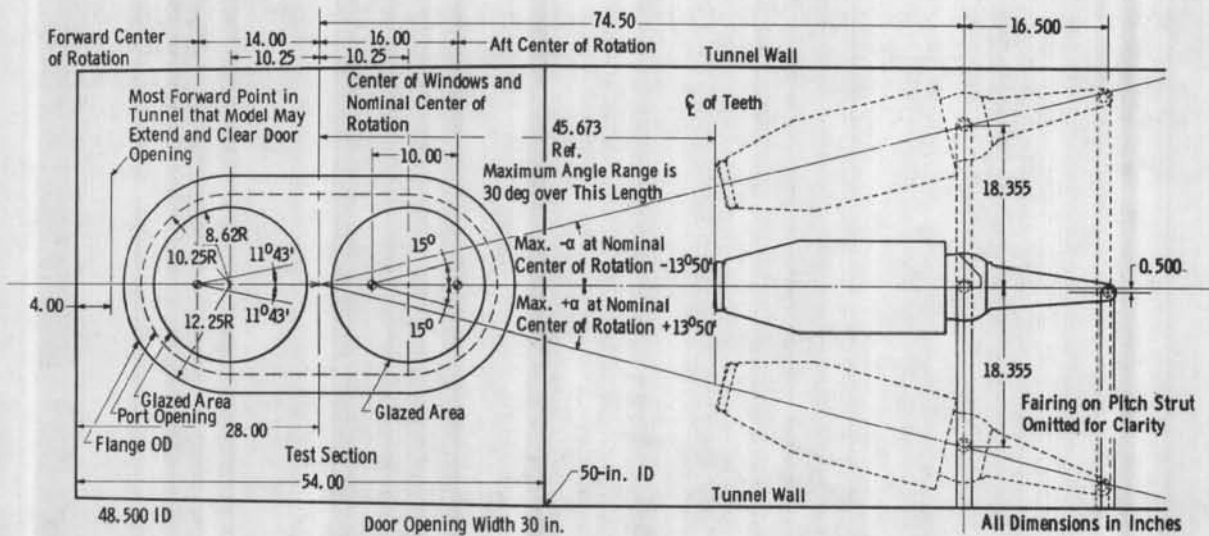


Figure 3.6 Test section (elevation), Tunnels B and C.

### 3.2.3 Instrumentation

Tunnels B and C are each equipped with a complement of permanently installed instrumentation for measuring such parameters as pressure and temperature. In general, this equipment provides visual indications for monitoring purposes

as well as output signals for the data acquisition systems. These systems can accept 98 digital signals (including constants) and 32 analog signals. The normal sampling rate is 3,500 samples per second, but other rates can be provided to meet special requirements. The format of the digital signals can be either 17-bit binary or 4-digit BCD plus sign. Analog signals may range from  $\pm 5$ -mv full scale to  $\pm 10$ -v full scale. These signals are converted to a 4-digit BCD format. During operation, the data system is connected on-line with the DEC 10 computer.

### 3.3 TYPES OF MATERIALS TESTS

#### 3.3.1 Test of Insulating Panels

A sketch of a wedge that has recently been used for material testing is shown in Fig. 3.7. The basic wedge angle was 33.6 deg; however, during recent tests, prebent stings were used in conjunction with the model pitch mechanism, which provided for wedge angles from 0 to 38 deg. In addition to the material samples, an instrumented "calibration plate" was used to define the local conditions on the wedge for various wedge angles. The calibration plate was instrumented to measure both pressure and heat-transfer levels. To provide a turbulent boundary layer, trip spheres were installed 3 in. from the leading edge of the wedge as illustrated in Fig. 3.7.

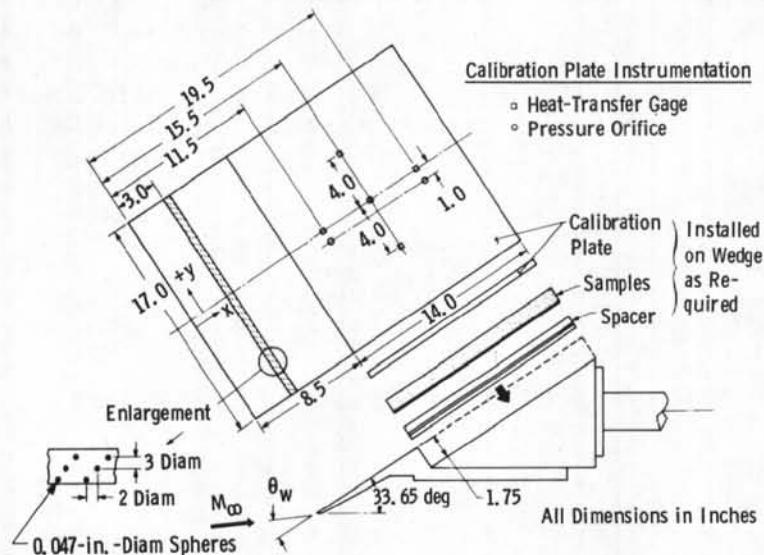


Figure 3.7 Sketch of test hardware.

The use of a large wedge as a holder for material samples actually provides two possible test regions as illustrated in Fig. 3.8. Region I is limited in height by the distance of the bow shock above the wedge boundary layer at the base of the wedge. Because of this severe limitation, a significantly larger test core is being planned for a future facility which will be discussed in Section 3.4. Much larger samples can be tested in Region II, and, in fact, samples up to 25 in. in length have recently been used. This region can be utilized for low-density ablative materials which may be required in locations of interference heating or as a general surface covering.

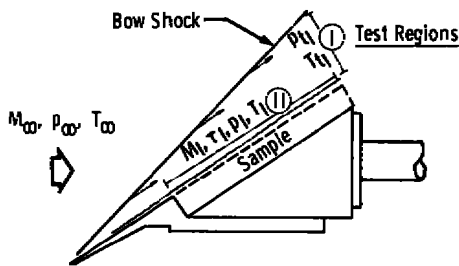


Figure 3.8 Wedge sketch illustrating nomenclature.

In Region II, duplication of local shear stress ( $\tau_1$ ) is probably the most relevant parameter for the given total temperature level ( $T_{t1}$ ), whereas in Region I duplication of total pressure ( $p_{t1}$ ), total temperature ( $T_{t1}$ ), and Mach number would be required. This is accomplished by setting the proper tunnel stilling chamber conditions as illustrated in Fig. 3.9. A summary of the supersonic flight conditions which can be duplicated in the AEDC-VKF hypersonic tunnels is presented in Fig. 3.10. This envelope covers a significant portion of the operating envelopes of current aircraft and missiles. The application of the capability to a specific example can now be illustrated.

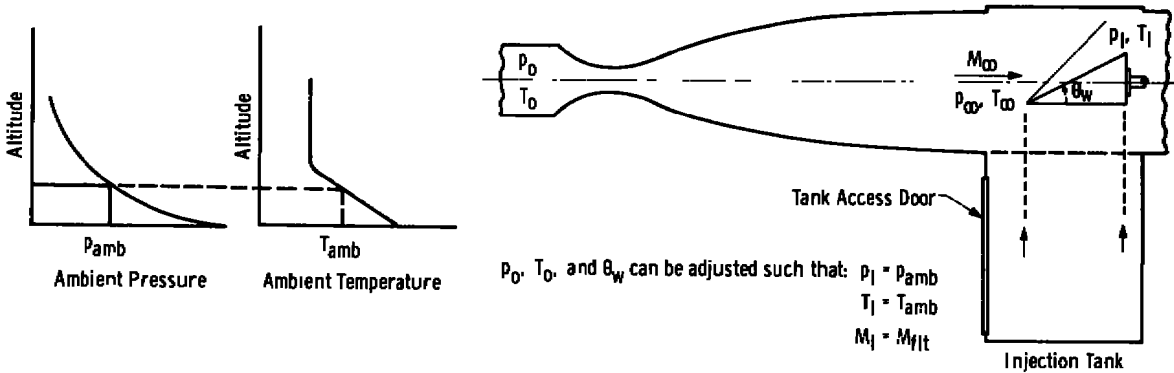
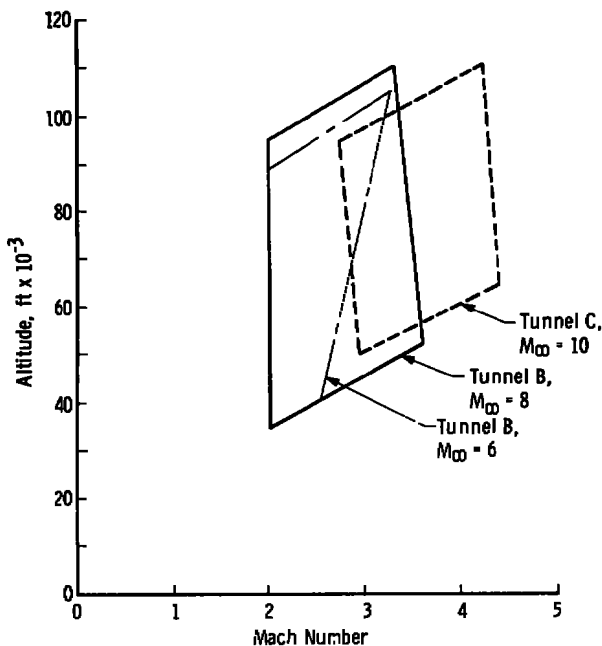


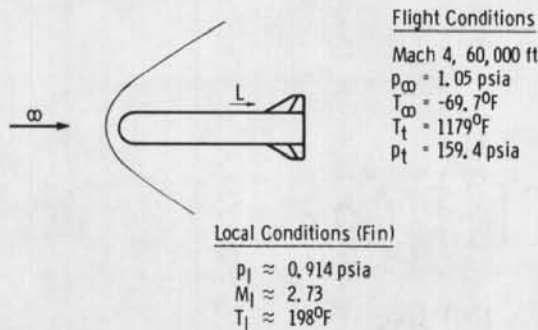
Figure 3.9 Illustration of testing technique used to duplicate flight conditions.



**Figure 3.10 Summary of flight conditions which can be duplicated in VKF continuous-flow tunnels by wedge technique.**

Consider an air-launched missile traveling at Mach 4 and 60,000 ft for a flight duration time up to 30 sec. Will the radome material withstand this environment, and what is the minimum amount of material required for the fin and in the fin interference region? The flight environments for the nose and fin regions are shown in Fig. 3.11a. Figure 3.11b shows the wind tunnel conditions required to duplicate these environments. The actual flight radome and radome support hardware could be tested in the facility described in Section 3.4. The fin and the material to be used in the interference region could be tested in Region II. A test somewhat similar to this example has recently been conducted for NASA in Tunnel C. The objective of this specific test was to observe the behavior of a low-density insulator in the region of a 1-in.-diam cylindrical protuberance. A schlieren photograph of the flow-field disturbance is presented in Fig. 3.12, and the timewise effect on the material is presented in Fig. 3.13. The horizontal dark lines in this figure were projected onto the samples to provide a system for determining material recession rate. Upstream "movement" of the grid lines corresponds directly to the amount of material eroded as will be discussed later. The left-hand photograph in Fig. 3.13 shows that the interference flow field caused by the protuberance was sufficient to

erode completely through the 1-in.-thick layer of this particular material sample in just 4 sec.



These conditions can be determined from analytical or experimental techniques.

**a. Flight environment**

Utilizing AEDC-VKF Tunnel C,  $M_{\infty} = 10$  (Real Gas Corrections < 4%)

<u>Nose</u>	<u>Fin</u>
Test Region I (See Fig. 3.8)	Test Region II (See Fig. 3.8)
for $\theta_w = 21$ deg	for $\theta_w = 29.7$ deg
$p_0 = 2000$ psia & $T_0 = 1179^{\circ}\text{F}$	$p_0 = 965$ psia & $T_0 = 1265^{\circ}\text{F}$
The Flow Conditions Are:	The Flow Conditions Are:
$M_{lwt} = 4.0 = M_{\infty ffit}$	$M_{lwt} = 2.73 = M_{lffit}$
$T_{t lwt} = 1179^{\circ}\text{F} = T_{t ffit}$	$p_{lwt} = 0.914$ psia = $p_{lffit}$
$p_{t lwt} = 159.4$ psia = $p_{t ffit}$	$T_{lwt} = 198^{\circ}\text{F} = T_{lffit}$

**b. Wind tunnel conditions required to duplicate flight environment**  
**Figure 3.11 Illustration of test technique.**

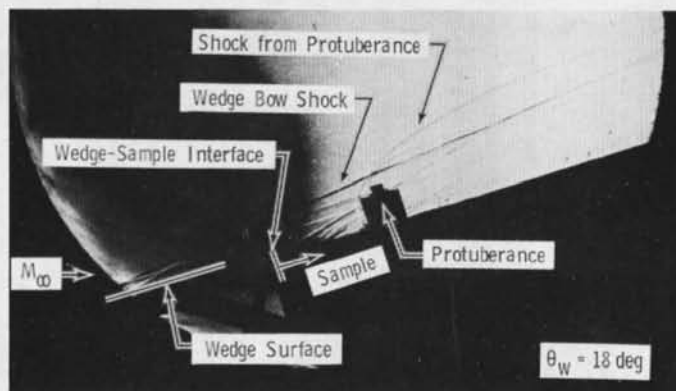


**Figure 3.12 Typical Schlieren photograph.**

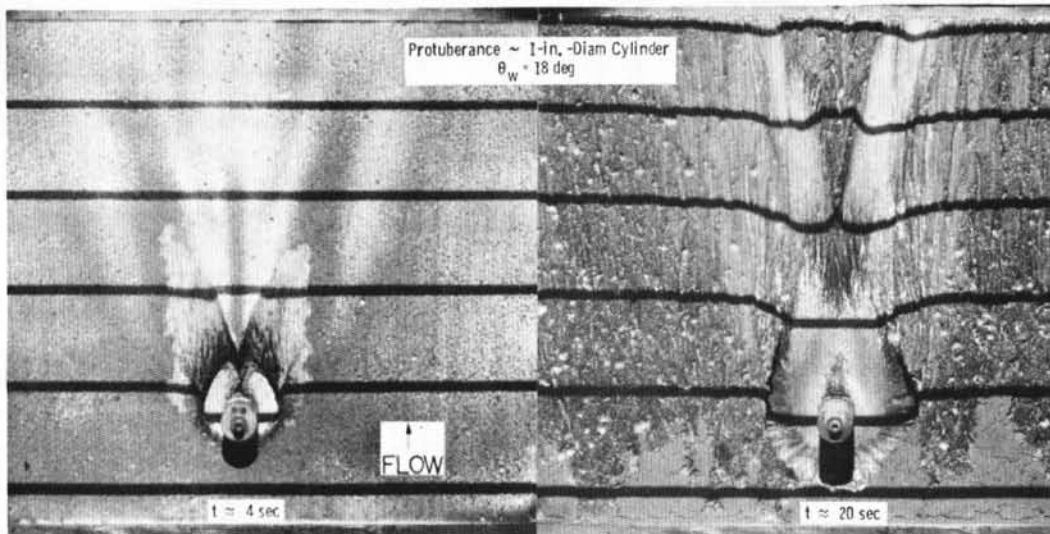


**Figure 3.13** Photographs illustrating interference effects of protuberance.

The unique grid line projection system mentioned above is illustrated in Fig. 3.14. A standard slide projector was mounted on top of the tunnel, and a slide was made such that grid lines spaced about 2 in. apart were projected onto the sample at an acute angle. As the material surface receded, the projected lines translated toward the leading edge as viewed from the position of the 70-mm camera. This system was calibrated for each wedge angle and camera installation

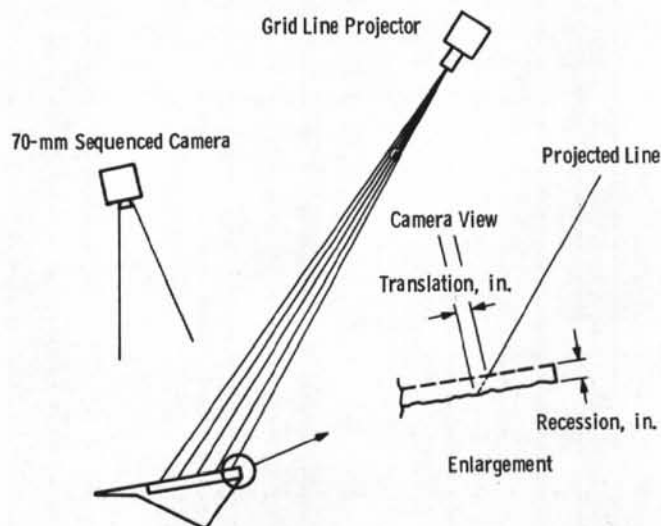


**Figure 3.14** Illustration of grid line projection system.

by photographing a sample level with the wedge surface and then removing a known thickness of spacers and again photographing the sample. An enlarger was used to measure the translation of each grid line so that "scale factors" could be determined. This provided a means of obtaining quantitative measurements of the recession rate during the run since the samples were photographed at a nominal rate of one frame every two seconds.

Photographs of a sample without a protuberance are shown in Fig. 3.15. The grid line projection system clearly illustrates the formation of large grooves in this particular sample. As a result of these tests, some modifications were made to the material to improve the performance in this environment.

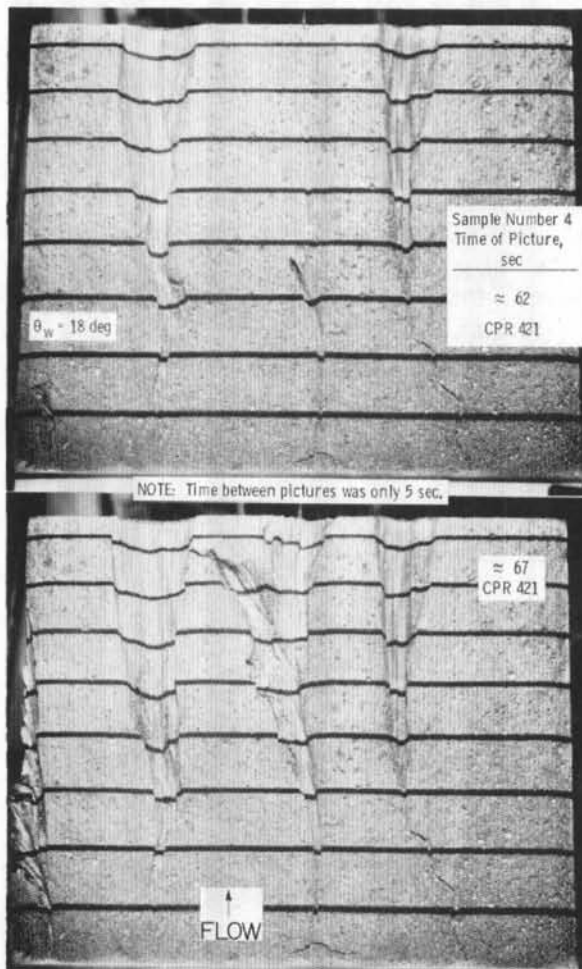


Figure 3.15 Photographs illustrating an example of groove formation.

In addition to photographing the sample, it was also desirable to obtain temperature measurements on the front and back surfaces of the samples. The back surface temperatures were measured with a thermocouple attached to the aluminum plate (substrate), and the front face temperatures were measured with an infrared scanning system. The camera used was an AGA model 680 which has a detector sensitive to the 2- to 5- $\mu$  wavelength band. Radiant flux is converted to an electronic signal which is then viewed on a color monitor which displays the thermal image in ten distinct color bands. Figure 3.16 illustrates typical results from these temperature measurements on a silicone foam sample. Since these materials are good insulators, the surface temperature rises very quickly to an equilibrium value, while the back face temperature remains less than 160°F.

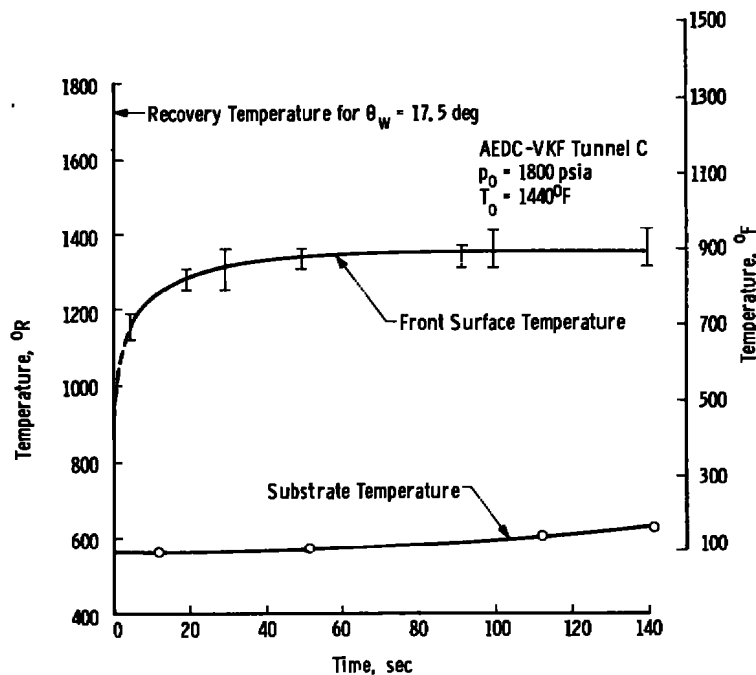


Figure 3.16 Silicone foam temperatures for  $\theta_w = 17.5$  deg.

### 3.3.2 Test of Windshield Materials

Another example of this wedge technique is the recent series of tests conducted on candidate windshield materials.

The design of supersonic aircraft windshields is strongly influenced by aerodynamic heating. The windshield must be

able to withstand the severe heating environment and still provide an undistorted view for the pilot. A windshield composed of several laminated plies of clear plastic materials is being considered for use in supersonic aircraft by the Air Force Flight Dynamics Laboratory (AFFDL/FEW). The objective of these tests was to evaluate the performance of three candidate windshield materials to determine the amount of optical distortion caused by the repeated exposure of the materials to the combined aerodynamic heating and pressures.

Nominal flight conditions of Mach 2.5 at an altitude of 50,000 ft were chosen to be simulated. The tests were conducted in the Hypersonic Wind Tunnel (B) of the von Kármán Gas Dynamics Facility (VKF) at a nominal free-stream Mach number of 6.0.

For simplicity, and because of model size limitations, flat windshield sections (test panels) approximately 8 by 10 in. were tested in the two-dimensional flow field existing behind the wedge. The test panels were subjected to the flow for nominal 200-sec cycles, and photographs were taken after each cycle to evaluate the relative condition of the test panels.

3.3.2.1 Model

The model shown in Fig. 3.17 consisted of a wedge that served as the flow generator and a test panel attached directly behind the wedge. Four panels were tested: three windshield panels and one instrumented panel.

Region	Environment
①	Free-Stream Conditions $M_{\infty} = 6.05$ $T_0 = 885^{\circ}\text{R}$ , $p_0 = 210 \text{ psia}$
②	Approach Conditions $M = 2.27$ $T_0 = 885^{\circ}\text{R}$ , $p = 2.41 \text{ psia}$
③	Windshield Conditions $M = 1.81$ , $p = 4.60 \text{ psia}$ $T_0 = 885^{\circ}\text{R}$ , $Re_{\xi} \approx 4.2 \times 10^6$
④	Inboard Face Conditions $\approx 0.1 \text{ psia}$

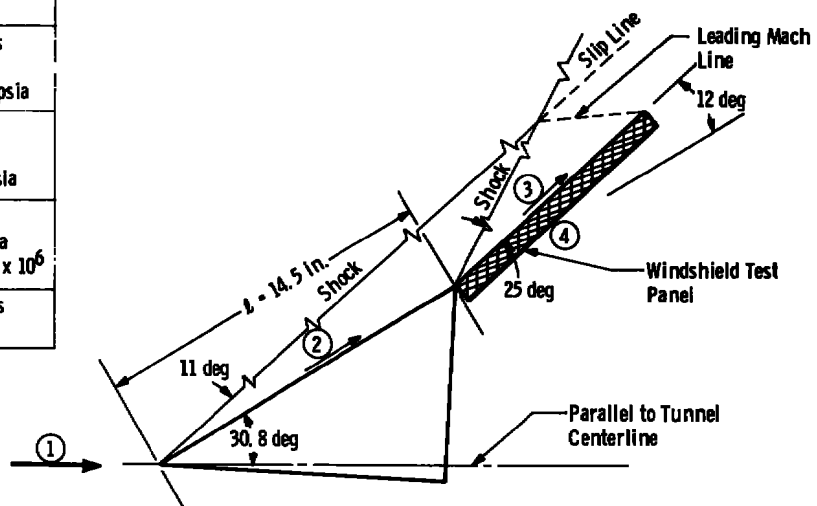


Figure 3.17 Windshield test environment.

The three windshield panels, provided by Pittsburg Plate Glass Industries under AFFDL contract, were of identical construction except for the outboard surface plies of the laminated plastic material. The windshield panels were composed of alternate layers of plastic materials.

An instrumented panel was used to determine the heat-transfer rate and pressure environment on the outboard surface of the windshield panels tested. Ten pressure orifices and nine Gardon-type heat-transfer-rate gages were located on the surface of the instrumented panel.

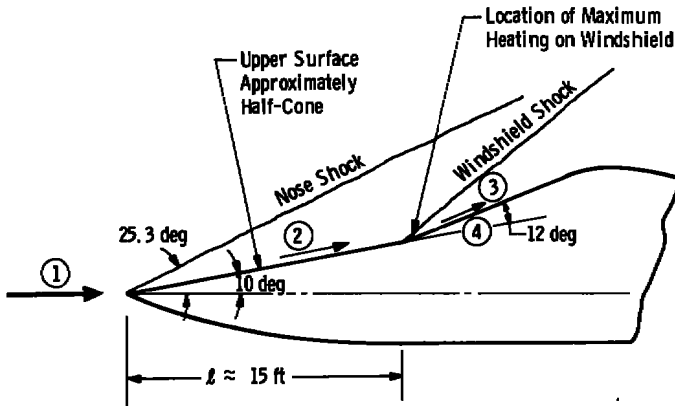
To evaluate the relative deterioration of the optical quality of the windshield panels, photographs were taken of a grid pattern viewed through the windshield panels. These photographs were taken prior to the test and after each time a panel was exposed to the tunnel flow. The photographs were taken with a Hasselblad camera which was mounted on a bracket located behind the model. The bracket was permanently mounted to the model support, while the camera was installed for the grid photographs and then removed before the model was injected into the tunnel. The camera was located 26 in. behind the windshield panel, and the camera line-of-sight was 22 deg (same as pilot's view) relative to the panel.

Flow-field photographs were taken periodically by a standard refocused shadowgraph system. General coverage 16-mm color motion pictures were obtained at 24 frames/sec.

### 3.3.2.2 Test Conditions

The area of an aircraft windshield which would normally receive the highest heating, and therefore the area that would probably fail first because of overheating, is that area directly behind the aircraft nose and on its centerline. A typical supersonic aircraft nose shape with the flow environment depicted in the area of interest is shown in Fig. 3.18.

For simplicity, a two-dimensional wedge model was chosen to simulate the approach flow conditions of the aircraft nose. A two-dimensional, inviscid, oblique-shock solution was assumed to determine the appropriate Mach number and pressure to simulate the flight environment. Because of size limitations, the approach length of the aircraft nose could not be simulated. However, conditions were such that fully turbulent boundary-layer flow approached the test panel, as was expected to be the case for the flight environment. The test environment predicted by the inviscid two-dimensional solution is shown in Fig. 3.18.



Region	Environment
①	Free-Stream Conditions $M_\infty = 2.5$ at 50,000 ft $T_\infty = 393^\circ\text{R}$ , $p_\infty = 1.69$ psia $T_0 = 885^\circ\text{R}$ , $p_0 = 28.8$ psia
②	Approach Conditions $M = 2.27$ $T_0 = 885^\circ\text{R}$ , $p = 2.41$ psia
③	Windshield Conditions $M = 1.81$ , $p = 4.60$ psia $T_0 = 885^\circ\text{R}$ , $Re_\ell \approx 45 \times 10^6$
④	Cabin Conditions $535^\circ\text{R}$ , 11 psia

Figure 3.18 Windshield flight environment.

### 3.3.2.3 Test Procedure

At the beginning of the test, a single injection of the model (with the instrumented panel installed) was made to determine the test environment of the windshield.

Each windshield panel was preheated to approximately  $140^\circ\text{F}$  (to simulate the expected temperature under normal flight conditions at subsonic speeds), installed behind the wedge model, and then injected into the tunnel flow for a nominal 200-sec period. Shadowgraph photographs were taken at 4-sec intervals, and motion pictures were taken continuously to observe any panel deterioration. The thermocouples embedded in the windshield panel were recorded continuously while the windshield panel was exposed to test conditions. Photographs were taken of a grid pattern through the windshield panel prior to the test, and each time the model was retracted after exposure to test conditions. After each injection, the windshield panel was cooled to approximately  $140^\circ\text{F}$  on the inboard surface. This process was repeated for ten injections or until the windshield panel failed.

### 3.3.2.4 Materials Evaluation

The primary objective of the tests was to determine the amount of optical distortion caused by the repeated exposure of the windshield materials to the combined aerodynamic heating and pressures. The relative optical distortion due to exposure to test conditions can be determined from the sequence of grid photographs shown in Figs. 3.19 and 3.20. A posttest photograph of Panel 3 (Fig. 3.21) shows the extent of surface deterioration. Large bubbles formed under the top ply of this panel causing the surface to crack severely.

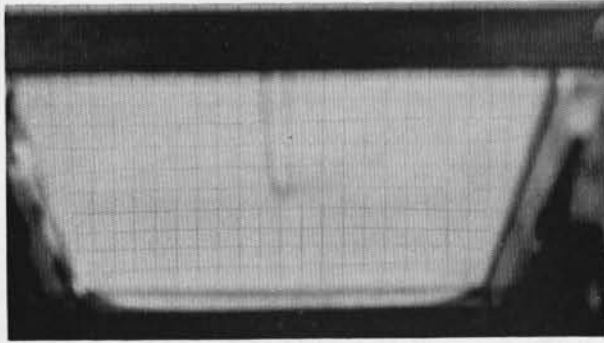


Figure 3.19 Panel No. 3 before testing.

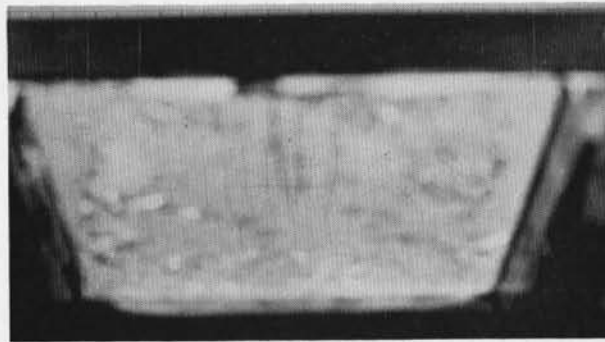


Figure 3.20 Panel No. 3 after test completion  
(test time = 405 sec).

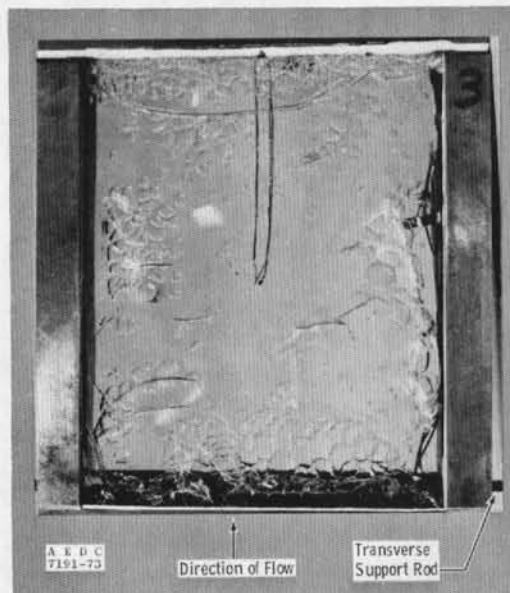


Figure 3.21 Panel No. 3.

### 3.4 FUTURE CAPABILITIES

The existing aerothermal testing capabilities in Tunnels B and C are primarily designed for testing large flat samples or small hemispherical noses. In recent years, the need for aerothermal testing of full-scale infrared domes (or radomes) has also become important.

Current high-performance aircraft are capable of flight Mach numbers in the 2.0 to 2.5 range for brief periods of time. Flight at these conditions can produce aircraft skin temperatures in excess of 400°F. Advanced aircraft will be capable of sustained flight at Mach 3, which increases skin temperatures to over 700°F. And finally, for these aircraft to be effective, they must carry weapons which operate in the Mach 4-plus regime. As a result, stagnation temperatures can exceed 1,100°F (see Fig. 3.22). When missiles are

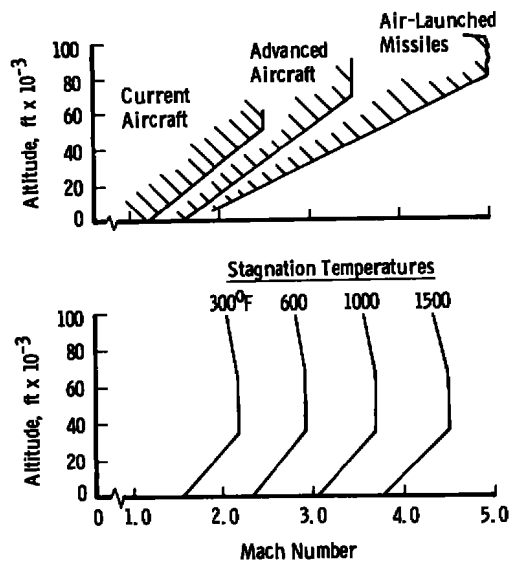


Figure 3.22 Definition of environment.

launched and accelerate to their design Mach number, the protruding domes which house the guidance equipment and provide its "view" of the target may experience these large temperature increases in a very short time period. This "thermal shock" can be severe enough to cause structural failure of the domes as illustrated in Fig. 3.23. In less severe cases, the structure of the dome may survive, but the sophisticated guidance system may receive a distorted "image" through the dome. To demonstrate the operational reliability of these domes and to utilize the "best" dome materials, ground tests are needed to screen and qualify materials.

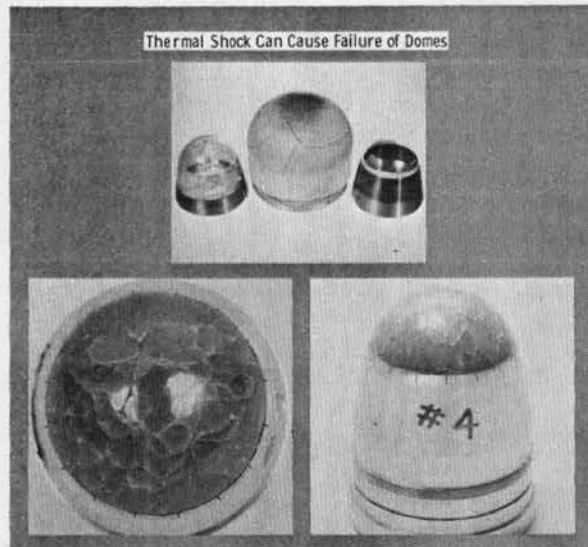


Figure 3.23 Thermal shock damage.

Having discussed some of the aerothermal problem areas, let us now look at the existing capabilities or tools which can be used to help solve these problems. The advantages and disadvantages of the various approaches are listed in Table 3.4. While each approach has its advantages, there are still several undesirable characteristics associated with each technique. The proposed aerothermal test capability can eliminate many of the "undesirable characteristics" and, therefore, provide a unique test capability for the flight regime of current interest.

Table 3.4 Pros and Cons of Existing Capabilities

Technique	Pros	Cons
Flight Testing	Real World No Assumptions	Very Expensive Long Lead Times Required Flight Safety Approval Difficulties
Track Test	Real Hardware Severe Test Environment (High $T_0$ )	Short Exposure Times Requires Extrapolation High Cost
Radiant Heating Test	Real Hardware Relatively Inexpensive Versatile	Poor Duplication of Flight No Pressure-Loading No Shear Forces
Analytical Solutions	Inexpensive Fast Versatile	Unrealistic for Complex Flow Unrealistic for Complex Geometry Requires Many Assumptions
Existing Wind Tunnels	Relatively Inexpensive Versatile Simulation of Pressure and Shear	Cannot Duplicate Temperatures Requires Extrapolation
High-Enthalpy Facilities (Arc Jets, Combustion Heaters, etc.)	Can Produce High Temperatures Relatively Inexpensive	"Dirty" Flow (Particles, Grit, or Foreign Gases) Usually Small Test Core Undefined Aerodynamic Environment

Development of an improved aerothermal test capability should, of course, address the weaknesses of existing capabilities and, for economic reasons, incorporate their positive factors. Because the VKF is basically an aerodynamic test facility, its strength and experience lie in providing high quality (clean) aerodynamic ground testing. Our approach, therefore, follows these guidelines.

The approach used in the planning of the improved aerothermal test capability was to study the existing AEDC air supply systems to determine how they could be utilized to achieve an increased capability. Emphasis was placed on duplication of flight conditions in the supersonic Mach number regime.

Basically, an improved aerothermal capability can be obtained by providing a new stilling chamber and nozzle in place of the existing Mach 10 nozzle in Tunnel C. The design of this modification has been completed under AEDC sponsorship. Figure 3.24 emphasizes the interchangeability between the existing Mach 10 nozzle and the planned Mach 4 nozzle. With the Mach 4 nozzle installed, the facility will provide an important supersonic aerothermal test capability. Mach 10 performance of Tunnel C will be retained requiring only a few days to interchange nozzles.

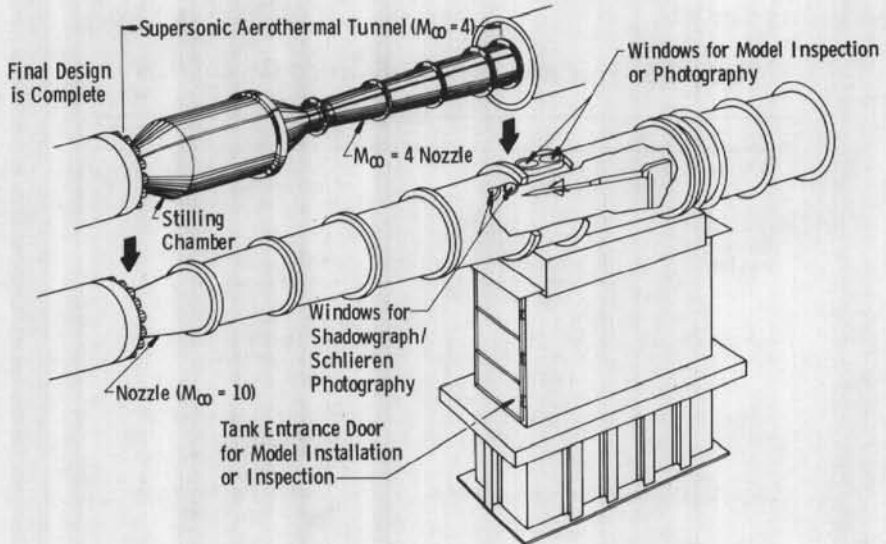


Figure 3.24 Interchangeability of Mach 10 and Mach 4 nozzles.

The specific features of the aerothermal test capability are listed as follows:

1. 25-in.-diam Test Section
2. Continuous Mach Number 4 Flow
3. Duplicate Pressure and Density Altitudes from 55,000 to 100,000 ft, (i.e.,  $24 \leq p_0 \leq 200$  psia)
4. Duplicated Stagnation Temperatures up to  $1,180^\circ\text{F}$
5. Provisions for Mach Number 3 Nozzle
6. Nozzles Are Interchangeable with Current Mach Number 10 Nozzle
7. Vastly Improved Supersonic Heat-Transfer Testing Capability

Duplicated pressure and density altitudes mean that the free-stream pressure and temperature in this tunnel will be identical to those in the U. S. Standard Atmosphere for the altitude range shown. To provide these matched conditions down to sea level would require a major facility with plant and heater capabilities significantly greater than those which exist today. However, since Mach number 4 flight at sea level is not commonly encountered, such a facility is not considered essential at the present time.

A significant "spinoff" of the aerothermal capability will be improved quality of supersonic heat-transfer data which can be obtained in this facility as compared with current capabilities (see Fig. 3.25). The quality of heat-transfer data is proportional to the difference between the

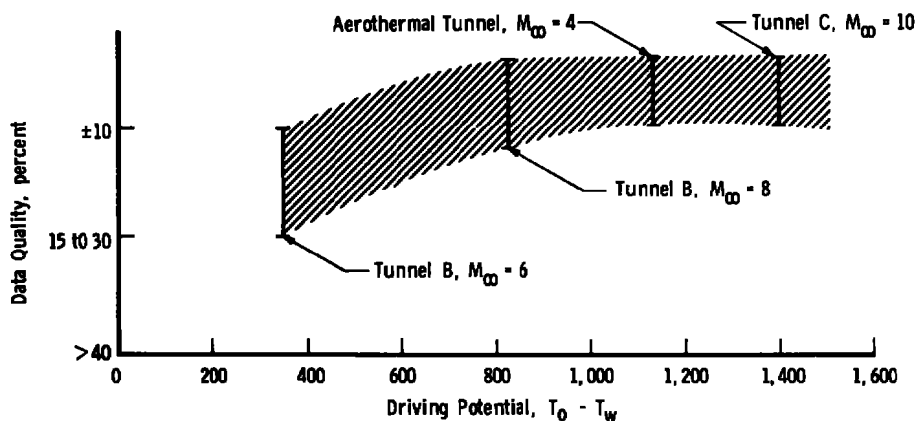


Figure 3.25 Improved heat-transfer capability.

tunnel stagnation temperature and the model wall temperature. That is, the larger  $(T_o - T_w)$ , the better the quality of the heat-transfer data. Heat-transfer tests in the supersonic speed regime are currently conducted in the VKF/Tunnel A, which was not originally designed (Tunnel A was designed in the early 1950's and became operational about 1958) for heat-transfer testing. The aerothermal tunnel will provide a temperature difference  $(T_o - T_w)$  of about  $1,000^{\circ}\text{F}$ , which will enable measurement of heat-transfer data to better than  $\pm 10$  percent.

**4.0 HYPERBALLISTIC RANGE (G)**

**4.1 Facility Description . . . . . 56**  
**4.2 Types of Materials Tests . . . . . 69**  
**4.3 Facility Limitations . . . . . 72**  
**4.4 Future Capability . . . . . 73**  
**4.5 Concluding Remarks . . . . . 74**



#### 4.0 HYPERBALLISTIC RANGE G

The thorough evaluation of materials selected as candidates for external surfaces of reentry vehicles requires clean air ablation, erosion, and boundary-layer transition testing in ground-based test facilities. To obtain ground test data that are directly applicable to the reentry flight case, it is frequently necessary to duplicate rather than just simulate important aspects of the reentry environment. For example, in obtaining materials data applicable to reentry vehicles with large ballistic coefficients, a major problem is to duplicate simultaneously velocity, stagnation enthalpy, and stagnation pressure corresponding to a point in the reentry trajectory. The significant advantage of the aeroballistic range in this regard is that it does have the capability to duplicate simultaneously the very high levels of stagnation enthalpy and pressure at Mach numbers corresponding to peak heating portions of reentry trajectories. In addition, the quiescent environment of the range facilitates simulation of various types of erosive encounters by means of free-falling particles which closely resemble those found in the natural environment in terms of size, concentration, and structure.

Historically, the free-flight Range G has been adapted to meet a wide range of test requirements other than its originally intended mission. Concentrated efforts during the past ten years in such areas as model launching techniques, test environment simulation, and specialized instrumentation have resulted in the emergence of Range G as a viable and versatile facility for testing reentry materials. Interest in providing the Range G with a model guidance capability to further improve test capability began in 1970. The concept was shown to be feasible but was generally considered to be unjustifiable by the ablation testing need alone. However, in 1972, the justifiability for such a capability was markedly increased by the need for ground test simulation of RV nosetip encounter with atmospheric hydrometeors. Thus, a decision was made to initiate a joint project between AEDC and ABRES to install a track and recovery system in Range G. Subsequently, a 160-ft, 1-5/8-in.-diam system was developed and studied. This system was installed in Pilot Range K and used extensively to develop a technology base for the design and operation of the Range G track, which was placed in operation in March 1977. The track system includes a retraction capability so that the free-flight mode of operation is

retained. Thus, materials tests may be conducted in free-flight or with track guidance.

To acquire meaningful data under realistic test conditions, a state-of-the-art technology has been developed for Range G to overcome facility limitations associated with the severe model launch and in-flight environment, the short test time, and the acquisition of data from a hypervelocity test article. In particular, this advanced technology is manifest in the following capabilities: (1) model guidance for trajectory control, (2) models suitable for ablation, erosion, boundary-layer transition, and heat-transfer testing, (3) measurement of material response to aerothermal and erosive environments, (5) model recovery, and (6) advanced data reduction techniques.

The test techniques and hardware, which have been developed for use in the Range G track and which collectively comprise its materials testing capability, are described in the following sections.

#### 4.1 FACILITY DESCRIPTION

The major subsystems which comprise the Range G track facility are (1) a model launcher device, (2) a model guidance system including the track and its ancillary hardware, (3) a model recovery system that is used to dissipate the kinetic energy of the test article without significant damage, (4) a test model that is either a full- or reduced-scaled flight vehicle, (5) an environmental system, the basic component of which is the 10-ft-diam range tank, to provide a wide range of environmental simulation such as high-altitude flight in clear air, erosive particle encounter, or special chemically inert environments, and (6) an instrumentation system capable of in-flight data acquisition. Each of the subsystems is described in detail in the following sections.

##### 4.1.1 Model Launcher System

Range G is equipped with a 2.5-in.-caliber, two-stage, powder-hydrogen gun approximately 150 ft long. This gun, referred to as the GO4 launcher, is the fourth generation two-stage gun that has been developed for use with Range G. It has been in use for about eight years and has launched over one thousand models. A conservative limit of performance for this launcher based on structural considerations for a range of models and sabots that have been tested extensively in

Range G is shown in Fig. 4.1. Model/sabot combinations that exceeded the limit curve by a considerable margin have been successfully launched many times; however, a "harder" than average launch package has been required for reliable operation in this regime. In this regard, it is likely that experience with track models which do not require a separate sabot will result in definition of a new limit curve displaced to the right of the present curve.

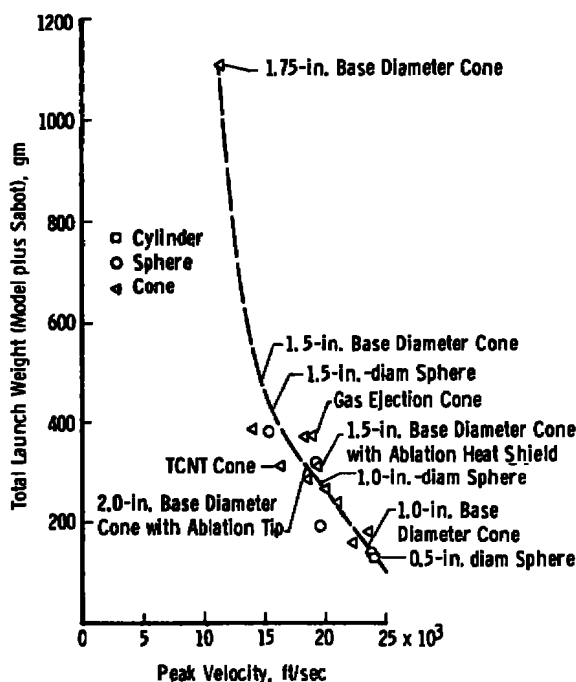


Figure 4.1 Range G launching capabilities - typical models.

#### 4.1.2 Guidance and Recovery Systems

The concept of trajectory control which has been utilized for the Range G track is to confine the test article to a straight-line trajectory by four surrounding guide rails as shown schematically in Fig. 4.2. The main advantages obtained by trajectory control are that the model can subsequently be recovered for posttest examination, and significant latitude is gained in many critical areas of design such as instrumentation and erosive field systems. The main components of the track installation (Fig. 4.3) are: a launch tube extension to reduce muzzle pressure, a muzzle adapter/recoil section to allow for gun recoil, approximately 910 ft of guidance track formed by four rails in a cruciform pattern inside a 7-in.-ID steel tube, and a support/stowage system. Quick-operating valves at

range bulkheads are provided so that the test pressure or range gas composition may be staged along the track.

At the end of its guided flight, the test model enters a recovery device where its energy is dissipated in the compression of gas in a long tube. Model recovery is particularly useful for certain types of tests where in-flight photography cannot fully characterize model surface features because of either resolution limits or hidden contours.

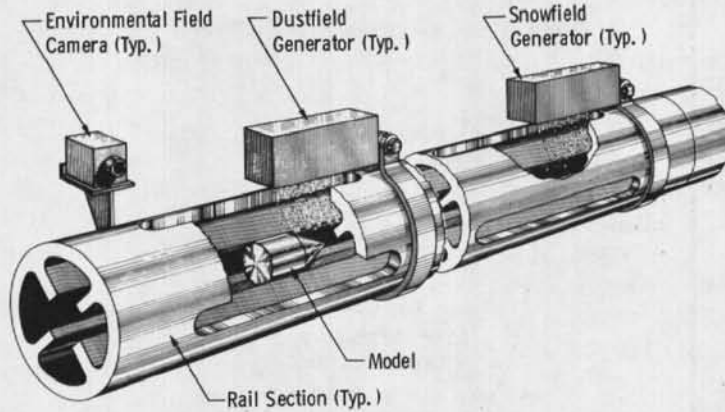


Figure 4.2 Range G track guidance system.

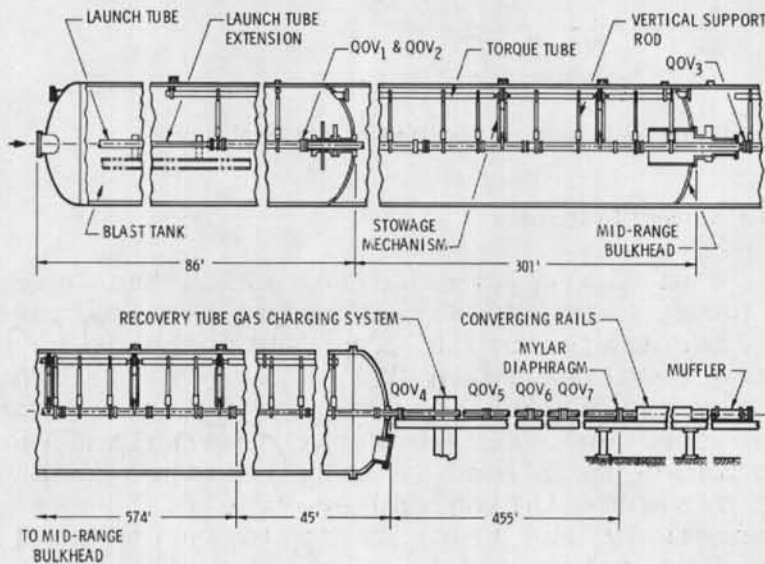


Figure 4.3 Range G track installation.

### 4.1.3 Test Models

A Range G track test model is required to withstand acceleration loads of up to 200,000 g's during launch (at 18,000 ft/sec), survive extreme heating rates and erosive particle encounters during the test period, and finally withstand deceleration loads of up to 120,000 g's during recovery. In addition, the ballistic coefficient must be large in order to minimize timewise variation in test conditions. For the free-flight case, these requirements were satisfied for materials testing applications by the development of a model/sabot package which combined an open base sabot with a heavy model (Fig. 4.4). Adaptation of this model concept to track guidance was accomplished by making the sabot an integral part of the model which forms the track "runner." An additional benefit of this concept is that retention of all the launched weight in the test model results in improvement in model ballistic coefficient, and hence less velocity decay in flight. A more comprehensive description of models developed for specific test applications is given in a later section.

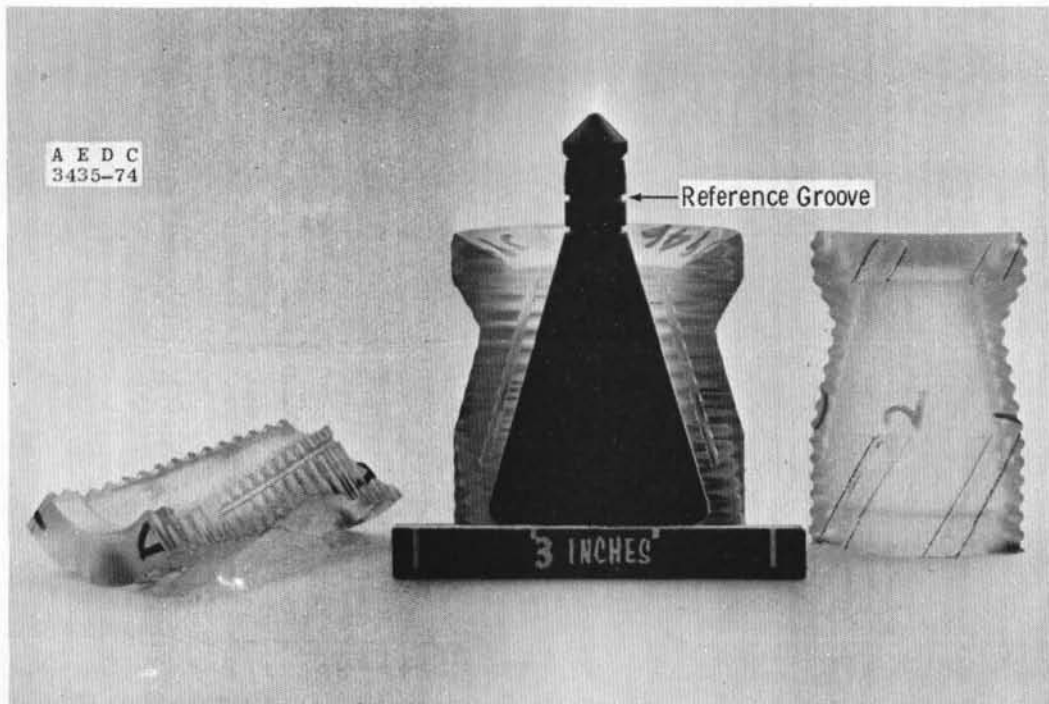
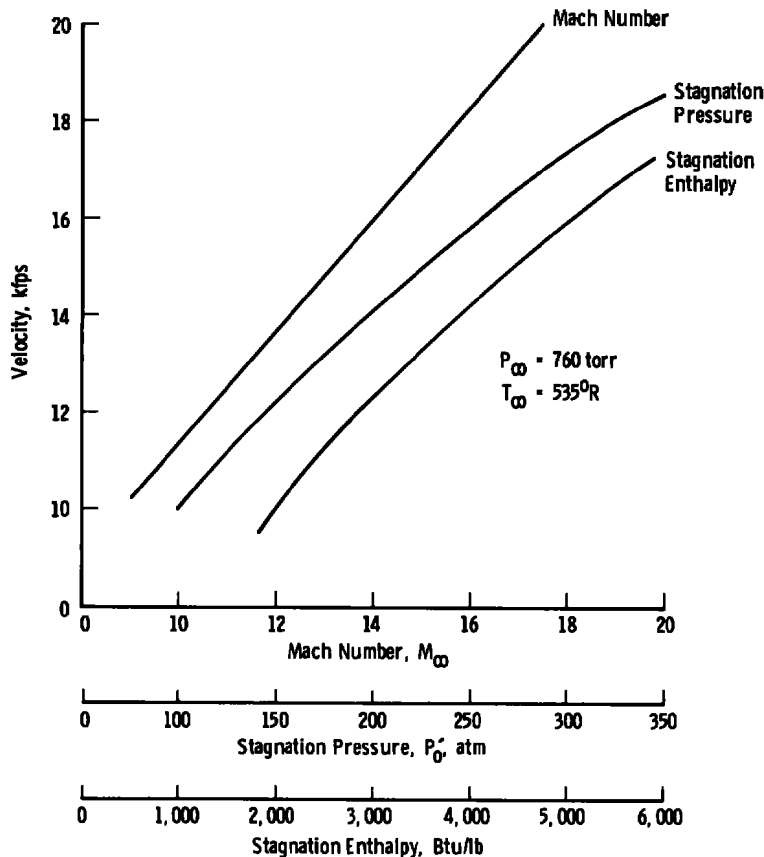


Figure 4.4 Typical free-flight material test model.

**4.1.4 Environmental Systems**

A major advantage of the Range G track facility is the straightforward manner in which erosive particle fields may be simulated because of its quiescent free-stream environment. The range tank itself is the basic component of the environmental system and provides an operating pressure range of 0.2 torr to one atmosphere. The aerothermal environment to which a test article is exposed is determined by its velocity and the ambient pressure and temperature. It is shown in Fig. 4.5 that the velocity range of interest for materials testing can produce stagnation pressures in excess of 350 atm and stagnation enthalpies of almost 6,000 Btu/lb. Any arbitrary level of stagnation pressure enthalpy may be obtained by appropriate test velocity and ambient pressure combination.



**Figure 4.5 Aerothermal simulation capabilities for materials testing.**

The technology required for generation of free-falling particulates was developed for Range G free-flight testing and has subsequently been adapted to track operation.

Types of environments which have been developed include: (1) snowfields consisting of dendritic-crystal snowflakes, (2) dustfields consisting of spherical particles of various sizes and materials, (3) water droplet clouds consisting of particles less than 100  $\mu\text{m}$  in diameter, and (4) rainfields consisting of approximately 1-mm raindrops. However, at the present time, hardware is fabricated and installed for only dust and snow testing on the track. All the erosive fields which have been developed for range testing meet the simulation requirements in regard to realistic field concentration and impact frequency. This is illustrated for dust in Fig. 4.6, where it is shown that number density and particle size combinations may be chosen to produce a very wide range of field concentrations. The interaction which occurs between a nosetip and erosive particles during encounter is shown in Fig. 4.7 for the case of a free-flight graphite nosetip passing through a snowfield. Bow shock distortions and a plume of debris from the surface are apparent. Although most environmental fields are simulated in air, specialized environments (nitrogen, argon, helium, et al.) can be satisfactorily introduced for unique test requirements.

Techniques for conducting single particle impact tests have been developed to an operational status. Water drops of uniform size and spacing can be generated under actual test conditions using a monodisperse drop generator. In addition, a dust capability has been provided by suspending single dust particles on 15- $\mu\text{m}$ -diam silk threads.

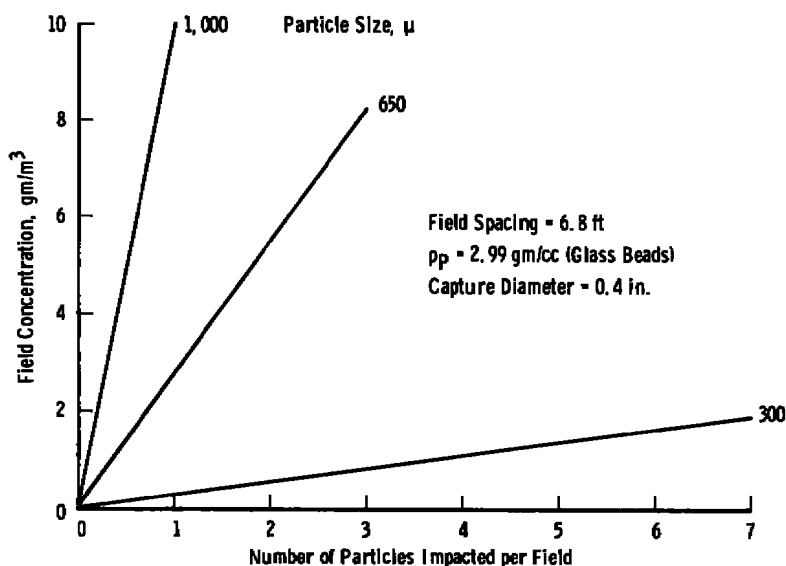


Figure 4.6 Erosive field concentration in terms of particle size and number density.

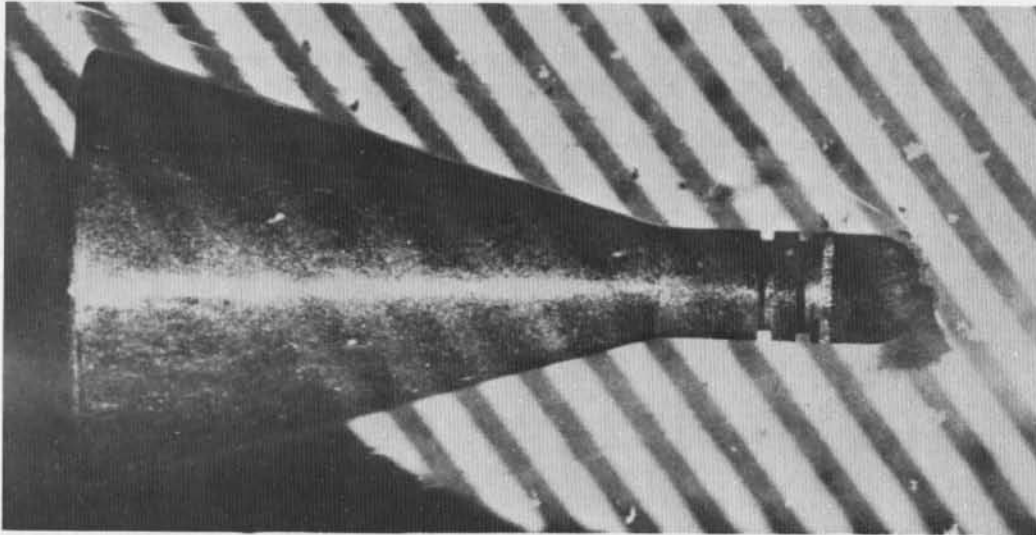


Figure 4.7 Graphite nosetip passing through snowfield.

#### 4.1.5 Instrumentation Systems

The instrumentation for the Range G track facility consists of specially designed high-speed photographic, electro-optical, and electronic systems. The various instrumentation systems, along with the primary intended function for each, are listed in Table 4.1. These systems are described briefly in this section.

Table 4.1 Range G Instrumentation Systems for Materials Testing

System	Number of Stations*	Primary Functions
Front-Light Laser Photography	7	To Provide in-flight photographs from which nosetip-recession data may be obtained.
Stereo Laser Photography	1	To Provide in-flight stereo photographs from which mass eroded and roughness data may be extracted.
X-Ray Shadowgraphs	7	To provide photographic data (with fiducial marks) for use with time data for accurate determination of model velocity.
Photopyrometers	4	To provide in-flight surface temperature data.
Environment Cameras	15	To provide photographs for characterization of erosive fields.
Five-Frame Sequential Laser Photography	1	To provide photographic coverage of high-speed events such as erosive particle/bow shock interaction.
Model Detectors	30	To provide pulses for accurate triggering of photographic system light sources and camera shutters.
Data Acquisition and Control System (DACS)	1	To sequence events necessary for track operation and to acquire and record all timing information.

\* Number of systems is the number currently proposed and is subject to change depending on measurement requirements, funding situations, etc.

#### 4.1.5.1 Laser Photographic Systems

Laser photography is used in Range G to provide in-flight measurements of model nosetip recession. The standard front-light laser photography systems which were developed for free-flight testing in Range G have been modified to take advantage of the fact that test models on the track are confined to a known flight path. Large viewfields and depths-of-field are not required as they are in the free-flight case, and hence higher magnification, and, therefore, better photographic resolution, is achieved.

A schematic of a typical laser photographic system for Track applications is shown in Fig. 4.8. This optical arrangement provides a combination of diffuse front and back lighting through appropriate slots in the track tube. This arrangement produces a magnification of approximately 0.7, and peak photographic resolvability of such a system has been shown to be approximately  $25\ \mu\text{m}$ . For comparison, the resolution of the laser photography systems configured for free-flight testing is  $200\ \mu\text{m}$ . This improvement in photographic resolution reduces the average uncertainty of nosetip recession measurements from  $\pm 2.5$  mils to about  $\pm 1$  mil, respectively.

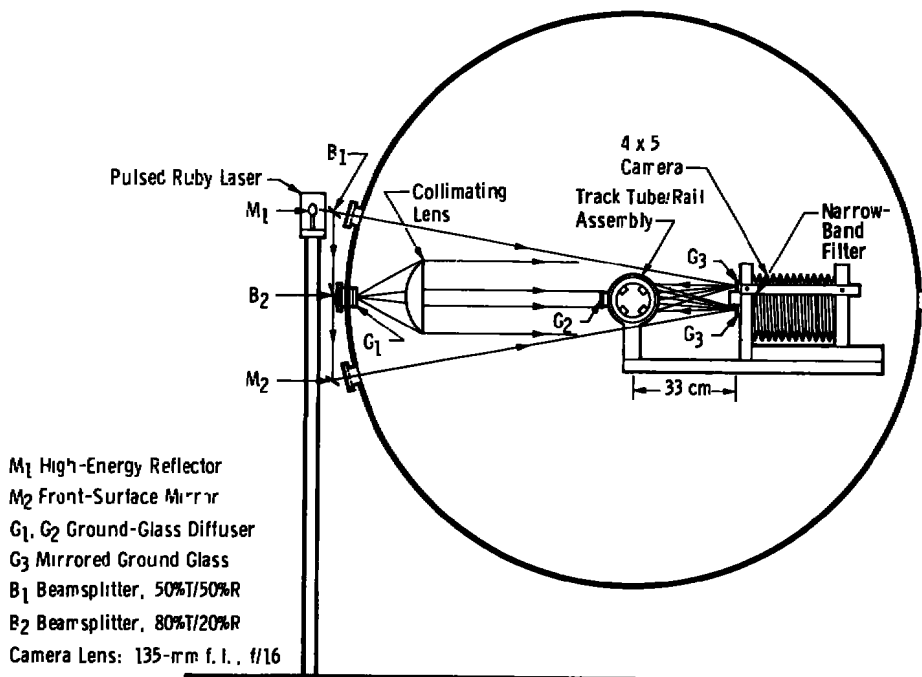


Figure 4.8 Track front-light/back-light laser photography system.

#### 4.1.5.2 X-Ray Shadowgraphs

X-ray shadowgraph systems provide the primary means for model velocity measurements in Range G. By surveying the locations of fiducial markings within each viewfield and by digitally recording the times of each X-ray exposure, model velocity can be measured with an overall uncertainty on the order of  $\pm 0.1$  percent. The possibility of adding fiducial references to the laser photographic systems so that these systems may be used for additional velocity measurement stations has been investigated. Preliminary indications are that this can be done with approximately the same measurement uncertainty as with the X-ray systems.

Another important application of the X-ray shadowgraph systems is for cases where either the model surface is obscured by an opaque shock layer or where knowledge of some internal feature of the model is desired. The former situation arises where massive model erosion precludes meaningful interpretation of laser photographs. During certain metal nosetip ablation tests, for example, ablation material completely fills the dimension reference grooves on the model, obscuring them in laser photographs. In such instances, X-ray shadowgraphs, although of poorer optical quality than laser photographs, allow visualization of the reference grooves and determination of nosetip recession.

Knowledge of internal features of the model during flight is desired for certain types of tests, such as, where fluid is expelled from a cavity by movement of a piston. An example of such a model is one developed for testing transpiration-cooled nosetip concepts. The coolant mass flow rate history is deduced from the position of the piston for a series of times during flight. These times correspond to points along the range at which X-ray shadowgrams are obtained and from which piston position may be measured.

#### 4.1.5.3 Photographic Pyrometry Systems

These systems are employed in Range G for in-flight model surface temperature measurements as shown schematically in Fig. 4.9. The photopyrometry systems feature image intensifier cameras and optics to afford viewing angles of approximately 17 deg from head-on. Proximity-focused image intensifiers with fiber optic coupling to the recording film (Generation I image intensifiers) are employed in two photopyrometry systems, and more sensitive Generation II image intensifiers featuring microchannel plate amplifiers are used in two other systems. All intensifiers have S-20R spectral responses; i.e., they respond to visible and near-infrared radiation out to a

wavelength of approximately  $0.93 \mu\text{m}$ . It is estimated that the lower temperature measurement limits for the photopyrometers are approximately  $1,600^\circ\text{K}$  for the Generation I systems and approximately  $1,200^\circ\text{K}$  for the Generation II systems. The upper measurement limit for all systems is approximately  $4,500^\circ\text{K}$ . Measurement uncertainty for either system is approximately  $100^\circ\text{K}$ .

Systems were designed so that the image intensifier cameras can be removed conveniently from the range and transported to the laboratory for calibration. Graphite-arc lamps and other lower temperature blackbody sources are maintained as temperature standards in the laboratory.

To ensure that the photopyrometry systems detect only incandescent radiation from the model surface and thus provide accurate measurements of model surface temperature, it is necessary to quench or considerably decrease chemiluminescence and shock cap radiation. This is achieved in the range via use of helium-filled chambers at each photopyrometry measurement station. Each photograph (viz; surface temperature measurement) is made while the model is temporarily in "flight" within an inert helium atmosphere.

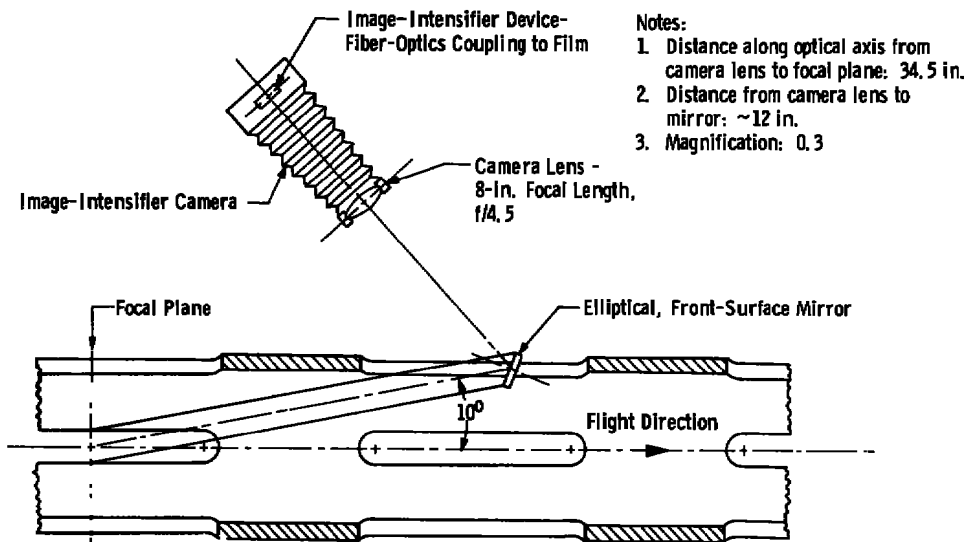


Figure 4.9 Track photopyrometer geometry.

#### 4.1.5.4 Erosive Environment Photographic Systems

These systems provide photographs for use in the characterization of erosive fields. Back lighting with xenon flash lamps is used to provide good definition of particle edges. Photographic systems for track application were designed

with "quick disconnect" features to facilitate and expedite installation on or removal since removal of the systems is necessary before placing the track in its stowed position. The light source, field optics, and camera for each system are mechanically fixed with respect to one another and can be removed (or installed) as a unit without disturbing the optical alignment. Photographic resolution of Track G systems has been measured to be on the order of  $50\ \mu\text{m}$ , whereas resolution of comparable Range G systems is approximately  $175\ \mu\text{m}$ . Depth-of-field for the  $50\text{-}\mu\text{m}$  resolution with the Track G system is approximately 25 mm.

#### 4.1.5.5 Sequential Laser Photography System

An innovative sequential laser photographic system has been designed for Range G and successfully applied in Pilot Range K for the observation of one-on-one encounters between erosive particles and the test model/bow shock. This system, shown schematically in Fig. 4.10, consists essentially of five individual backlight laser photography systems located very close to one another. Images formed by the five individual backlight systems are separated from one another geometrically; i.e., light from one particular laser enters only one particular lens of the multi-lens camera. Specially designed electronics allow the time between laser firings (photographic exposures) to be varied from 100 nsec to  $100\ \mu\text{sec}$ . At the minimum time between frames of 100 nsec, an effective framing rate of  $10^7/\text{sec}$  is achieved.

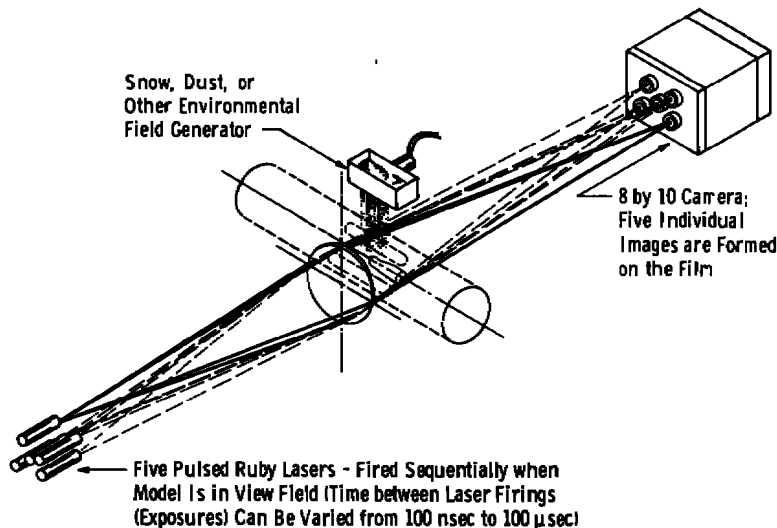
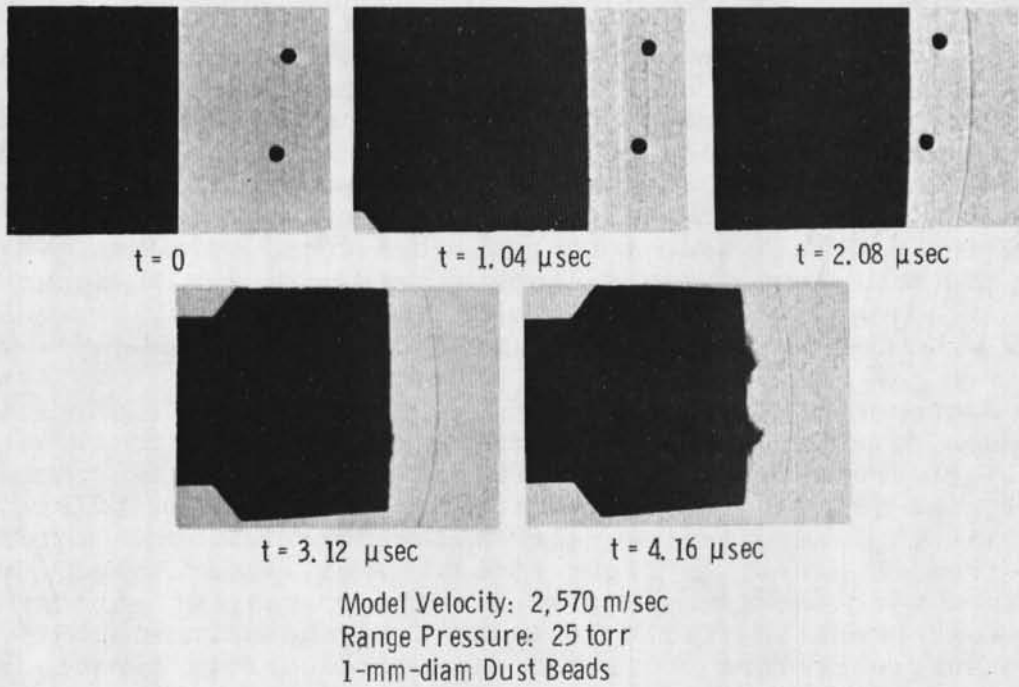
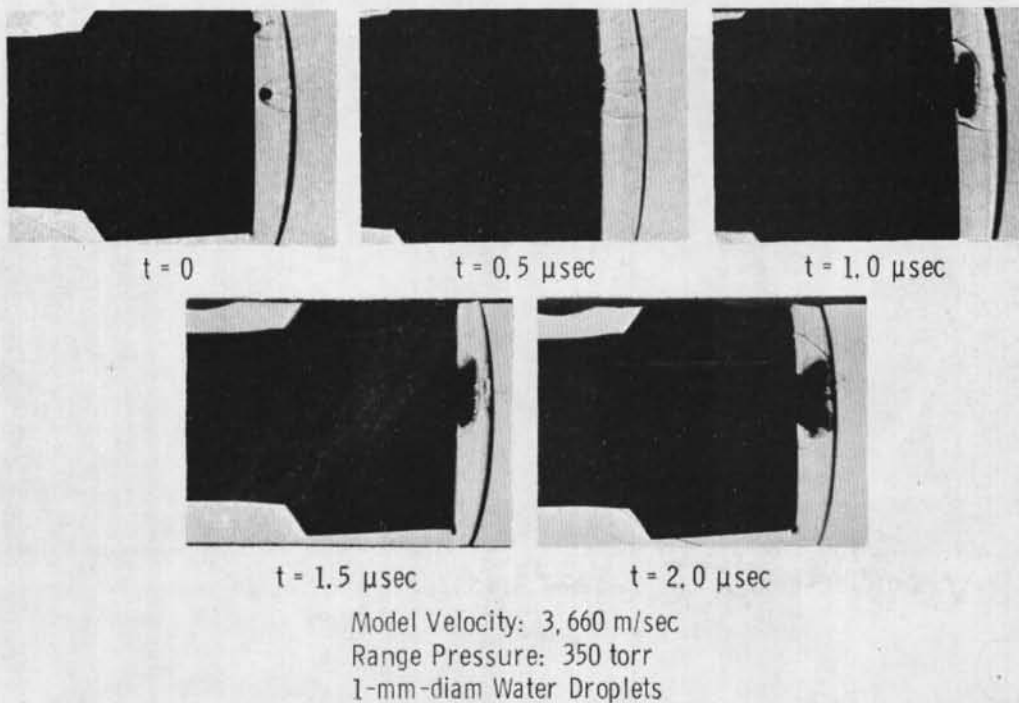


Figure 4.10 Sequential laser photography system.



**Figure 4.11** Sequential laser photographs depicting model and bow shock interactions with water droplets in Range K.

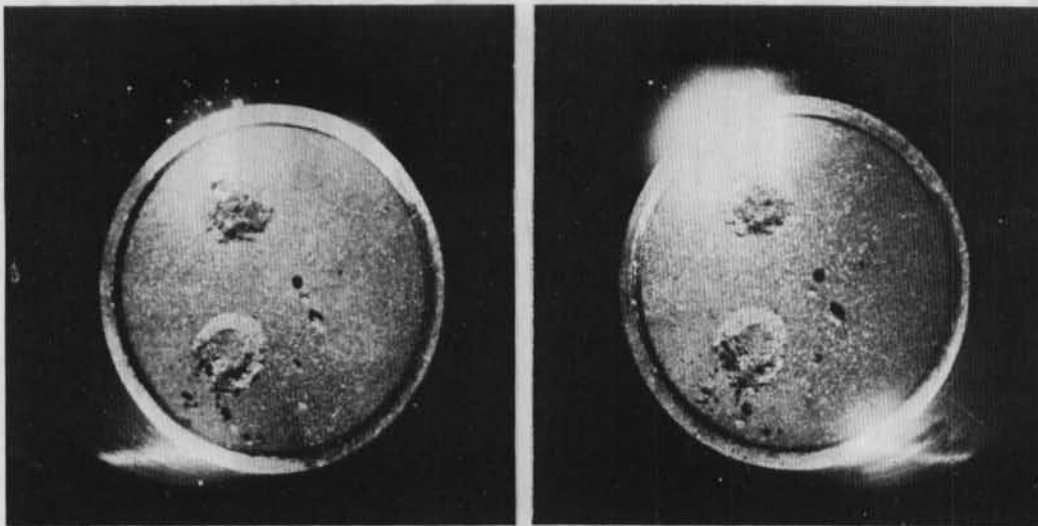


**Figure 4.12** Sequential laser photographs depicting model and bow shock interactions with water droplets in Range K.

Examples of the use of the sequential laser photography system in Range K are shown in Figs. 4.11 and 4.12. In Fig. 4.11, the encounters of first the bow shock and then the model with two 1-mm-diam dust beads are pictured. The dust beads were suspended on very fine silk threads. In Fig. 4.12, 1-mm-diam water droplets in free fall are shown between the model and its bow shock, and then the encounter of one of the water droplets with the model surface is depicted over a period of 2  $\mu$ sec, at a framing rate of  $2 \times 10^6$ /sec.

#### 4.1.5.6 Stereo Laser Photography Systems

A stereo photography technique using Laser illumination has been developed in Range K track as a method for obtaining in-flight crater and surface roughness measurements. The model nose is illuminated by diffuser laser light (pulsed ruby laser), and a stereo pair of cameras views the model nose from the left and right at angles of approximately 20 deg from head-on. An example of a stereo pair of photographs of a test model in flight in Range K is shown in Fig. 4.13. Two discrete craters on the model nose caused by impacts with water droplets are readily discernible, as are surface ejecta resulting from the impacts.



Model Velocity: 2,440 m/sec (8,000 ft/sec)  
Total Angle between Cameras: 40 deg

**Figure 4.13** Stereo photographs of laser-illuminated Range K model.

Stereo photographs such as those shown in Fig. 4.13 require further processing to produce elevation contour maps of the nose region and the desired crater and surface roughness data. The use of stereo plotter devices that provide reconstruction of the three-dimensional image is being investigated for this purpose.

## 4.2 TYPES OF MATERIALS TESTS

Types of materials-related tests which have been conducted in the Range G include (1) ablation, (2) erosion, (3) nosetip transition, (4) heat transfer, and (5) transpiration cooling. The various types of high-temperature materials which have been tested include various grades of bulk graphites; carbon/carbons of several different constructions, carbon phenolics of various kinds, quartz phenolic, and a number of high-temperature tungsten alloys. In all, close to a thousand shots have been fired over a period of eight years in support of materials development programs. For materials testing in the aeroballistic range, discussion of models and types of testing are not clearly separable because of their interdependence. Therefore, types of material testing discussed in this section are illustrated with particular models which have been devised to meet specific requirements.

A typical model configuration for nosetip ablation/erosion/transition testing is shown in Fig. 4.14. The external model components are (1) carrier, (2) carrier heat shield, (3) specimen holder, and (4) test specimen. In this case, a single model is useful for different types of testing because the differences are in the test environment for example, ablation testing requires a high-velocity, high-pressure clear air environment; erosion testing requires the addition of erosive fields; and transition testing requires a relatively low-pressure clear air environment. Obviously, these types of testing may be combined for special purposes; for instance, such as might be required for investigation of effects of erosion-particle induced roughness on clear air ablation or transition.

The 2.5-in. diameter of the track permits hemispherical test specimens of up to 2.25 in. in diameter to be tested. A cut sphere nosetip which has been utilized in free-flight erosion testing offers the advantage of simulating up to 3 in. in nosetip diameter with only a minor flow-field modification. Ballistic coefficients for typical models of this type are expected to range from 50 to 100 lb/ft<sup>2</sup>.

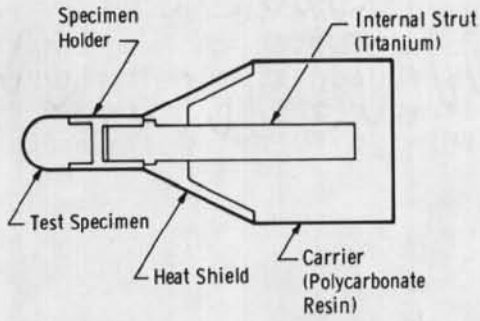
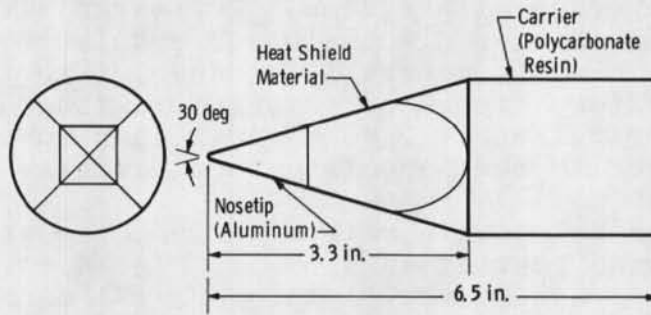
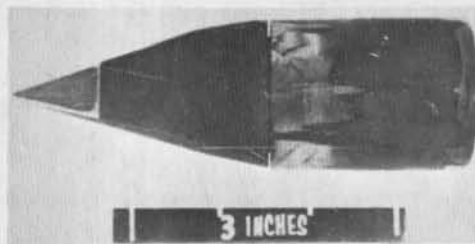


Figure 4.14 Typical nosetip ablation/erosion/transition model.

A heat shield model which has been used in erosion tests is shown in Fig. 4.15. This design features the basic carrier with a four-sided pyramid-type forebody. A portion of each surface is comprised of an ablation test specimen mounted at an oblique angle to the flow to simulate the heat shield case. Specimens cut from four different full-scale heat shields can be evaluated simultaneously.



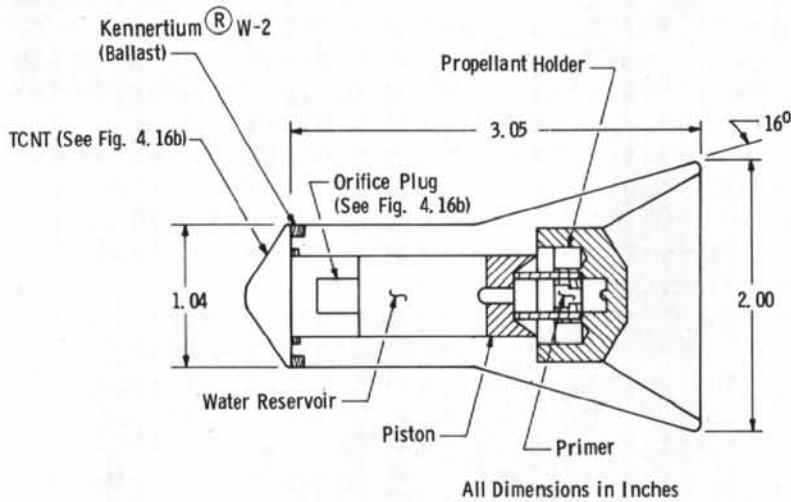
a. Model design



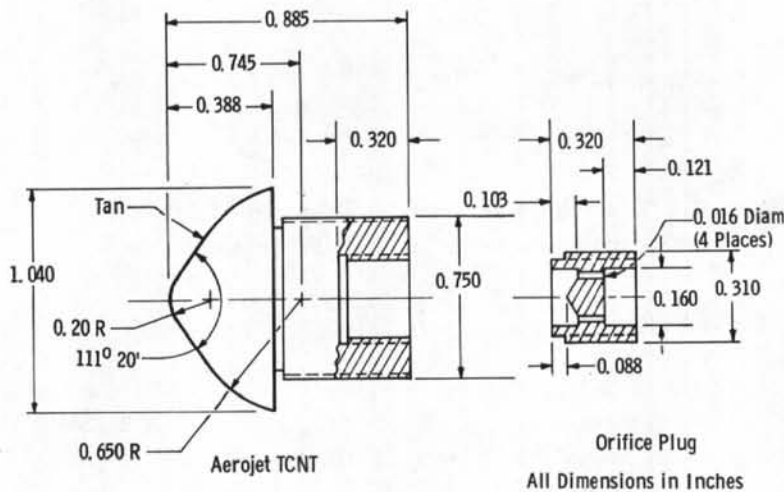
b. Recovered model

Figure 4.15 Heat shield ablation model.

An area of current interest in the field of RV nosetip technology is that of transpiration cooling. Testing requirements in this area have been addressed by development of a model, shown in Fig. 4.16, which incorporates an innovative pressurized fluid reservoir. Nosetips of this type which have been tested were of metallic construction and utilized discrete shots for transpirant injection.



a. Model base



b. Aerojet TCNT and orifice plug  
 Figure 4.16 TCNT model for free-flight testing.

Though not a materials testing capability per se, models have been devised for free-flight testing which melt during flight in such a way that heating rates can be deduced. Such models utilize a thin tapered outer shell fabricated from a high thermal conductivity metal which melts progressively from the trailing edge forward, as shown in Fig. 4.17. The relationship of this type of model to materials testing is that flow phenomenon, which plays a vital role in nosetip performance and which is manifest in the surface heating distribution, may be investigated at full-scale Mach numbers and boundary-layer thicknesses using this technique. Two studies which have been conducted using this capability have addressed effects of surface roughness and entropy layer swallowing on heating. Such a model concept could also be adapted to track testing.

Development of other specialized test models will be initiated in the future as dictated by test requirements.

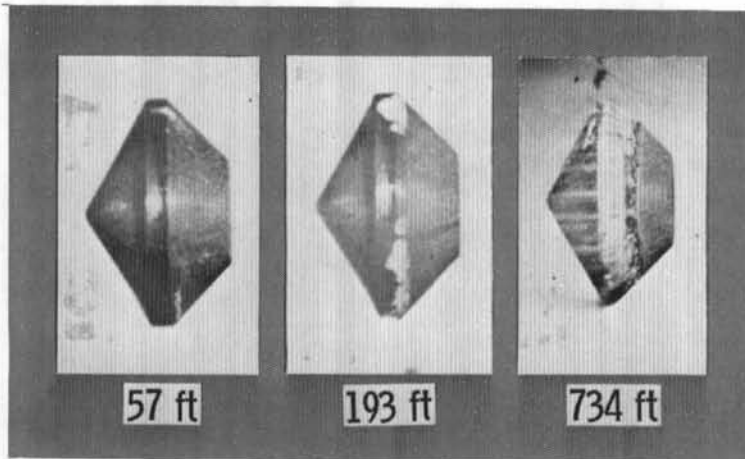


Figure 4.17 Sequence of laser photographs illustrating melt line measurement technique.

### 4.3 FACILITY LIMITATIONS

The facility limitations inherent in aeroballistic range testing are (1) short test time - which can be increased only by lengthening the range, and (2) model size limitation imposed by the diameter of launch tube and track system. Both these limitations have been addressed in feasibility studies of an upgraded facility. Launch tube/track diameters of up to 5 in. and range lengths up to 5,000 ft have been considered. Although such a new facility would be quite costly, the benefits which could be obtained may be justifiable. For example, one

aspect of nosetip testing to which the range is not currently applicable, and which no other ground test facility can address, is that of shape change phenomenology. A factor of five increase in the present range length would result in a significant capability in this regard in that sufficient test time would be available for a nosetip to ablate to a steady-state shape at a given test condition. This particular problem is one of much current interest, and inability to simulate simultaneously levels of Mach number and stagnation pressure and enthalpy encountered during reentry precludes this type of testing in either conventional wind tunnels or arc jets.

Another problem area which is encountered in aeroballistic range testing is frequency of model failure during launch. For types of models which have not been tested extensively, failure rates of up to 50 percent may be experienced. In addition to loss of data, such failures may result in damage to either the launch tube or track, or both. However, models which have been tested extensively frequently exceed 90-percent reliability. In addition, welding techniques have been developed by which launch tubes and track sections may be satisfactorily repaired without disassembly. Other facility problems peculiar to the track installation have not been fully assessed because of the limited operational experience which has been accumulated at this time.

#### 4.4 FUTURE CAPABILITY

The Range G materials testing capability is continually being upgraded for future testing in all areas. Developed models are available to meet currently anticipated test requirements, and improvements in this regard are expected to result in refinements to existing designs. Some activity is expected in the near future in support of asymmetric nosetip technology, and development of appropriate model types will require a fairly radical departure from current design types. Therefore, this development work is expected to be a difficult task.

In the area of erosive field generation, some interest in cirrus ice has been received from test sponsors. A technology base for generation of cirrus ice environments which closely simulates the particles encountered in the natural environment is currently under development. It is anticipated that this capability will be available for application to track testing in the near future.

In the area of instrumentation, the materials testing capability is being upgraded by development of new pyrometry systems with a lower temperature threshold. This capability is particularly important in boundary-layer transition tests where two of the important parameters are surface roughness and wall temperature. Nosetips for such tests are typically preablated in a high-enthalpy arc jet to simulate the surface condition produced during the high-altitude laminar flow portion of a reentry trajectory. It is important in testing this preablated ballistic range model that transition data be obtained before the known surface roughness is altered by subsequent ablation processes. This requires that such data be obtained as early in flight as is practical - which is equivalent to saying at as low a temperature as is possible. In addition, it is now known that, in the presence of surface roughnesses characteristic of graphitic materials, wall temperature has a stabilizing effect on the boundary layer. To fully characterize this phenomenon requires measurements over as wide a temperature range as can be achieved.

Other areas where new or additional capability may be profitably developed will be pursued as future trends as materials testing requirements emerge.

#### 4.5 CONCLUDING REMARKS

Hypervelocity Range G incorporates state-of-the-art hyperballistic range technology. It retains the range capability of simultaneously duplicating velocity, pressure, and enthalpy corresponding to a point on the reentry trajectory. In addition, its fixed trajectory capability permits improved characterization of the encountered particulates and high resolution in-flight photography. Model recovery is a characteristic of great significance since posttest material analyses hold the promise of providing insight into ablation/erosion mechanisms.

These facility characteristics of (1) real life test conditions, plus (2) realistic and well-characterized erosive fields, plus (3) accurate in-flight measurements, plus (4) posttest model examination represent a significant ground test simulation capability. Hypervelocity Range/Track G provides cost effective solutions to numerous present and future problems in the reentry physics field.

**5.0 HIGH-ENTHALPY ABLATION TEST (HEAT) FACILITY**

**5.1 Types of Testing . . . . . 78**  
**5.2 Facility Description . . . . . 79**  
**5.3 Facility Performance and Calibrations . . 88**  
**5.4 Future Capability . . . . . 96**



## 5.0 HIGH-ENTHALPY ABLATION TEST (HEAT) FACILITY

Reentry vehicles for ballistic missile systems commonly employ a covering of ablative material for heat protection. The nosetip of the vehicle is normally a spherically blunted cone in shape and is subjected to a much higher heating rate than the rest of the vehicle. The heating rate on nosetips increases with increasing reentry velocity and velocity at impact. This is the natural direction of performance evolution of ballistic missiles. There is a continuous development effort to provide better materials for nosetips. Ground test facilities are required to evaluate the performance of these materials in a timely and economical manner. Unfortunately, the performance of missiles has continuously outpaced the performance of the test facilities. No existing facility can duplicate simultaneously the enthalpy and pressure conditions encountered in flight by current reentry vehicles, and this deficiency becomes even greater for the vehicles under development for the future.

Arc-heated test facilities were first operated at the Arnold Engineering Development Center (AEDC) in 1962. The purpose of these facilities was to investigate nozzle throat cooling techniques applicable to large arc facilities. The original arc heater was an N4000 obtained from the Linde Company. The operating conditions of this heater were 37-atm chamber pressure and an energy balance enthalpy of 2,700 Btu/lb.

In mid-1966, the heater was combined with a multiple-position model injection system and data recording equipment to permit its use for ablation testing of RV nosetips and heat shields. Continuous studies and investigations have been made at AEDC to improve the arc-heater performance, and thereby the testing capabilities of the ablation facility. This improved arc heater has been moved to the second test leg of the High-Enthalpy Ablation Test (HEAT) Facility, and its performance has been upgraded to deliver more power to the airflow (Fig. 5.1). The first test leg of the HEAT Facility uses a large high-powered segmented arc heater as the heat and pressure source, thereby allowing testing in large test flows at very high enthalpies.

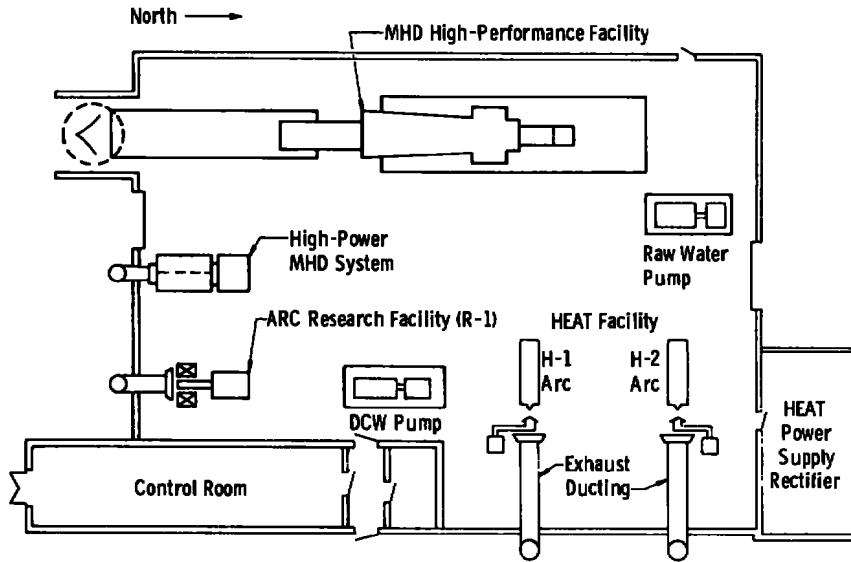


Figure 5.1 Layout of the AEDC high-temperature laboratory.

## 5.1 TYPES OF TESTING

A facility with the capability of HEAT operating on pure air can do many types of tests. Also, the addition of the second test leg (H-2) to the high-performance capability of the primary test leg (H-1) adds versatility that no other facility has. The model injection systems are similar, and the models are designed so that one can operate on either test leg.

The more standard tests that can be accomplished in these facilities are the ablation tests which require shape change, recession rate, and reentry simulation by model ramping. The facilities also are very amenable to transpiration-cooled nosetip testing. Either of the two test legs of HEAT can be equipped with a specially designed particle injection system and nozzle so that simultaneous ablation and erosion can be applied to the test articles. This system has been tested and is operational. A special test technique is available where models are exposed to ablation for a short time, thereby preconditioning nosetips that are later fired in the AEDC hypervelocity gun range.

Other types of testing are available but require three to four months lead time to fabricate. Some of these are: real time variation of model angle of attack during ablation, real time variation of model spin rate, sidewall testing of

either curved or flat walls, and large model testing in a coaxial shrouded flow of hot core flow and cold surrounding airflow. In the not too distant future, the facility will be upgraded to "fly" a reentry pressure-heat transfer profile in real time. The arc heaters will be continually upgraded in performance and versatility.

## 5.2 FACILITY DESCRIPTION

The HEAT Facility has two test legs. The main test leg will be used for ablation and combined ablation/erosion testing. The second will be used primarily for facility-oriented research and development. Both test legs share the same basic utilities including the d-c power supply capable of 40- to 60-MW output for several minutes. The air system can provide air at pressures up to 270 atm and flow rates up to 90 lbm/sec. The main test leg (H-1) utilizes a segmented arc heater scaled from the AEDC prototype segmented arc heater. This prototype heater has demonstrated that bulk enthalpy of the effluent stream will vary from approximately 8,500 Btu/lbm at a heater pressure of 25 atm to 4,000 Btu/lbm at 150 atm. The enthalpy profiles at the nozzle exit will be essentially flat in contrast to the peaked profiles characteristic of the Huels-type arc heater. The second test leg (H-2) is equipped with a nominal 12-MW Linde heater (Huels arc) for facility-oriented research, as a test bed for advanced arc-heater designs, and ablation tests. An aerial photograph of the HEAT Complex is shown in Fig. 5.2, and a facility schematic is shown in Fig. 5.3. Figure 5.4 is a photograph of H-1 showing relative location of components.

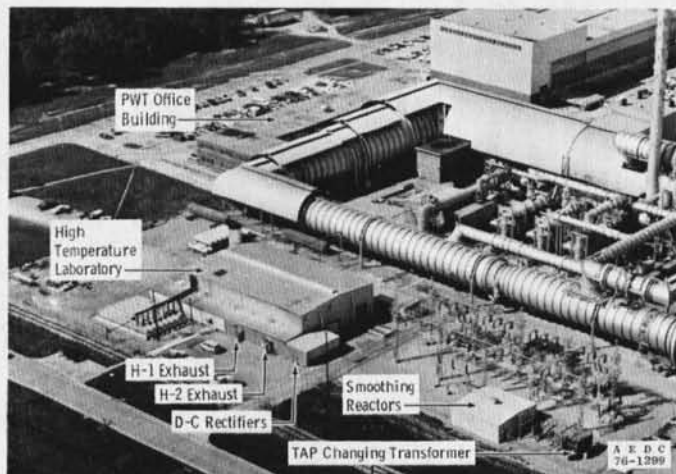


Figure 5.2 Aerial photograph of HEAT Facility.

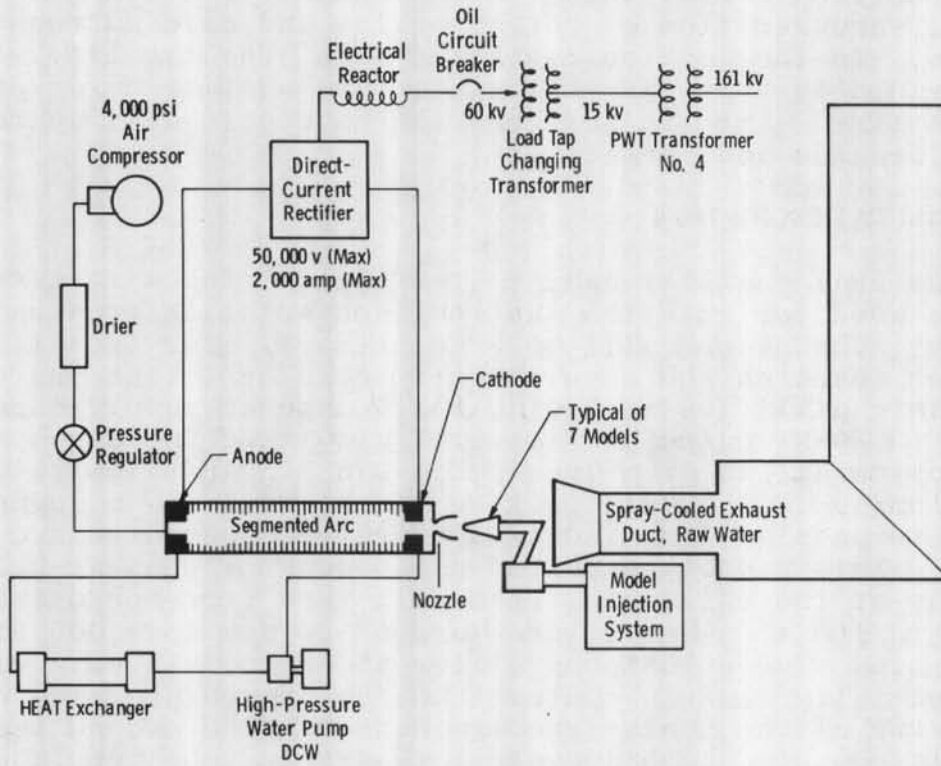


Figure 5.3 Schematic of HEAT Facility.

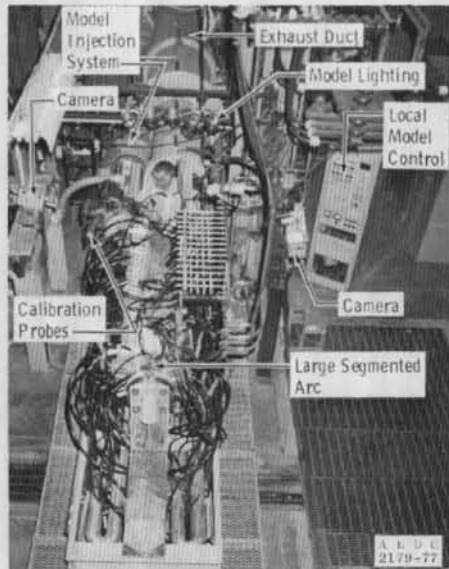


Figure 5.4 Photograph of HEAT H-1 leg.

### 5.2.1 Power Supply

The d-c power supply consists of a three-phase load-tap-changing transformer feeding a three-phase, full-wave bridge rectifier. The bridge rectifier consists of over 400 diodes series-paralleled to give a maximum open-circuit voltage of 50 kv. Maximum rated operating current is 2,000 amp. The maximum design power of the system is 60 MW. The power supply has a voltage tower for voltage measurements and inductive current measuring systems.

### 5.2.2 Water and Air Systems

The facility components are cooled by a closed-loop demineralized water system which supplies water at pressures up to 1,500 psi and flows of 1,300 gpm. The water is cooled by passing it through a tubed heat exchanger cooled by low-pressure lake water. Water for the arc heater passes through a distribution manifold to each component to be cooled.

The air system is connected to the VKF/AEDC main high-pressure air compressor and storage tanks with 8- and 10-in. piping. Air is stored at pressures up to 3,800 psi and can be flowed at rates up to 90 lb/sec at the facility. Normal airflow rates for the arc heaters are 0.5 to 4 lb/sec controlled by regulation and control valves. Airflow rate is continuously measured by a subsonic venturi and can be measured by calibrated choked venturis if necessary.

### 5.2.3 HEAT H-1 Arc Heater

The primary test leg of the HEAT Facility uses a large segmented arc heater as the wind tunnel (ablation) driver. This complex arc heater gives a performance 50 percent higher than conventional Huels arc heaters of equal power. A sketch of the arc heater is shown in Fig. 5.5 and a photograph in Fig. 5.6. The electrodes are fixed at each end of the arc heater separated by about 200 electrically floating segments. The arc heater is usually operated at voltages in excess of 10,000 v and currents in excess of 1,000 amp. Heater stagnation pressures of 150 atm can be obtained at very high stagnation enthalpies.

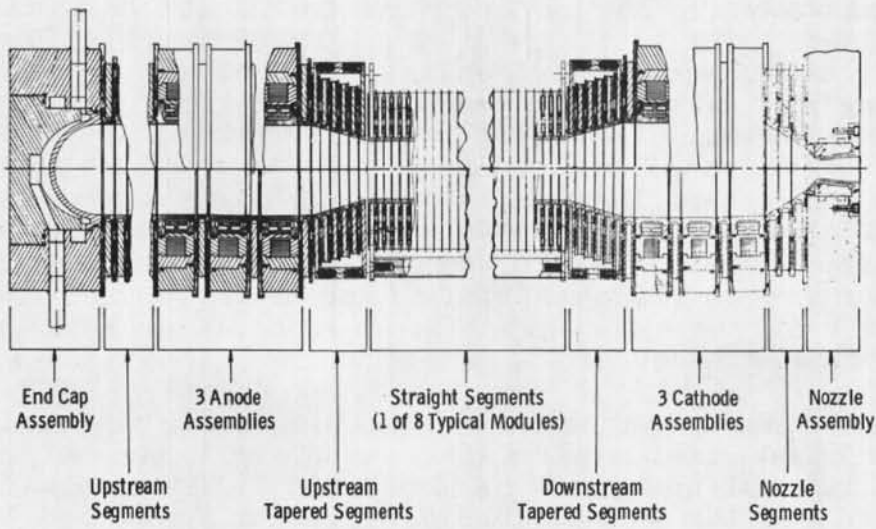


Figure 5.5 Sketch of the HEAT (H-1) segmented arc heater.

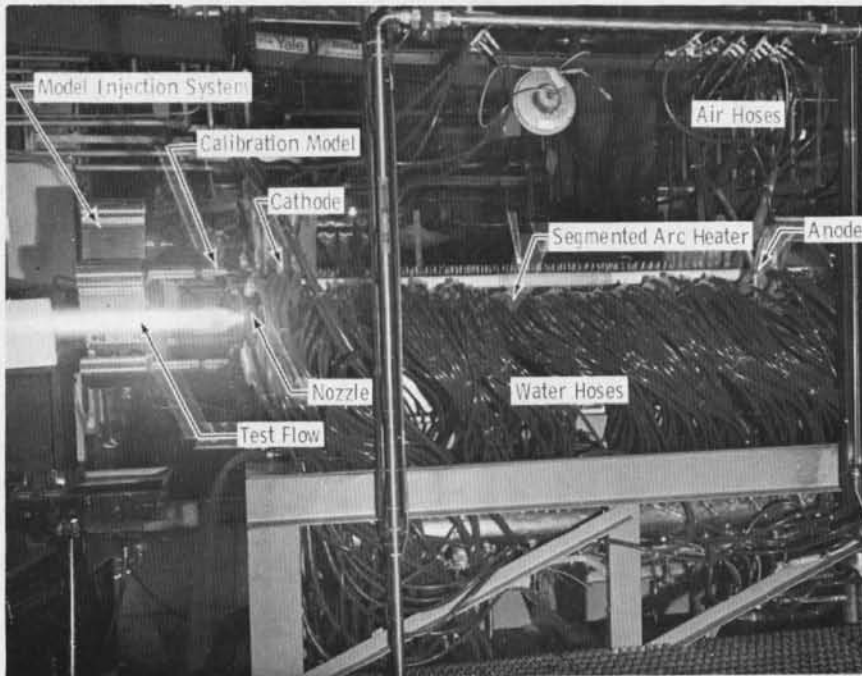


Figure 5.6 Photograph of HEAT (H-1) segmented arc heater.

An air mixing chamber is available to mix cold air with the arc-heated air if the user requires lower enthalpies and higher Reynolds numbers.

#### 5.2.4 HEAT H-2 Arc Heater

The second test leg of HEAT uses a conventional Huels-type of arc heater with cooled copper tubes as electrodes. These tandem electrodes allow the arc to seek its own length, hence some low-frequency fluctuations occur in the test flow. This heater is the same device previously used on the AEDC 5-MW Arc Heater Test Unit except it has been optimized for 15 MW of power input. It is capable of pressures of 180 atm with small nozzles and 130 atm with large nozzles. A sketch of the arc heater is shown in Fig. 5.7, and a photograph is shown in Fig. 5.8.

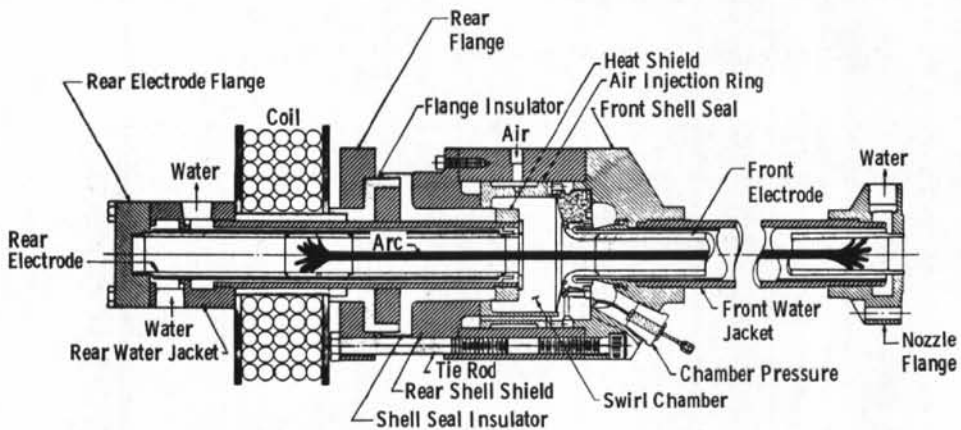


Figure 5.7 Sketch of HEAT (H-2) conventional arc heater.

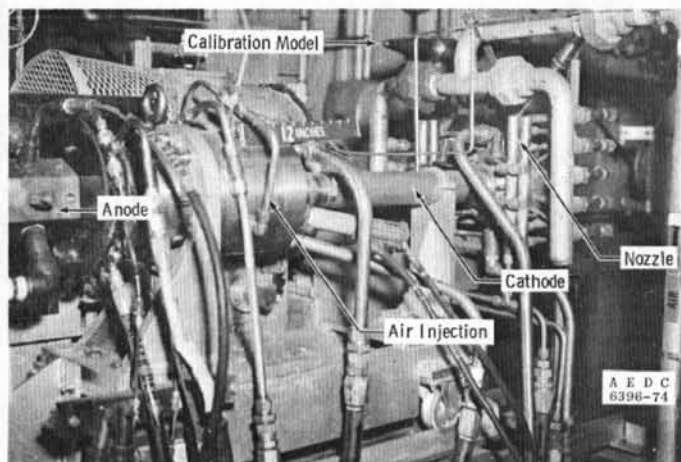


Figure 5.8 Photograph of H-2 arc heater.

### 5.2.5 Rotary Model Injection System

Each leg of the facility is equipped with a multiple-strut, remotely controlled rotary model injection system (Fig. 5.9). Normally, from one to seven models are positioned sequentially on the test stream centerline for pre-set dwell times from 0.5 sec to 5.0 min. The arc-heater conditions remain essentially constant for all models. Nearly constant injection velocity is provided during the index cycle between normal stop positions, and, by using 45-deg offset arms, transient calibration probes can be swept through the test stream at constant velocity. In this mode, sweep speeds from approximately 20 to 60 in./sec can be attained.

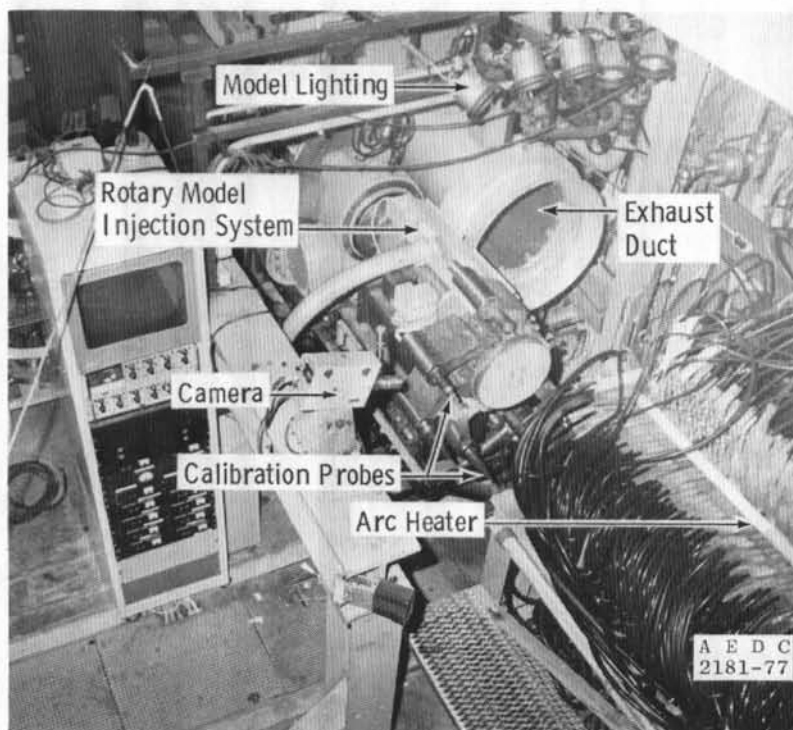


Figure 5.9 Rotary model injection system of HEAT H-1.

The model injection/support system can be operated with the carriage in a fixed position and with the support struts rotating in a fixed plane. In this case, the axial position of each model with respect to the nozzle exit is set by means of a frictional clamp between the model sting and the support strut. Model mounting interface and maximum outline dimensions are shown in Fig. 5.10. The user can either supply the specimen or entire holder.

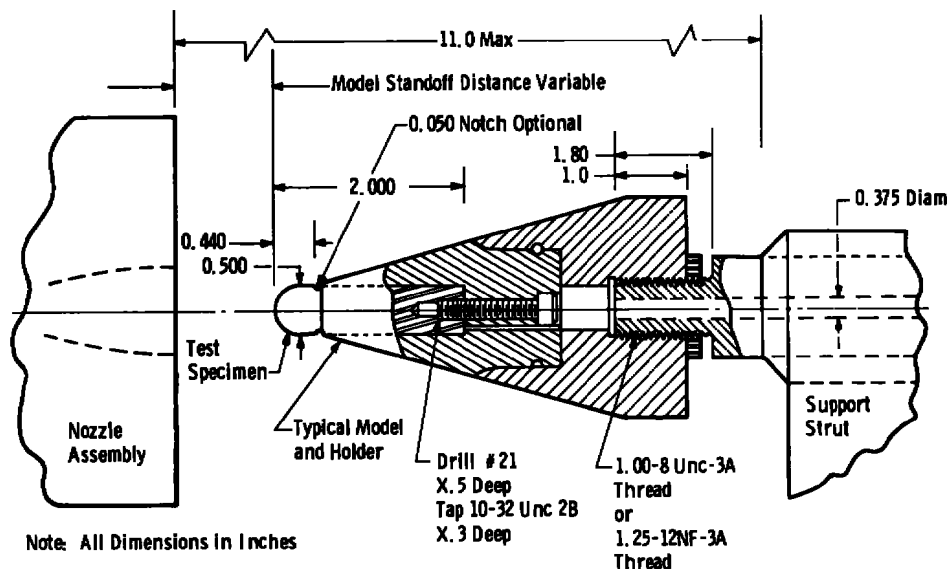


Figure 5.10 HEAT Facility model mounting interface.

The uniform flow regions in high-pressure arc facilities are limited in size because of power limitations, and the recession of an ablating model frequently moves the model out of the uniform flow region. To counter this problem, the entire model injection system is driven axially with a servocontrolled drive system to advance the model upstream at (essentially) the same rate at which it ablates downstream, thus holding the model front surface in the uniform flow field.

A schematic of the model advance system in relation to the H-2 test unit and a block diagram of the laser control system are presented in Fig. 5.11. The test unit model advance system includes a laser beam propagated through the centerline of the plasma stream and detected by a photocell sensor. When the laser beam is blocked by the model front surface to a preset beam percentage null point, a command signal is sent to the servovalve and hydraulic cylinder to stop forward movement. When the model recedes approximately 0.002 in. and the laser beam is partially uncovered, the photocell signals the axial drive system to move forward to the null point. The model front surface is thereby kept at virtually a fixed position with respect to a predetermined test station.

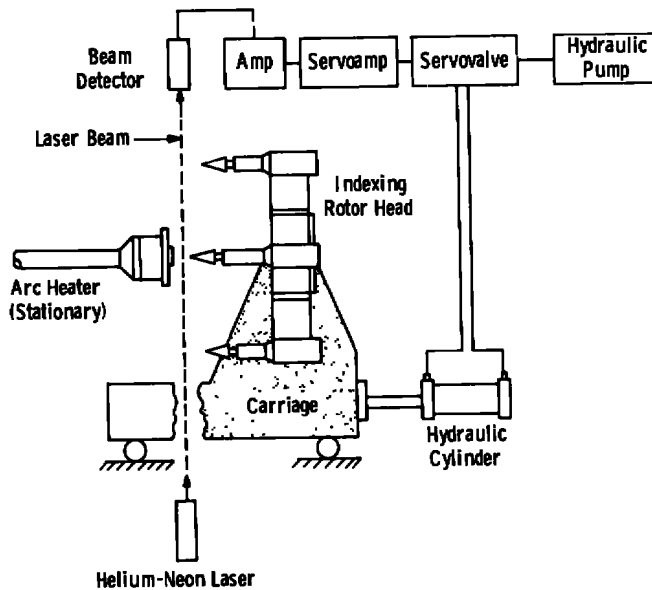


Figure 5.11 Laser-controlled model advance system.

This same axial drive system can be used to ramp the model forward in the flow field and simulate reentry. This system is useful in determining the onset of transition as the pressure is increasing. Ramp rates of about 0.5 in./sec are easily accomplished over a 5-in. length.

Control of the entire model injection system is performed using a Digital Equipment Company 1430 controller. This controller computer allows preprogramming of dwell times, camera sequences, and ramp rates.

## 5.2.6 Instrumentation and Data Reduction

### 5.2.6.1 Test Unit Instrumentation

The arc-heater performance and nozzle cooling loads are determined from the recorded data and presented to the operator on-line on a CRT. The water temperature rise through each component to be cooled is measured using thermocouples immersed in the cooling water. All flows are measured using standard turbine flowmeters. Data are amplified before entering the data system. A wide variety of strain-gage and piezoelectric crystal pressure transducers are available for use in the facility.

### 5.2.6.2 Data Acquisition and Recording

The two test legs share a common computer-based acquisition system (Fig. 5.12) which is built around a Digital Equipment Company, DEC 11/45 computer. In the normal or low-speed data mode, 192 channels are available for facility instrumentation. Up to 64 high-speed channels are available for the requirements of high-response probes. Typical sampling time for these data is 200  $\mu$ sec. All facility data, such as heater pressures, bulk enthalpy, voltages, current, and airflow rates, are continually calculated and presented on a CRT for the user and facility operator to monitor. Any of these channels and/or the high-speed channels can be recorded on a high-speed direct-reading oscillograph. All low-speed data are processed immediately after the run and printed using a high-speed electrostatic printer. All high-speed data are processed on the AEDC IBM 370/165 base computer.

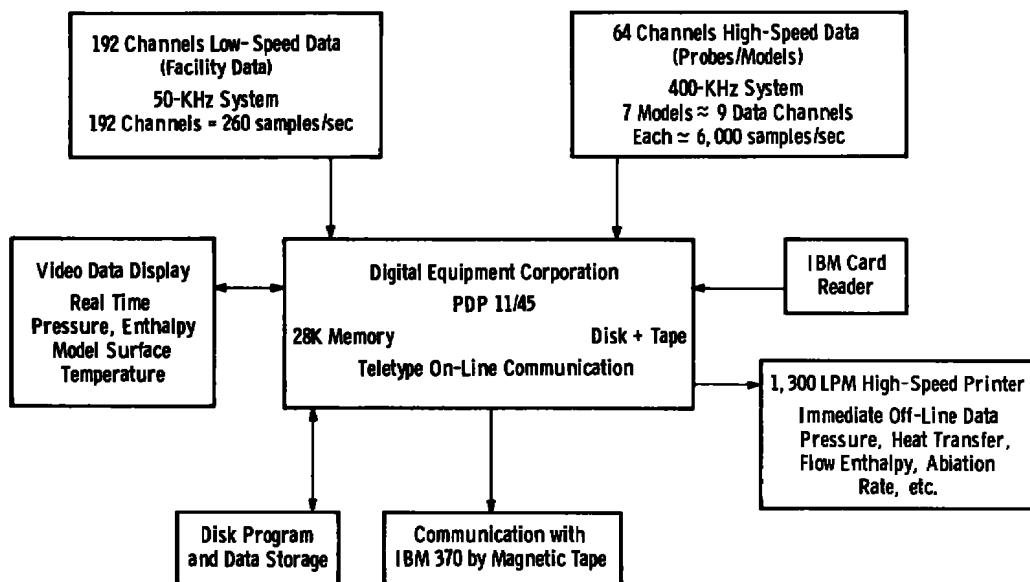


Figure 5.12 HEAT Facility computer-based data acquisition system.

### 5.2.6.3 Optical Instrumentation

Each of the two cells has three high-speed cameras available for model data recovery. Supplemental cameras can be added as required. One of the cameras has the capability to record 10 digits of data on the film in the margin. Typically, the test number and run number plus the computer time will

be input to the camera. Up to six cameras can be prepared by the model injection system controller to operate at a predetermined time. A table of photographic equipment is presented in Table 5.1. High-speed color motion-picture film is processed at AEDC every morning for viewing by the user. Copies can be made at AEDC within two days.

**Table 5.1 Available Photographic Equipment**

Camera Type	Negative Size	Framing Rate, Frames/sec	Film, Frames/ft	Magazine Capacity, ft	Number Available
Hycam	16 mm	6 to 10,000	40	400	3
Locam	16 mm	6 to 500	40	400	4
Locam*	16 mm	6 to 500	40	400	1
Veriton	70 mm	1	3.4	100	6
Cine Special	16	6 to 60	40	200	3
Millikan	16	6 to 100	40	400	1
Speedgraphic	4 x 5 in.	Single	---	---	1
Panasonic**	Television	30	71	2,150	3

\*Digital Data on Each Frame.

\*\*Slow Motion/Stop Split Screen.

Television cameras monitor the models and facility during testing for rapid determination of model survivability and facility safety. These images are recorded on a video tape recorder and can be played back using a multi-speed playback system with stop action.

#### 5.2.6.4 Data Reduction

All data are recorded on magnetic tape and reduced to engineering units immediately after the test using the facility minicomputer. Data obtained from flow probes are reduced and plotted using the AEDC IBM 370/165 computer with overnight service. Data such as heat flux, flow pressures, enthalpies, surface temperatures, TCNT flow rates, etc., can be plotted against time and/or probe position.

Feedback from the model injection system axial position sensor can be tabulated and/or plotted against time and recession rate calculated.

### 5.3 FACILITY PERFORMANCE AND CALIBRATIONS

Both test legs of the HEAT Facility have the capability to provide high pressures on the test specimen as well as

being able to generate a severe erosive environment when desired. Either leg can be run an average of once a day depending on the complexity of the test specimens. Normal run times are less than 2 min, depending on the user requirements and severity of the test conditions. The flow contamination residual (particles in the flow for a clear air test) is greater on the H-2 facility because of the nature of the more standard arc heater. Flow contamination from the HEAT segmented arc (H-1) is almost nonexistent. The facility normal firing sequence does not allow for any cold airflow just prior to the arc firing. Cold flow can be made any time up to 15 min prior to arc firing. There are no provisions for direct visual observations of the test. All views of the flows are made with closed-circuit television systems and high-speed cameras. Both arc heaters could operate on gases other than air, but the capability currently does not exist at the facility. On rare occasions during extremely cold weather, the facility may be curtailed from operating during peak electrical use times of the day. This rarely happens and does not preclude operation at a different time of the same day.

The AEDC has developed a long list of diagnostic tools for the calibration of the ablation and ablation/erosion facilities. These probes and diagnostics are available to the user for any test that involves this facility. A list of these tools is presented in Table 5.2, and the list will grow through the ongoing research effort at the AEDC.

**Table 5.2 Diagnostic Tools Available to User  
to Check Facility Calibration**

Diagnostic	Direct Measurement	Range	Nose Radius, in.	Setup Lead Time, Days
Impact Pressure Probe	Flow Pressure Profile	5 to 100 atm	0.040	0.5
Heat-Transfer Probe	Stagnation Point Heat Transfer	1,000 to 20,000 Btu/ft <sup>2</sup> -sec	0.250	0.5
Transient Enthalpy Probe	Total Enthalpy	500 to 6,000 Btu/lbm	0.125	1.0
Pressure Distribution Probe	7-Channel Pressure Distribution Model	1 to 100 atm	0.250	1.0
Pressure Distribution Probe	7-Channel Pressure Distribution Model	1 to 100 atm	0.500	1.0
Heat-Transfer Distribution Probe	7-Channel Heat-Transfer Distribution Model	200 to 20,000 Btu/ft <sup>2</sup> -sec	0.250	1.0
Heat-Transfer Distribution Probe	7-Channel Heat-Transfer Distribution Model	200 to 20,000 Btu/ft <sup>2</sup> -sec	0.500	1.0
Laser Velocimeter	Erosion Particle Velocity	1,000 to 8,000 ft/sec	---	5.0
Pyrometer	Ablating Surface Temperature	1,500 to 6,500°F	---	1.0

### 5.3.1 HEAT H-1 Leg

The facility has at present (Fall 1977) undergone a partial calibration at high arc-heater pressures. All performance information that will be presented here is calculated except where experimental calibrations are noted. Table 5.3 shows a list of nozzles including size, pressure, enthalpy, and Mach number available for use in this test leg. The  $M = 2$  (0.85 in.) and the  $M = 2.65$  (1.40 in.) nozzles have undergone primary calibration and are expected to be typical of all nozzles.

**Table 5.3 HEAT H-1 Available Nozzles**

Throat Diameter, in.	Exit Diameter, in.	Exit Mach	Model Pressure Arc Pressure	Maximum Arc Pressure-Enthalpy (Flow Enthalpy)*	Erosion Particle Velocity, ft/sec
0.625	0.770	1.80	0.800	120 to 3,100(7,000)	5,400(140 $\mu$ ), 6,800(75 $\mu$ )
0.625	0.850	2.00	0.700	120 to 3,100(7,000)	
0.625	0.850	1.80	0.773	120 to 3,100(7,000)	
0.625	1.120	2.50	0.461	120 to 3,100(7,000)	
0.625	1.600	3.00	0.282	120 to 3,100(7,000)	
0.700	1.400	2.65	0.400	120 to 3,100(7,000)	5,800(140 $\mu$ ), 7,000(75 $\mu$ )
0.700	1.400	2.52	0.416	120 to 3,100(7,000)	
0.900	1.350	1.80**	0.800	120 to 2,000	

\*Inferred from Pressure and Heat-Transfer Measurements Using Laminar Heating Relationships

\*\*Flared

Figure 5.13 shows typical pressure profiles and heat-transfer profiles of the flow from the Mach 2 nozzle. Note that these profiles are replots of computer plotted data with no smoothing applied and still show no significant peaking even at high pressure. The profiles at the 70-atm case are typical of 20 profiles taken at this condition. These data are for nominal half-power conditions of the facility and should be considered lower limits of heat-transfer rates that can be obtained without mixing cold air with the arc flow. The heater has a mixer available which allows cold air to be mixed with the heater air, resulting in a lower enthalpy, higher Reynolds number flow.

Sym	$P_0$ , atm	$H_{0g}$ , Btu/lbm	$H_0$ (Effective), Btu/lbm
○	71	3,350	6,600
□	115	3,122	6,400

Based on Measured Heat-Transfer, Pressure, and Laminar Fay-Riddell Equations

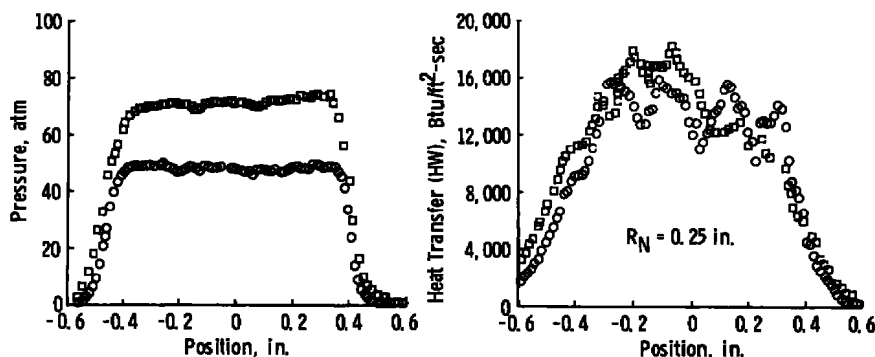


Figure 5.13 Typical calibration results for HEAT (H-1) Facility.

### 5.3.2 HEAT H-2 Leg

This test leg of the HEAT Facility has the same capability of the AEDC 5-MW Facility plus the ability of using all the nozzles that H-1 uses. The main difference is that the enthalpy of H-2 is lower than H-1 because of the difference in the arc heaters. Table 5.4 shows a list of nozzles including size, pressure, enthalpy, and Mach number available for use in this test leg.

Table 5.4 HEAT H-2 Available Nozzles

Throat Diameter, in.	Exit Diameter, in.	Exit Mach	Model Pressure Arc Pressure	Maximum Arc Pressure-Enthalpy (Flow Enthalpy)*	Erosion Particle Velocity, ft/sec
0.375	0.428	1.60	0.889	160 to 2,400(4,000)	5,100(140 $\mu$ ), 6,000(75 $\mu$ )
0.375	0.465	1.80	0.880	160 to 2,400(4,000)	
0.375	0.518	2.00	0.700	160 to 2,400(4,000)	
0.375	0.617	2.30	0.551	160 to 2,400(4,000)	
0.500	0.570	1.60	0.889	160 to 2,600(4,400)	
0.625	0.770	1.80	0.800	120 to 2,300(3,900)	
0.625	0.850	2.00	0.700	120 to 2,300(3,900)	
0.625	0.850	1.80	0.773	120 to 2,300(3,900)	
0.625	1.120	2.50	0.461	120 to 2,300(3,900)	
0.625	1.600	3.00	0.282	120 to 2,300(3,900)	
0.700	1.400	2.65	0.400	120 to 2,300(3,900)	5,350(140 $\mu$ ), 6,300(75 $\mu$ )
0.700	1.400	2.52	0.416	120 to 2,300(3,900)	
0.750	0.800	1.30**	0.978	100 to 2,300(3,900)	
0.750	1.800	3.20	0.230	100 to 2,300(3,900)	

\* Inferred from Pressure and Heat-Transfer Measurements Using Laminar Heating Relationships

\*\*Conical Nozzle

Many tests run in this facility use very large wedge or hemisphere models which require testing in the flow plume. Figure 5.14 is a descriptive sketch of the flow showing the plume size, flow angularity in the plume, and Mach number distribution for an  $M = 2$  nozzle using a 0.375-in. throat. Figures 5.15 and 5.16 show the distribution of impact pressure and stagnation point heat transfer in the expanded plume.

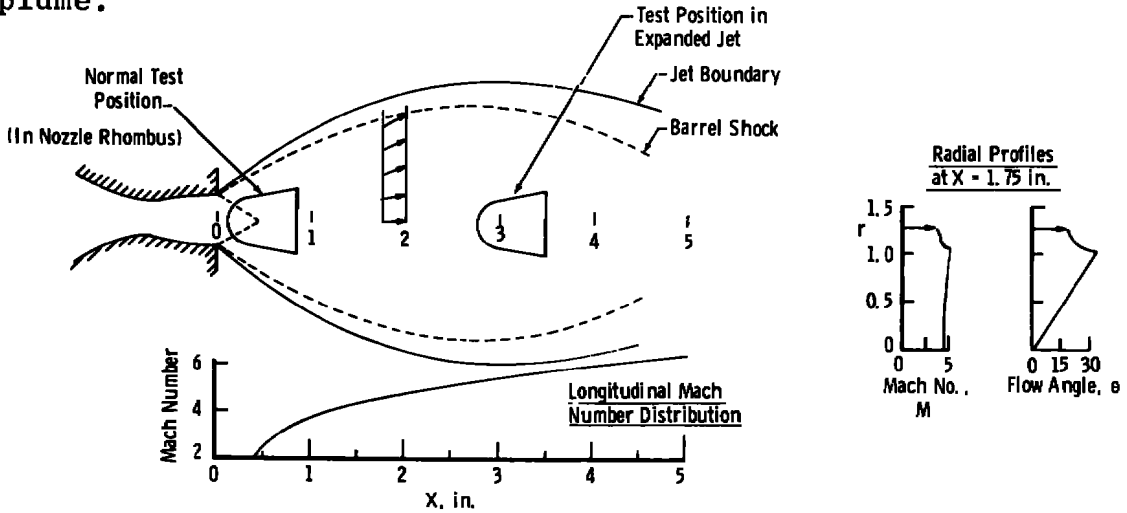


Figure 5.14 Descriptive sketch of plume from HEAT (H-2).

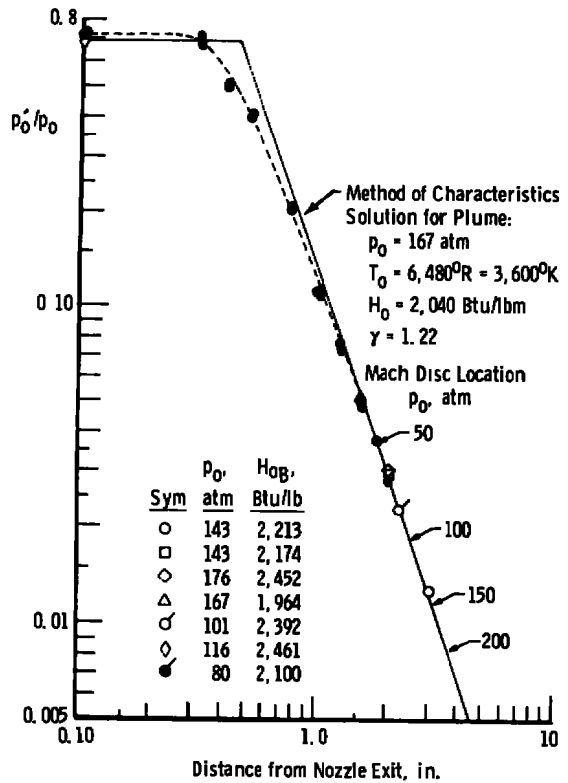


Figure 5.15 Impact pressure distribution in plume from  $M = 2$  nozzle.

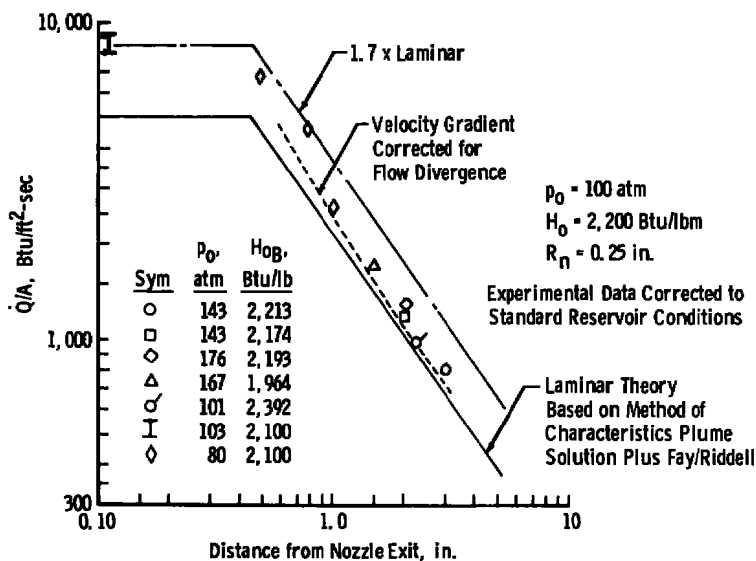


Figure 5.16 Stagnation point heat transfer in plume from  $M = 2$  nozzle.

### 5.3.3 Ablation/Erosion Capability

Both legs of the HEAT Facility have the capability of graphite particle injection and acceleration for ablation/erosion testing. This unique capability is accomplished by injecting various size graphite particles in a chamber just upstream of the nozzle and allowing them to drag-accelerate to hypersonic velocities. There are two systems available for particle injection (Fig. 5.17), each with a different range of particle flow rate. The particle/binder rod system provides positive control of the rate of low flows up to 6 gm/sec. The other system provides particle flow rates by dust injection of flow rates up to 60 gm/sec. There are two nozzles currently available for particle acceleration. The smaller one is a nominal  $M = 1.8$  nozzle with a 0.85-in. exit diameter. This nozzle has the advantage of high impact pressures at fairly high particle velocities. The maximum pressure and calculated velocities are shown in Fig. 5.18. The second nozzle is larger but at the sacrifice of model pressure. This nominal  $M = 2.52$  nozzle has an exit diameter of 1.4 in. The calculated particle velocities are shown in Fig. 5.19. Kinetic energy fluxes of the particles have been calculated for both nozzles for a range of particle velocities and are shown in Fig. 5.20. Energy fluxes in excess of 3 kw/cm<sup>2</sup> have been measured in the facility.

Although all the velocities shown in the figures were calculated by drag acceleration, AEDC has had considerable experience in particle velocity measurement in similar facilities. Figure 5.21 shows a comparison of measured versus

calculated velocity for various systems using three different measurement techniques. A program is planned for verification of the calculated velocities in the HEAT Facility by direct measurements, using both high-speed fast shutter photography and a laser velocimeter. There is no method available to measure particle size in the flow field, but the important parameters, such as kinetic energy flux, can be measured.

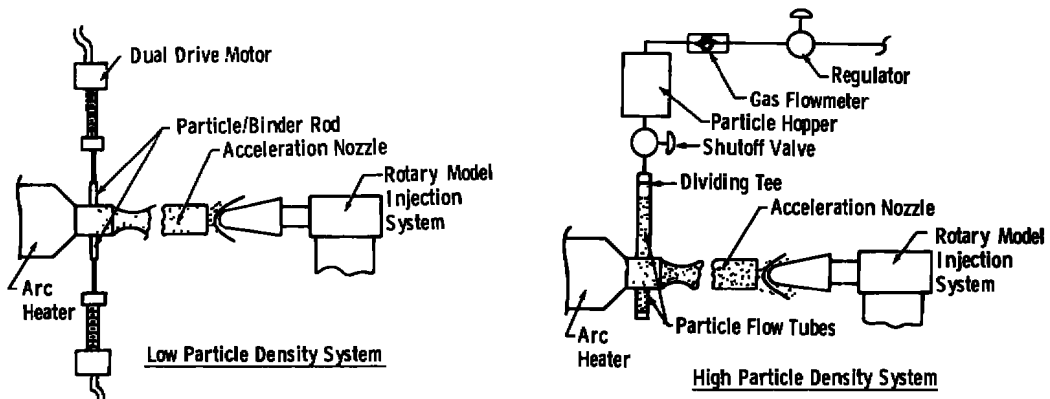


Figure 5.17 Particle injection systems.

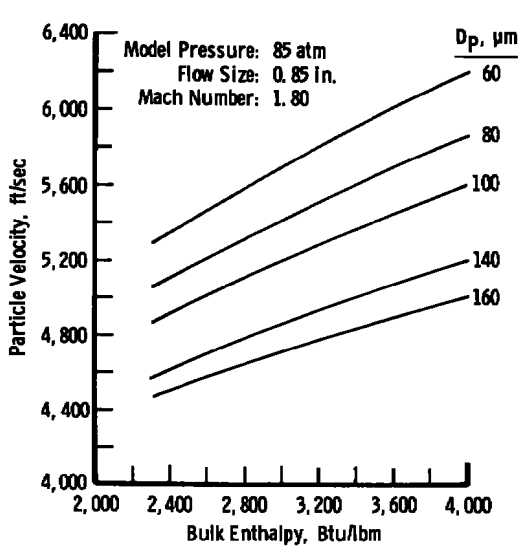


Figure 5.18 Particle velocity versus bulk enthalpy for arc-heater pressure of 120 atm and the M = 1.80 nozzle.

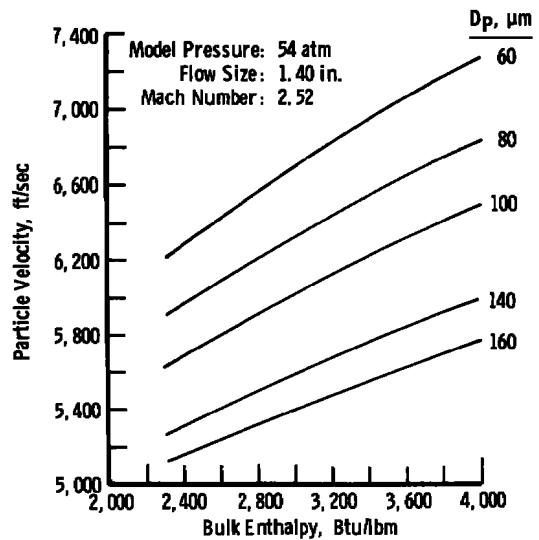
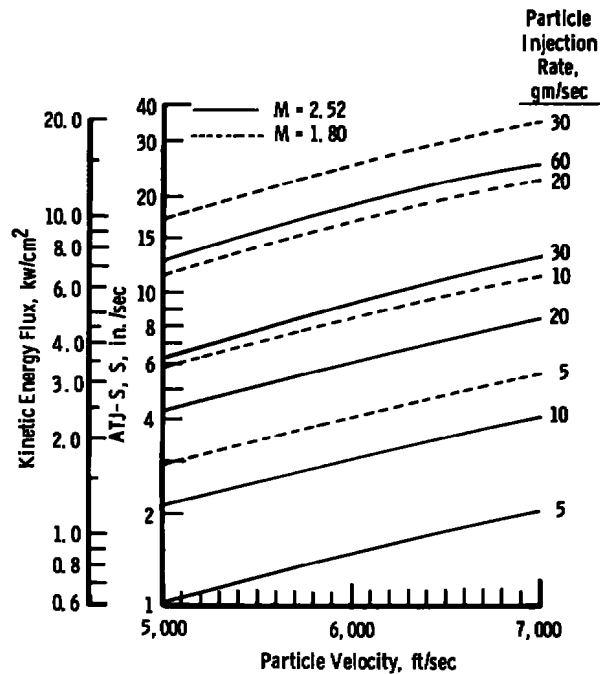
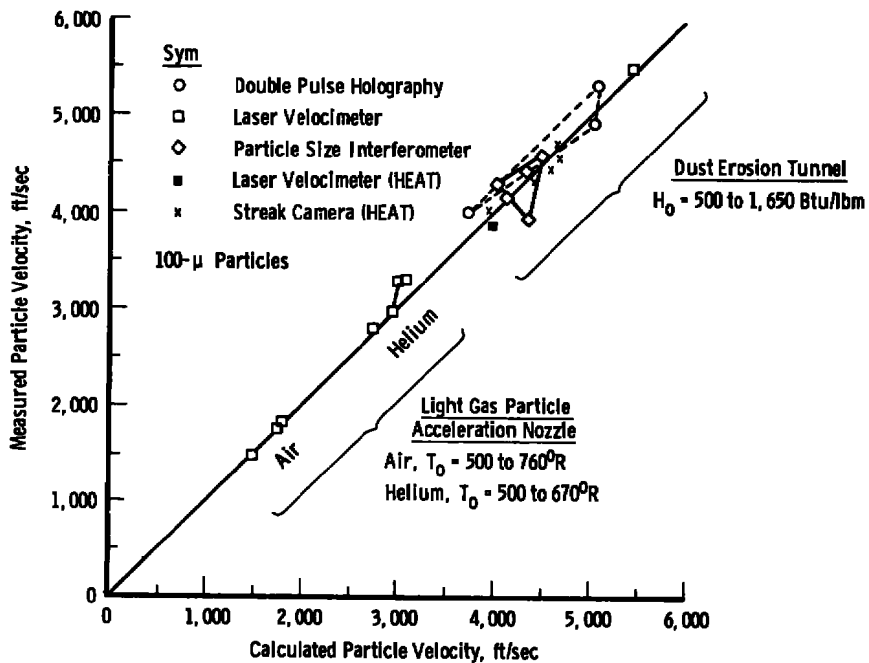


Figure 5.19 Particle velocity versus bulk enthalpy for arc-heater pressure of 120 atm and the M = 2.52 nozzle.



**Figure 5.20 Theoretical kinetic energy flux and ATJ-S graphite erosion rates for various particle velocities.**



**Figure 5.21 Summary of particle velocity measurements with three different techniques in two different facilities; comparison with one-dimensional program prediction.**

## 5.4 FUTURE CAPABILITY

The facility (especially H-1) has great growth potential in its ability to satisfy the user. Several items of research are under development which when fully operational will greatly increase the flexibility and performance of the facility. The most near term increase in capability will be a significant power increase when the current is increased. Ongoing research at AEDC on particle acceleration should double particle velocities within the next few years. A better calibration of the particle flow field will result from development of a particle sizing interferometer. The facility will be augmented with the capability of preprogrammed power and pressure which will allow a test specimen to "fly" a trajectory with nearly full simulation of pressure and heat transfer in real time.

Long-term future capabilities lie in increased arc-heater pressures, i.e., increased model pressure and higher power operation. Both of these items will also result in larger flow diameters. At present, the AEDC power distribution system will support a d-c power supply of up to 200 MW. By 1982, this will increase to about 500 MW.

**6.0 DUST EROSION TUNNEL (DET)**

<b>6.1</b>	<b>Types of Testing</b>	<b>99</b>
<b>6.2</b>	<b>Facility Description</b>	<b>101</b>
<b>6.3</b>	<b>Facility Performance</b>	<b>104</b>
<b>6.4</b>	<b>Future Capability</b>	<b>114</b>

## 6.0 DUST EROSION TUNNEL (DET)

Ballistic or other missiles flying at high velocities near the earth's surface may be required to traverse dust clouds formed by surface bursts of nuclear weapons. Dust erosion of heat shields, fins of various kinds, antennas, and windows or other items in subsurface cavities will occur during the penetration of such dust clouds. Natural snow and rain, and water/ice formed by the rapid expansion of nuclear fireballs also pose erosion problems. The phenomenological bases of particle erosion are not completely understood, and there are large undocumented gaps in some flight regions where empirical correlations could be formulated for use in practical design problems.

The AEDC Dust Erosion Tunnel (DET) was the first tunnel designed specifically to drag-accelerate solid particles to velocities greater than 5,000 ft/sec on a continuous (>5 min) basis. A feasibility study on the use of an existing electric arc heater for the DET driver was concluded affirmatively in calendar year 1970 at AEDC. Subsequent to the conclusion of the feasibility study, USAF/AFSC-SAMSO contracted with the Boeing Company to design and fabricate a dust tunnel to be installed and operated at AEDC. The first shipment of tunnel components arrived at AEDC May 3, 1971; installation was completed on May 30, 1971; shakedown tests were completed June 18, 1971; and calibration of the tunnel, highlighted by the use of laser holography for dustfield characterization, was begun June 21, 1971, and extended into calendar year 1972. Concurrent with the tunnel calibration, the first test series was completed during the period November 30, 1971, through April 7, 1972. This first test series, sponsored by SAMSO, involved a study of the ignition and combustion of titanium, first observed during a sled track test at Holloman Air Force Base. From the conclusion of this test until the present time, the DET has been used to investigate the erosion resistance of a wide spectrum of materials, ranging from graphite through carbon-carbon composites and from beryllium through titanium.

### 6.1 TYPES OF TESTING

Historically and primarily, the DET has been used to document the effects of high-velocity solid particle impacts on a wide variety of materials. The tunnel was specifically designed as a particle drag-accelerator, using a shallow-expansion-angle nozzle 207 in. (17.25 ft) in length for simulation of a point on the ascent trajectory of an ICBM. Since this long nozzle was of sectional construction, and since

requests for testing at off-design Mach and Reynolds numbers began to arise, tests were run with nozzle lengths of 127.5 and 75 in. to exploit the built-in capabilities for the expansion of the range of these variables.

Model geometries for erosion testing have varied greatly; e.g., thin-walled hemispheres from 1- to 3-in. diameter; spherically blunted cones, thin-walled, with 1- and 3-in.-diam spheres joined to 18-deg half-angle cones having base diameters of 2 and 6 in., respectively; flat-faced cylinders or thin disks ranging from 1 to 3 in. in diameter; material samples attached to wedge holders ranging up to 20 deg; and a solid 2-in.-diam hemisphere with a 1/16-in.-diam orifice at the stagnation point, used in a recent test to obtain gas samples for laboratory analyses. Thin-walled models were instrumented with thermocouples, and the outputs were used to calculate heat-transfer rates. Witness bars, plates, and rods of different materials have been used for tunnel calibration and special purposes.

In addition to solid particle erosion testing, other kinds of tests have been accomplished: e.g., a test where the effect of surface roughness (caused by particle impacts) on heat-transfer rates was investigated, taking advantage of the fact that the core flow of the DET is laminar, while that in the thick boundary layer is turbulent; a test where the tunnel was used to supply hypersonic, particle-laden jets for developmental testing of a laser-powered particle sizing interferometer with simultaneous velocity-measuring capability; and a test where water was injected into the tunnel to investigate the effects of the presence of water on the surface chemistry of a hot titanium hemisphere undergoing erosion.

Interest has been expressed in using the DET to simulate the effects of an aluminum-laden rocket motor exhaust jet impinging on an RV surface, for use in the development of an acoustical particle impact counter, and for use in the development of a pressure transducer designed for use on a heat shield undergoing erosion.

Other possible uses are: development of erosion-resistant materials for endo-atmospheric, hypersonic aircraft (windshield, leading edge, control surface, radome, or EM window materials, for example); conditioning, by controlled amounts of erosion, with attendant roughness, models to be subsequently launched in a gun range; and, perhaps, impacting models continuously with liquid water droplets or snowflakes, contingent upon the feasibility of such operation. Even though water has been injected into the tunnel in a recent

test, there were no means available to characterize the water field either as to droplet size or velocity. Facility development tests structured to generate snowflakes or ice have never been attempted, primarily because, up to now, they have not been proposed. There may be a possibility that snow or ice could be generated by the condensation of injected steam, when operating the tunnel at minimum or ambient enthalpy.

Higher particle velocities, using air as the carrier gas, could be obtained by replacing the present tunnel driver with one that can operate at higher pressures and enthalpies, or by developing the capability to use helium as the carrier gas.

## 6.2 FACILITY DESCRIPTION

The AEDC-DET is a hypersonic, continuous-flow (>5 min), open-circuit facility, designed to drag-accelerate particles to high velocities. A schematic plan of the tunnel is shown in Fig. 6.1, power supply not included. Power is supplied

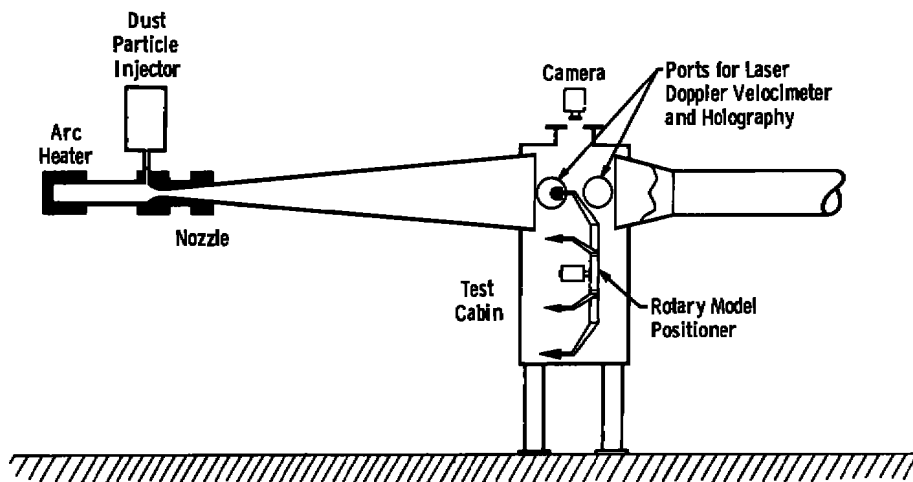


Figure 6.1 Schematic view of DET.

through a network of 3-phase a-c transformers and converted to d-c power with a 3-phase, full-wave ignitron rectifier. Arc-heater power is regulated by the use of a tap-changing-under-load transformer on the a-c side. A resistive ballast on the d-c side can be used for arc stabilization, if required. Air is heated to high temperatures by the electric arc heater, is then ducted through the adapter section and the dust injection section, and then into the expansion nozzle. If enthalpies less than about 1,500 Btu/lbm are required, a mixing section is placed between the adapter and

dust injection sections to temper the heater effluent. Just downstream from the plane where the flow exits from the expansion nozzle into the closed test cabin, a rotary injection system (see Fig. 6.2) moves the test models into the jet in a required sequence. Nine model mounting stings are available, with the tenth being empty for facilitation of starting the nozzle flow. The test jet is not walled in as with conventional wind tunnels, and generally, the nozzle exit flow is slightly overexpanded but with no effect on the model flow field. After the dust-laden flow impacts the test model, it exits the cabin through a diffuser and then is ducted into the ETF exhaust compressors and discharged into the atmosphere. Tunnel photographs are shown in Fig. 6.3.

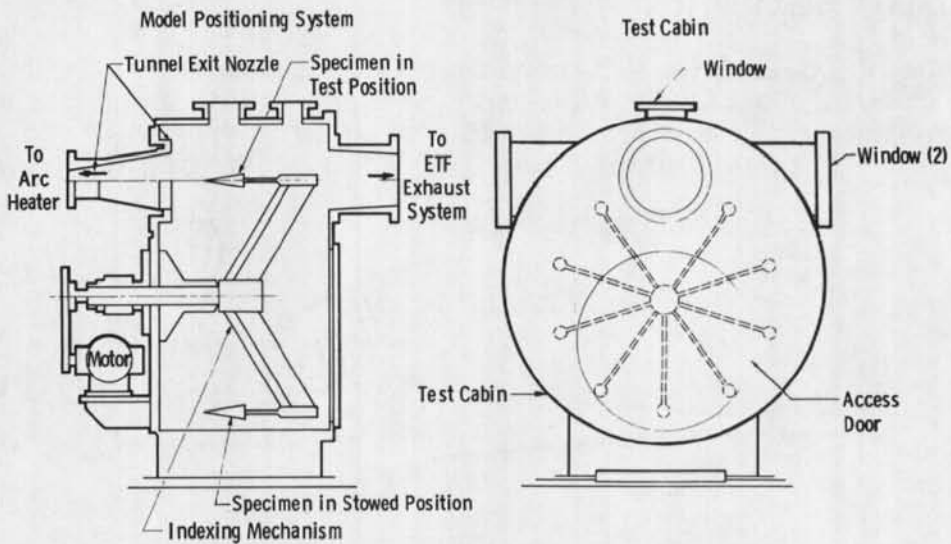
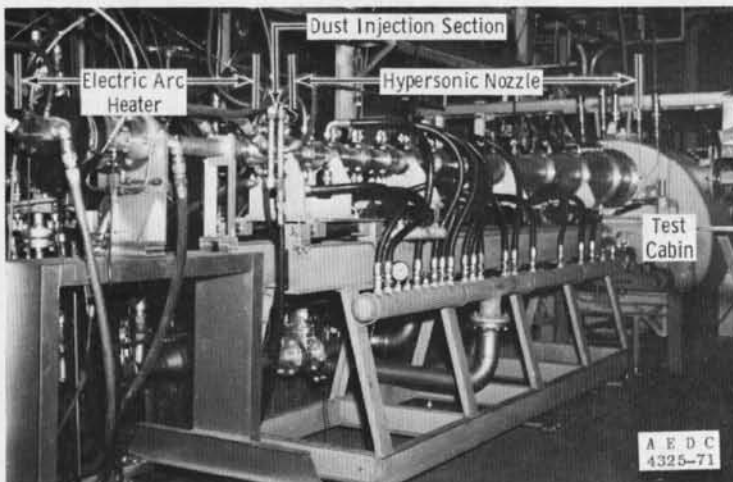
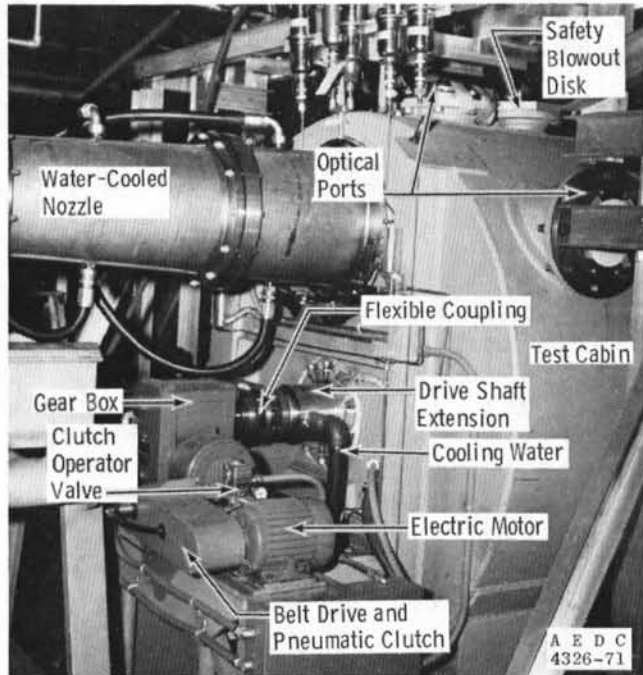


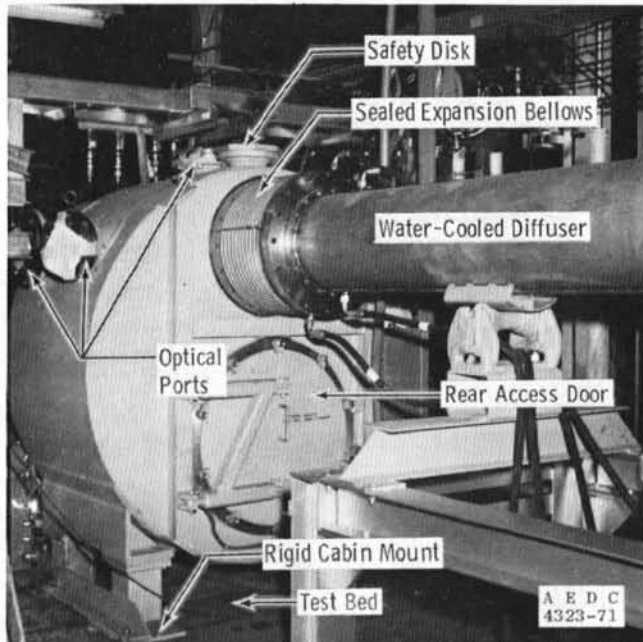
Figure 6.2 Test cabin and model positioning system.



a. Heater and expansion nozzle  
 Figure 6.3 Photographic view of DET.



**b. Test cabin and model positioner drive**



**c. Test cabin and diffuser**

**Figure 6.3 Concluded.**

High-pressure air to the arc heater and mixing section is supplied by the high-pressure air pumping system of the VKF. Cooling water for the arc heater and nozzle liner is supplied from demineralized and raw water pumping systems.

Dust hoppers pressurized by GN<sub>2</sub> are used to inject particulate matter into the hot airstream. Materials used to simulate dust have been magnesium oxide (50, 100, 650 μm), silicon carbide (100 μm), and glass spheres (100, 200, 650 μm). Two-micron titanium dioxide was used for an in-house research program. Laser shadowgraph equipment is also available but cannot be used concurrently with the laser holograph since they both must use the same optical window in the test cabin. One week is required for shadowgraph installation. High-speed cameras with 400 ft of 16-mm film capacity (16,000 frames) are available, with framing rates up to 10,000 sec<sup>-1</sup>. A closed-circuit television system with the screen located in the DET control room is used for model viewing during a test run.

A water-cooled pressure probe is available for measuring pitot pressure. For tunnel enthalpies less than 900 Btu/lbm, a probe is available for measurement of total temperature. Model temperatures and pressures can be recorded on magnetic tape using a 96-channel recorder with signal sampling rates of 6 msec or less, depending on the number of channels scanned.

### 6.3 FACILITY PERFORMANCE

The DET was designed to accelerate solid particles, and all other requirements were secondary to this purpose. Table 6.1 is a summary of tunnel aerodynamic conditions for the three lengths of nozzle used for testing: 75, 127.5, and 207 in. Included in this table are the nozzle diameters and wall angles, and velocities for 100-μm MgO particles. Tunnel conditions are 400, 800, 1,400, and 1,800 Btu/lbm enthalpy and 1,000 psia, the nominal heater enthalpy operating range and pressure, respectively. A limited number of test runs have been made at 500 psia.

To achieve the fullest use of the DET, it is useful to know the aerodynamic conditions at the various stations. Table 6.1 shows that the nozzle boundary layers are quite thick. These data are from boundary-layer calculations by Dr. A. W. Mayne, Jr., AEDC-VKF. Velocity profiles are shown in Fig. 6.4, and calculations indicate that the flow at these stations may be merged. The values of unit Reynolds numbers in Table 6.1 indicate that the flow at each station is

**Table 6.1 Tunnel Performance at Three Nozzle Stations, Including 100- $\mu$ m MgO Particle Velocities.**

Tunnel Variable	Nozzle Station, 75 in.				Nozzle Station, 127.5 in.				Nozzle Station, 207 in.			
	1,000				1,000				1,000			
$p_0$	400	800	1,400	1,800	400	800	1,400	1,800	400	800	1,400	1,800
$h_0$	6.0	5.8	5.6	5.5	7.7	7.1	6.7	6.7	9.6	9.0	8.6	8.5
M	28	26	23	22	10.0	11.3	11.2	9.6	3.6	3.8	3.6	3.2
$p_0$	8.0+6	3.0+6	1.6+6	1.2+6	4.6+6	1.5+6	7.1+5	5.3+5	2.3+6	8.0+5	3.6+5	2.6+5
Re	4,150	5,875	7,765	8,795	4,275	6,050	8,000	9,060	4,340	6,140	8,125	9,210
v	3,100	4,700	5,100	5,100	3,750	4,550	5,200	5,480	3,750	4,570	5,240	5,520
$v_p$	4.34	4.34	4.34	4.34	8.30	8.30	8.30	8.30	15.34	15.34	15.34	15.34
D	1.61	1.77	1.72	1.65	3.22	3.94	3.91	3.57	6.09	7.54	7.63	7.58
$\delta$	1.75	1.75	1.75	1.75	2.5	2.5	2.5	2.5	2.5	2.5	2.5	2.5
e	54	130	231	297	33	85	161	196	20	50	91	113
$(q\sqrt{R_N})_{SP-CW}$												

**Nomenclature**

- $p_0$  Tunnel total pressure, psia
- $h_0$  Energy balance enthalpy, Btu/lbm
- M Mach number
- $p_0$  Pitot pressure, psia
- Re Unit Reynolds number, 1/ft
- v Gas velocity, ft/sec
- $v_p$  Particle velocity, ft/sec
- D Nozzle diameter, in
- $\delta$  Boundary-layer thickness, in
- e Nozzle wall angle, deg
- $(q\sqrt{R_N})_{SP-CW}$  Sphere stagnation point, cold-wall (540°R), clear air heat-transfer rate,  $(\text{Btu}\cdot\sqrt{\text{in}}/\text{m}^2\cdot\text{sec})$ , from Fay-Riddell theory. Measured values will lie within  $\pm 15$  percent of these values.

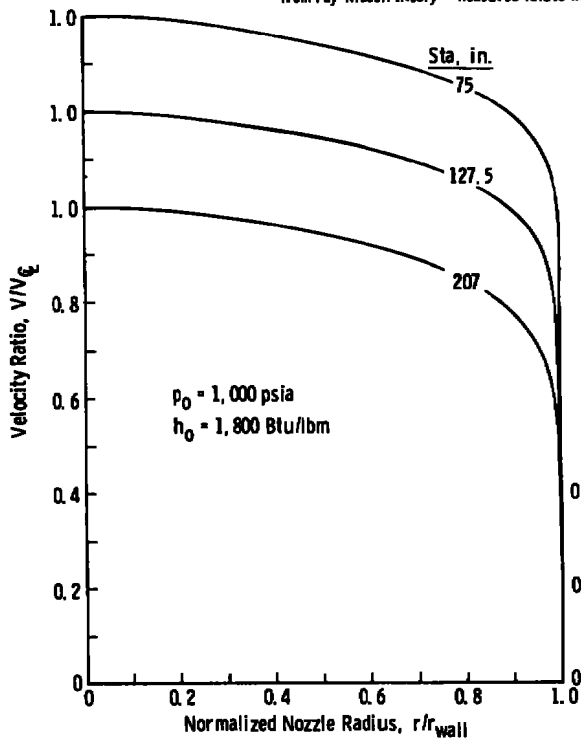


**Figure 6.4 Typical velocity profiles for three nozzle lengths.**

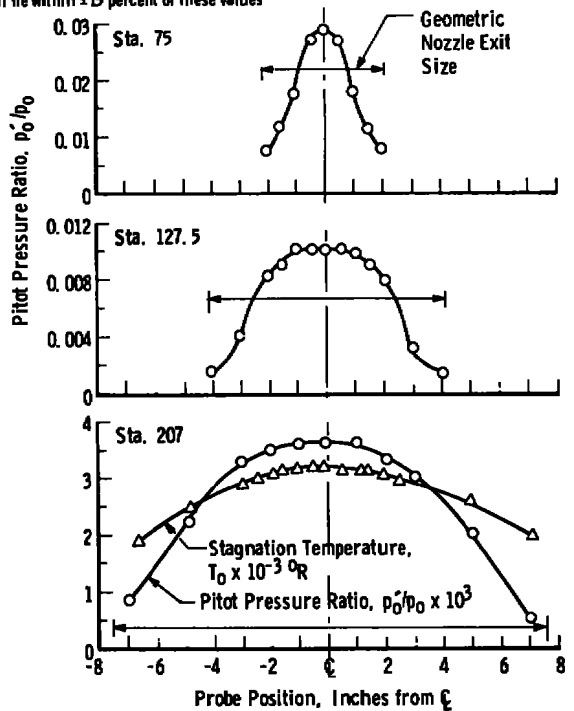


**Figure 6.5 Pitot pressure profiles and temperature profile,  $p_0 = 1,000$  psia,  $h_0 = 445$  to 490 Btu/lbm.**

turbulent; however, stagnation point heat-transfer measurements made on hemispheres placed on the tunnel centerline show that the core flow is laminar. The Table 6.1 values of heat-transfer rate to the stagnation point of a cold-walled hemisphere with a 1.0-in. radius were calculated using the Fay-Riddell theory, and past experience has shown that 95 percent of the measurements lie within  $\pm 15$  percent of these values. As the boundary layer is traversed, the effects of turbulence are in evidence; this conclusion was reached by examining power spectral density plots from dynamic pressure measurements made in the boundary layer which exhibited the high-frequency roll-off associated with turbulent flows.

Pitot pressure profiles made during the tunnel calibration and shown in Fig. 6.5 indicate reasonably uniform core flow diameters of about 7, 4, and 1.6 in. for the 207-, 127.5-, and 75-in. nozzles, respectively. Also, the temperature profile for station 207 shows reasonable uniformity.

To date, the majority of the erosion tests have used mainly magnesium oxide (MgO) as the erosion agent in the 100- $\mu\text{m}$  (nominal) particle size. A few test runs have used 50- and 650- $\mu\text{m}$  MgO; several test runs in the early tests used 100-, 200-, and 650- $\mu\text{m}$  glass beads; and two runs were made with 100- $\mu\text{m}$  silicon carbide (SiC). Several runs were made during an in-house research project with 2- $\mu\text{m}$  titanium dioxide, but no holograph documentation was obtained because the optics of the existing system establish a lower size resolution limit of about 30  $\mu\text{m}$ . The system optics could be reworked so that particles as small as 10  $\mu\text{m}$  could be seen, but this would probably require several months time plus funds for the design, fabrication, and checkout work involved.

Nominal 100- $\mu\text{m}$  MgO dust as obtained from the supplier has been found to have a size spectrum of 10 to 200  $\mu\text{m}$ , with 90 to 95 percent of the particles being in the 100 to 200 range. Figure 6.6 shows typical radial profiles of particle velocity obtained from double-pulse holograms at station 207 for nominal 100- $\mu\text{m}$  dust. The sizes observed range from 20 to 190  $\mu\text{m}$  shown in  $\Delta D_p$ 's of 20  $\mu\text{m}$ . The profiles are fairly uniform over the 7-in. core, and the cloud centerline is very nearly coincident with the tunnel centerline. Centerline particle velocities range from about 5,000 ft/sec for the 150- to 190- $\mu\text{m}$  bin to about 6,600 ft/sec for the 20- to 40- $\mu\text{m}$  bin. The distributions are parabolic, showing the influence of the gas velocity profiles shown in Fig. 6.4. Also shown in Fig. 6.6 is the radial distribution of particle number density, which is seen to be uniform over the 7-in. core. The core value shown represents an average number density of about 0.5 particle/cm<sup>3</sup>. Dust particle concentrations are

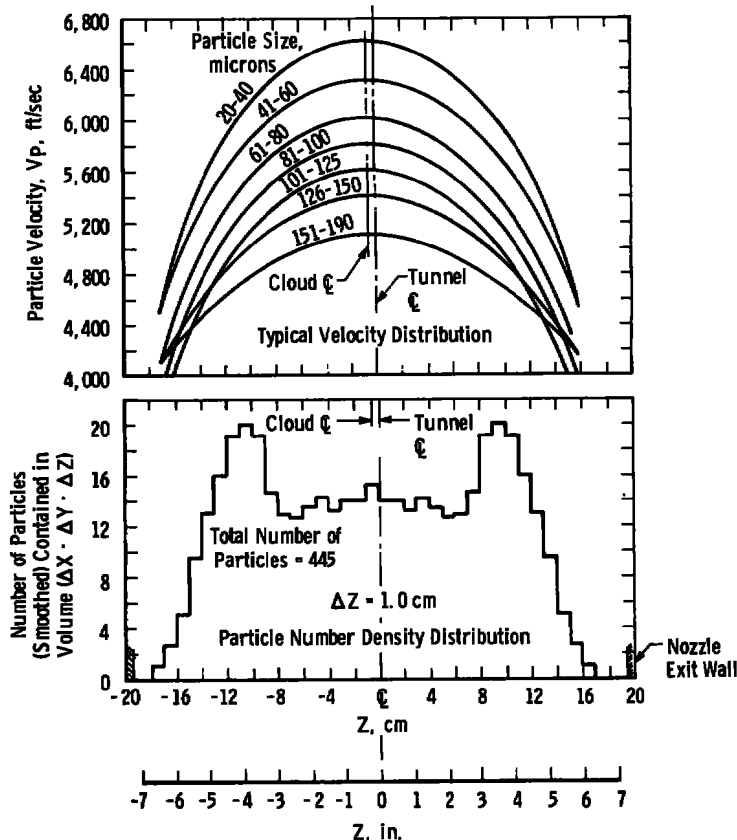
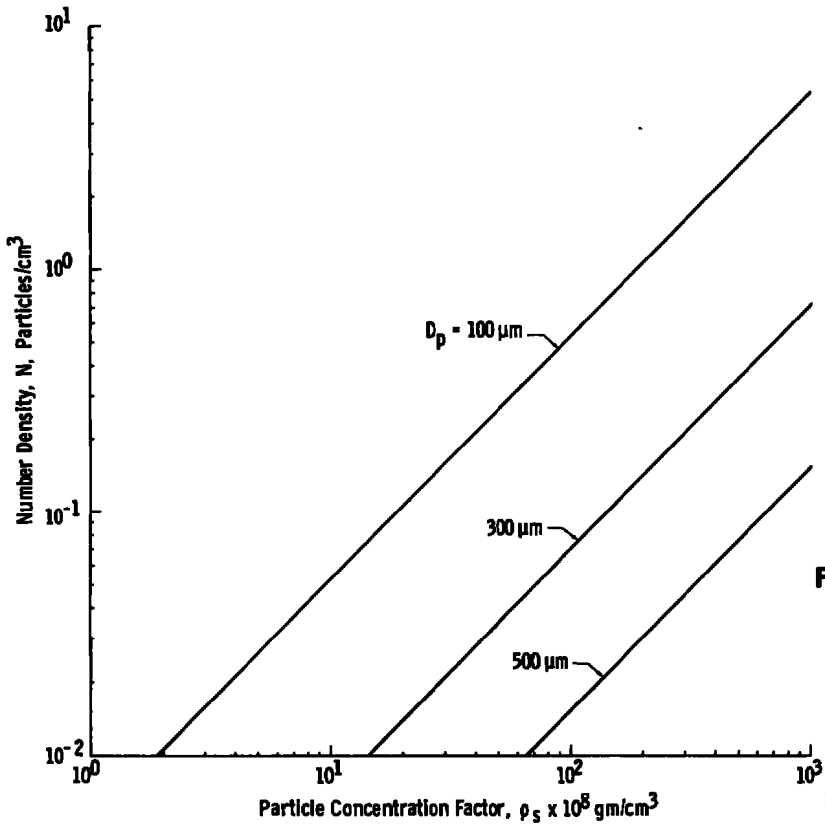
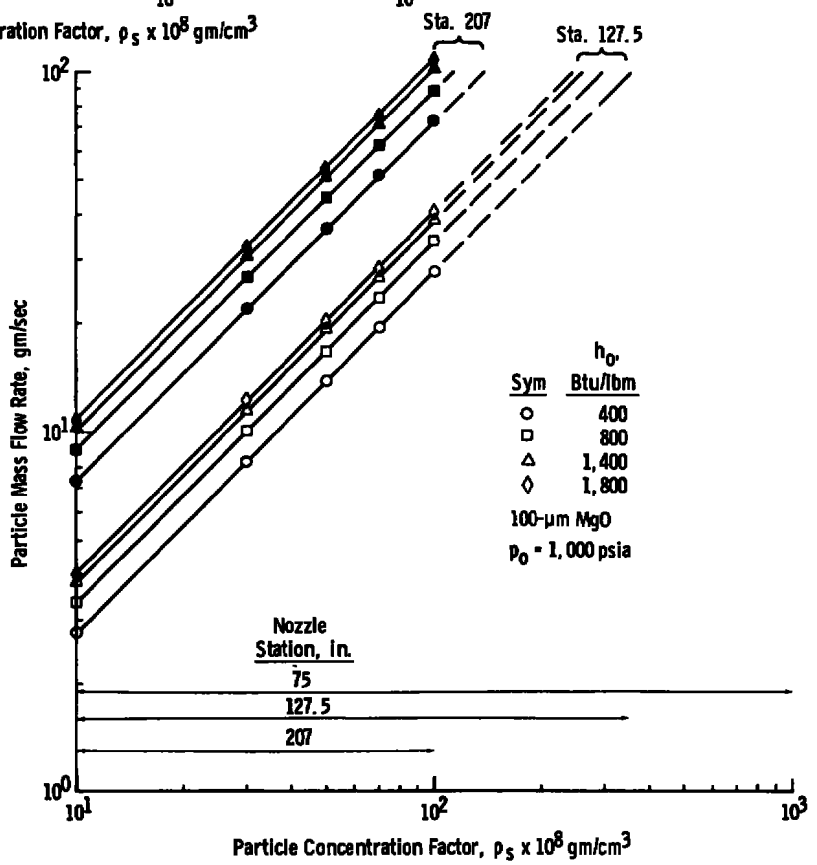


Figure 6.6 Velocity and number density profiles, station 207, nominal 100- $\mu\text{m}$ , MgO particles.

customarily specified by a concentration factor (C.F.) which is equal to the dust spatial density,  $\rho_s$  (gm/cm<sup>3</sup>) multiplied by 10<sup>8</sup>. With the present dust injection system a C.F. range of approximately 10 to 100 can be set with uncertainties ranging from about  $\pm 50$  percent at C.F. of 10 to  $\pm 20$  percent at C.F. = 100. For 100- $\mu\text{m}$  MgO particles (Fig. 6.7), C.F. = 10 corresponds to a number density of about  $5.34 \times 10^{-2}$  particles/cm, C.F. = 100 corresponds to about  $5.3 \times 10^{-1}$ , and C.F. = 1,000 to 5.3 particles/cm<sup>3</sup>. Figure 6.8 shows the particle material mass flow rate required for a given C.F. and enthalpy, for 100- $\mu\text{m}$  MgO and tunnel  $p_0 = 1,000$  psia. The data were calculated using the laser holographic information obtained during tunnel calibration. If the dust system could sustain a flow rate of 100 gm/sec of 100- $\mu\text{m}$  MgO dust, then the C.F. range at station 207 would be 10 to 100, and that at station 127.5 would be 10 to 350. Extrapolating these results to station 75 gives a C.F. range at that location of about 10 to 1,000. The use of dust materials greater than 100  $\mu\text{m}$  in diameter and composed of materials other than glass, SiC, or MgO would require additional dust cloud calibration.



**Figure 6.7 Particle number density versus concentration factor, 100- $\mu$ m MgO.**



**Figure 6.8 Particle mass flow rate versus concentration factor, with estimated C.F. range, 100- $\mu$ m MgO particles.**

Particle velocity as a function of tunnel stagnation pressure, stagnation enthalpy, and particle diameter is presented in Fig. 6.9, for spherical MgO particles at stations 75, 127.5, and 207. The calculated data shown were obtained by use of a computer code which calculates the boundary-layer growth on the nozzle surface and then integrates the drag equation for particles accelerated in the core flow, making use of the best sphere drag data available. The particle flow is assumed to have no effect on the gas dynamics. For a given enthalpy, increasing the pressure from 500 to 1,000 psia results in a substantial increase in particle velocity. No particle velocity calibration has been done at station 75; however, measurements using double-pulsed laser holography have been made at stations 127.5 and 207. Measured velocities are 0 to 8 percent higher than calculated at the 207-in. station and up to 12 percent higher at the

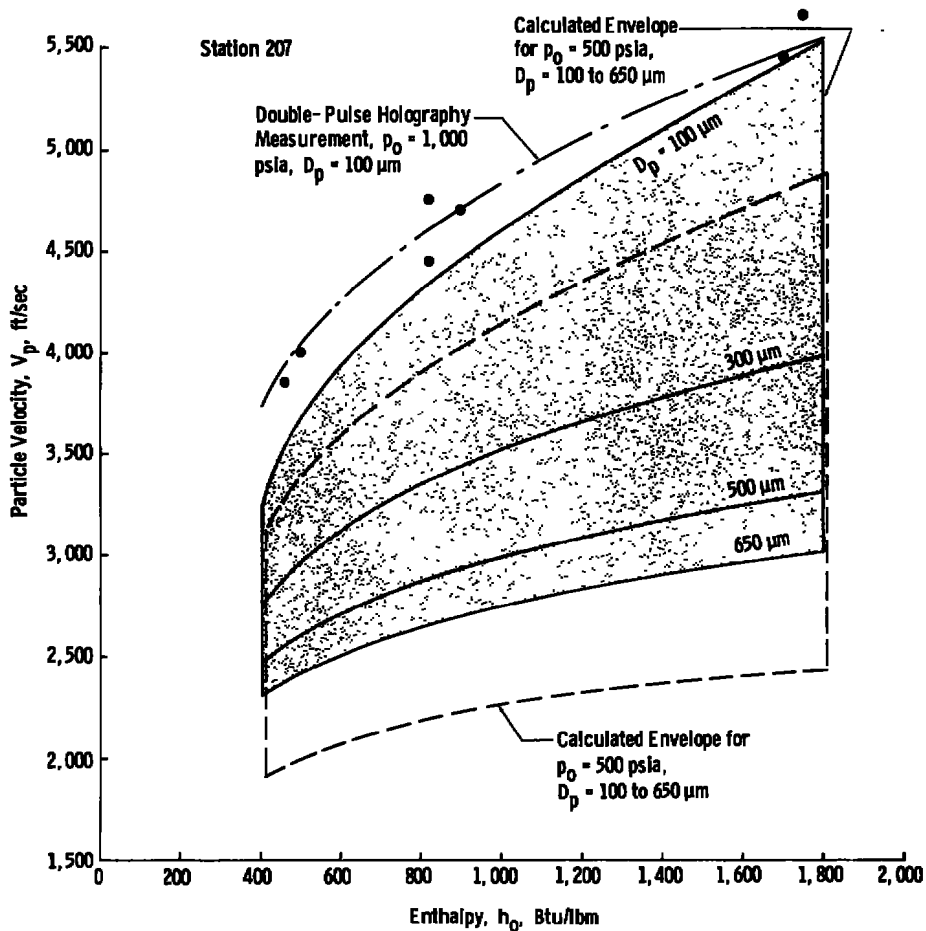


Figure 6.9 Particle velocity versus enthalpy envelopes for  $p_0 = 1,000$  psia and 500 psia.

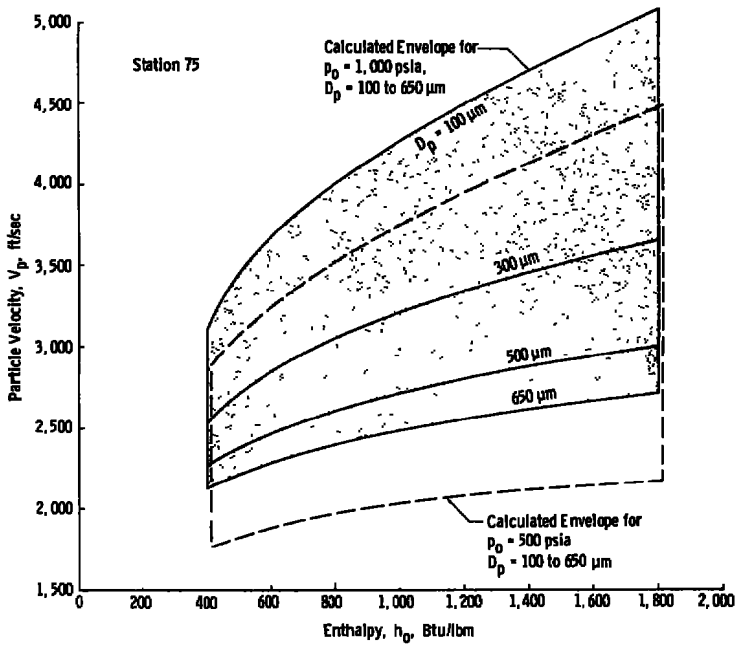
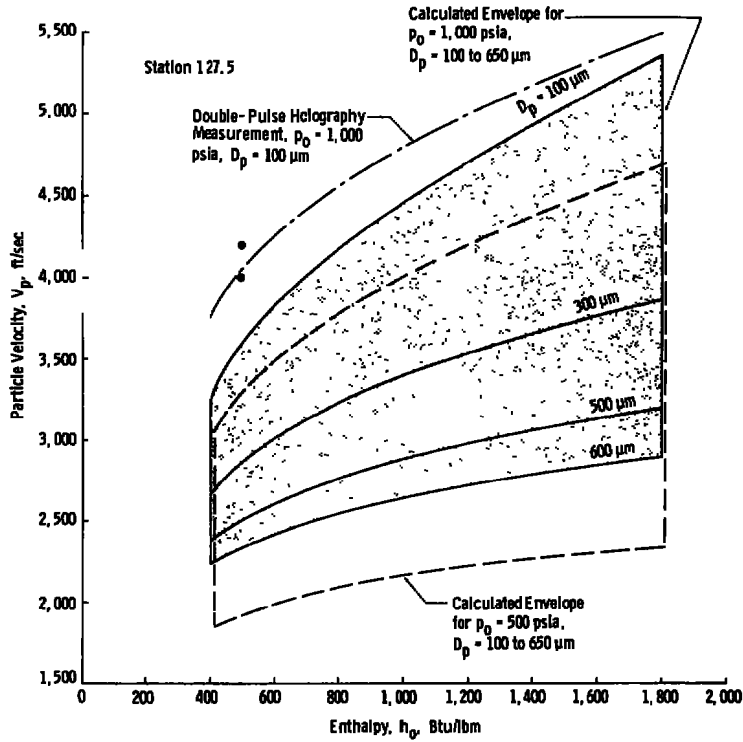


Figure 6.9 Concluded.

127.5-in. station, probably because the particles are irregular rather than spherical solids. Consequently, the actual drag coefficients are different from those used in the computer code, and apparently higher in value. Figure 6.10 shows that 95 percent of the particle acceleration has been accomplished when the particles arrive at station 127.5. A test model could be moved from station 207 to station 127.5 with no great loss in dust velocity, but values of Reynolds number and convective clear air heat-transfer rate would increase, and test stream diameter would decrease.

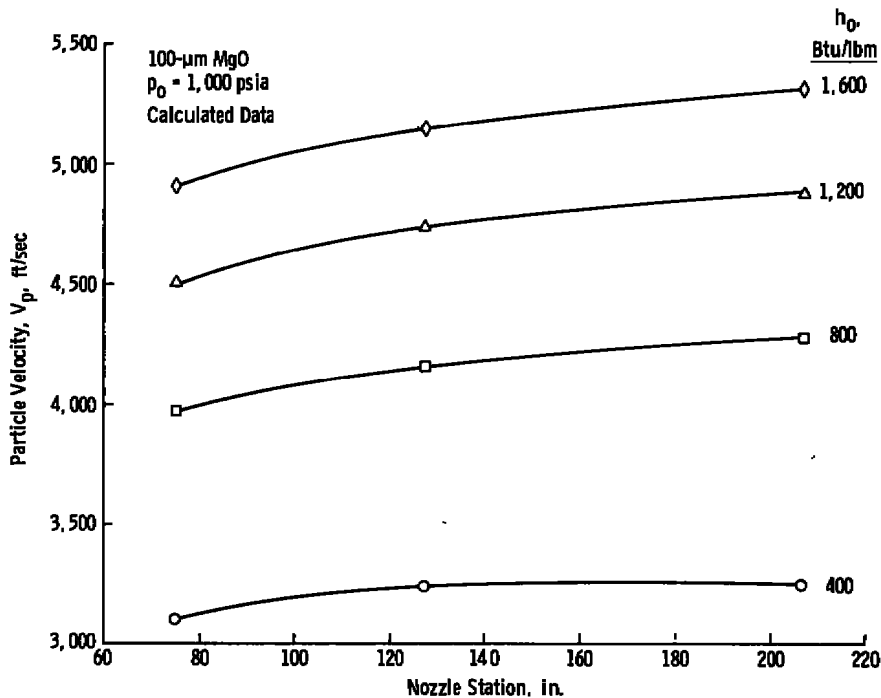


Figure 6.10 Particle velocity versus nozzle station and enthalpy,  $p_0 = 1,000$  psia, MgO particles.

Comprehensive blockage tests to determine allowable model sizes at various nozzle stations have not been made. Diameters of blunt, axially symmetric models which have been run, however, are given in Fig. 6.11, as well as probable limits inferred for two basic model shapes. If it is desired to test a model larger than heretofore run or a substantially different shape, a simple test run to determine blockage on a dummy model of the required characteristics should be made. Four-inch-wide wedge model holders (Fig. 6.12) with a 30-deg total angle (two 15-deg angles) have been used at station 207 only, but it

is believed that they could also be used at stations 127.5 and 75. If their use at these stations were required, a test run could be made to determine feasibility.

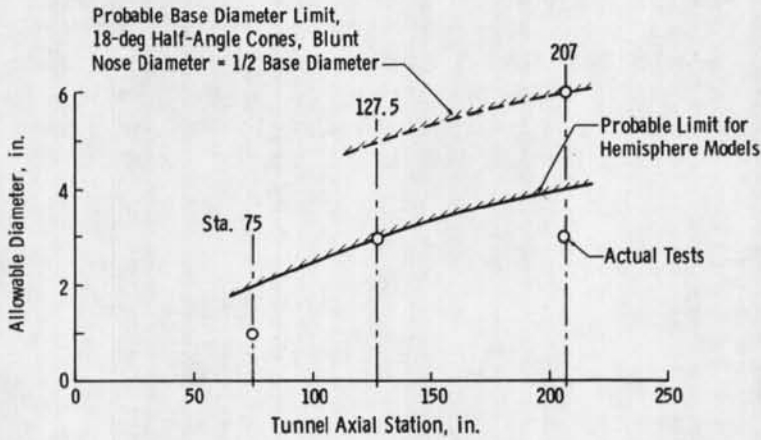


Figure 6.11 Allowable diameters of axially symmetric models for no blockage.

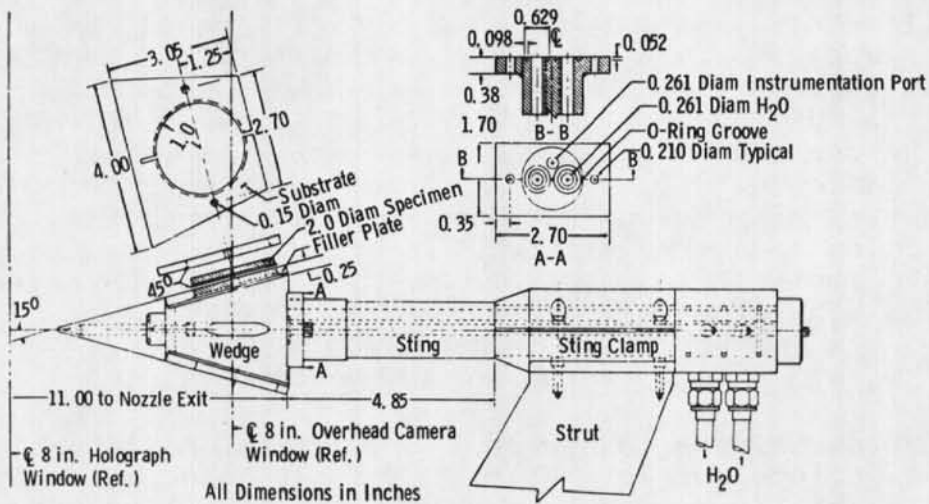
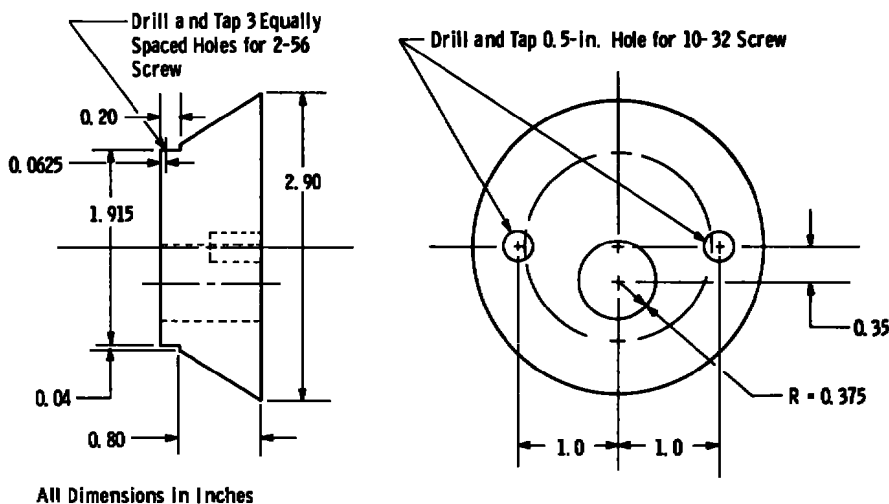


Figure 6.12 Water-cooled wedge model holder.

Model holders for various model geometries are available. Generally speaking, these holders can be modified to accommodate models not radically different from those used in past tests. Hemispheres of 1-, 2-, and 3-in. diameters, disks mounted on wedge holders, and also 90 deg to the flow have

been used in the past. A typical holder for a hemisphere model is shown in Fig. 6.13. This holder was designed for



**Figure 6.13 Sketch of model holder for 2-in.-diam hemisphere models.**

a 2-in.-diam hemisphere with a 0.040-in. wall. The off-axis 0.375-in. hole is for routing the back sidewall thermocouple leads. Hemisphere models are made with a 0.25-in. cylindrical skirt to facilitate mounting on the 0.20-in. lip projection using three equally spaced screws. Fifteen wedge model holders are available, and a typical one with its two surfaces inclined 15 deg to the flow is shown in Fig. 6.12. The leading edge is water cooled and the trapezoidal piece which holds the circular sample is uncooled. This piece could be modified to accommodate other than disk-shaped samples. The wedge holders have angles as follows:

<u>Angles, deg</u>	<u>No. of Holders</u>
9-9	3
6-12	3
2-15	3
15-15	3
4-20	3

Shims can be used to provide angles intermediate to the ones given.

The model injection system is integrated with the dust injection system through a remotely operated valve and timer

controls. A dust, no-dust schedule for up to nine models can be preprogrammed and executed automatically, with dusting periods up to 30 sec for each model.

#### 6.4 FUTURE CAPABILITY

The DET was designed and operated initially as a single-purpose test facility. There has already been an exploitation of test capability beyond the original design. Depending on missile and aircraft mission requirements, there is no doubt that the DET could have a greatly expanded utility. A segmented arc heater is now undergoing development at AEDC which has the possible capability of operation at 150 atm and 4,000 Btu/lbm. Analytical methods for nozzle optimization have been developed that could lead to shorter nozzles with thinner boundary layers, Mach numbers greater than 10, test section jet diameters of 20 to 30 percent greater size, and, in conjunction with the improved heater, particle velocities up to 7,000 ft/sec. The availability of modern data acquisition systems and microprocessors for control purposes would greatly enhance the data handling and delivery to test users.

Liquid water was injected into the tunnel in a recent test, with the purpose of documenting the effects of water on the surface chemistry of a hot, eroding titanium hemisphere. For this exploratory test, adequate instruments were not available to characterize the water field, but model temperature responses indicated that the injected water survived the acceleration process in liquid droplet form for at least some of the reservoir conditions tested. As previously mentioned, the possibility exists that the DET could become a continuous water/snow/ice erosion facility, if the means of supplying these erosive agents could be developed. The natural condensation of steam in the expansion nozzle is considered to be one method worthy of investigation.

## DISTRIBUTION

ADTC/ADBRL-2  
 ADTC/DLOS  
 Aeronutronic Ford Corp.  
 Aerotherm Corp./Hartman  
 Aerospace Corp./Dr. H. Dwyer  
 Aerospace Corp./Library  
 Aerospace Corp./S. Breshears  
 Aerospace Corp./P. Legende  
 AFATL/Eglin AFB/Major James Key  
 AFFDL/DOO  
 AFFDL/FXG/Melvin Buck  
 AFFDL/FXG/R. D. Neumann  
 AFFDL/FXM/Dr. G. K. Richey  
 AFFDL/FXS/Paul Lane  
 AFML/Dr. W. G. Frederick  
 AFML/Dr. Glenn Ornbrek  
 AFML/HBC/D. Schmidt  
 AFML/HKA/Fred Meyer  
 AFML/HKE/John Rhodehamel  
 AFML/HKS  
 AFRPL/DOZ  
 AFRPL/DY  
 AFRPL/RPF  
 AFRPL/RPMMA/Lee Meyer  
 AF Weapons Laboratory/Library  
 Ames Research Center/AFSC Liaison Office  
 Ames Research Center/Joe Marvin  
 Ames Research Center/J. W. Cleary  
 Ames Research Center/Tech. Library  
 AUL(SE)-83-508  
 AVCO Corp./Everett Research Lab.  
 AVCO Corp./Wilmington, DE/Dr. A. Pallone  
 AVCO Corp./Wilmington, DE/Research Library  
 AVCO Corp./Wilmington, DE/S. Sherman  
 Ballistic Research Lab./Anders S. Platou  
 Ballistic Research Lab./Tech. Library  
 Battelle Memorial Inst./Stephen A. Rubin  
 Bell Aerospace Co./Tech. Library  
 BMDATC/Tech. Library  
 BMDATC/Lee Webster  
 BMDSC/TEB/Commander  
 BMDSC/Commander  
 Boeing/Test Engr. and Lab./John Marsh  
 California Inst. of Tech./Prof. Lester Lees  
 California Inst. of Tech./Jet Propulsion Library  
 Calspan Corp./Library  
 Chrysler Corp./Defense Division/Tech. Info. Center  
 Chrysler Corp./Defense Division/Space Group  
 DDC  
 Department of the Navy/Special Proj. Office/S. S. Cooper  
 Effects Technology, Inc./Allan Hunt  
 Fluidyne Engineering Corp./Library  
 General Dynamics Corp./Convair Div./Research Library  
 General Dynamics Corp./Convair Div./H. Yoshihara  
 General Dynamics Corp./Fort Worth, TX/Jerry Beamish  
 General Dynamics Corp./Fort Worth, TX/Chief Librarian  
 General Dynamics Corp./Convair Div./E. Schwartz  
 GE Co./Philadelphia, PA/Dr. S. M. Scala  
 GE Co./Space and Research Div. Library  
 GE Co./Space and Research Div./D. E. Nestler  
 General Electric Research Lab./Dr. N. Nagamatsu  
 Grumman Aerospace Corp./I. G. Hedrick  
 Hq. SAC/WRI/STINFO Library  
 Hughes Aircraft Co./Culver City, CA/Tech. Doc. Center  
 Hughes Aircraft Co./Canoga Park, CA/Larry Wong  
 Johns Hopkins University/APL/Louis B. Weckesser  
 Johns Hopkins University/APL/W. B. Shippon  
 Johns Hopkins University/APL/Dr. F. K. Hill  
 Johnson Space Center/NASA/Library  
 Kaman Sciences Corp./A. P. Bridges  
 Langley Research Center/Charles Johnson  
 Langley Research Center/H. Harris Hamilton  
 Langley Research Center/Jim Dunnivant  
 Langley Research Center/Robert L. Trimpi  
 Langley Research Center/AFSC Liaison Office  
 Langley Research Center/Library  
 Lewis Research Center/AFSC Liaison Office  
 Lewis Research Center/Tech. Library  
 Lockheed/Burbank, CA/S. Elcan  
 Lockheed/Huntsville, AL/Frances G. Martis  
 Lockheed/Huntsville, AL/John Pond  
 Lockheed/Palo Alto, CA/Technical Inf. Center  
 Lockheed/Sunnyvale, CA/Howard Schultz  
 Lockheed/Sunnyvale, CA/L. E. Ericsson  
 Los Alamos Scientific Lab./Report Library  
 Manned Spacecraft Center/Dr. Donald M. Curry  
 Manned Spacecraft Center/Dorothy S. Lee  
 Manned Spacecraft Center/Ivy Fossler  
 Manned Spacecraft Center/R. G. Gonzales  
 Martin-Marietta Corp./R. Cramer  
 Martin-Marietta Corp./Charles Waugh  
 Martin-Marietta Corp./Engr. Library  
 Martin-Marietta Corp./Dr. Mark V. Morkovin  
 Martin-Marietta Corp./Dick Brakeen  
 Martin-Marietta Corp./Harry Carroll  
 Martin-Marietta Corp./Steve Copey  
 Martin-Marietta Aerospace/R. L. Kirlin  
 Martin-Marietta Aerospace/Research Library  
 Massachusetts Inst. of Tech./Aerophysic Lab.  
 McDonnell Douglas Astronautics/Bob Masak  
 McDonnell Douglas Corp./St. Louis, MO/Library  
 McDonnell Douglas Corp./Huntington Beach, CA/J. S. Murphy  
 Motorola, Inc./Dean Morris  
 Motorola, Inc./Tech. Library  
 NASA-MSFC/Jerry Vaniman  
 NASA-MSFC/Al Forney  
 NASA-MSFC/Homer B. Wilson  
 NASA-MSFC/Library  
 NASA-MSFC/S&E-AERO-AF/John Warnbrod  
 NASA Scientific & Tech. Inf. Facility  
 National Bureau of Standards/Library  
 Naval Air Development Center/Commander  
 Naval Air Engr. Center/Tech. Library  
 Naval Air Systems Command/Commander  
 Naval Research Lab./W. W. Atkins  
 Naval Research Lab./Director  
 Naval Ship R&D Center/Aerodynamics Library  
 Naval Surface Weapons Center/Tech. Library  
 Naval Surface Weapons Center/J. A. Iandolo  
 Naval Surface Weapons Center/Library  
 Naval Surface Weapons Center/C. Lyons  
 Naval Weapons Center/Tech. Library  
 Naval Weapons Center/Frank Markarian  
 North American Rockwell Corp./Anaheim, CA/Tech. Library  
 Office Director of Defense/Assistant Director  
 Office Director of Defense/Tech. Library  
 Ohio State University/Prof. G. L. Von Eschen  
 Rand Corp./Dr. Carl Garley  
 Raytheon, Inc./Henry Nadeau  
 Rentsch, Inc./John Reardon  
 Rome Air Development Center/Documents Library  
 SAMSO/Lt. K. C. Gaines  
 SAMSO/Lt. Col. M. Baran  
 SAMSO/MNRP  
 SAMSO/MNRR  
 SAMSO/RSN/Captain Joy  
 SAMSO/RSS  
 SAMSO/RSSB  
 SAMSO/RSSR/Lt. Col. Brininstool  
 SAMSO/ESTB  
 Sandia Corp./Livermore, CA/Tech. Library  
 Sandia Corp./Albuquerque, NM/Tech. Library  
 Sandia Laboratories/K. L. Goin  
 Spectrum Development Laboratory  
 Stanford University/Library  
 STD Research Corp.  
 Taylor Naval Ship R&D Center/Aero. Library  
 Taylor Naval Ship R&D Center/Dr. S. De Los Santos  
 Technion, Inc./Dr. G. L. Cann  
 Texas Instrument/Harry Barnard  
 TEW, Inc./Cleveland, OH/Elizabeth Barrett  
 TEW, Inc./Redondo Beach, CA/Document Acquisitions  
 United Technology Corp./Viola Thoren Kress  
 University of California/Library  
 University of Tennessee/Library  
 University of Tennessee Space Institute/Library  
 University of Texas/Dr. John I. Bertin  
 USAF Academy/DFAN  
 USAF Academy/DFSLB/Library  
 US Army Missile Command/Commanding General  
 US Army Missile Command/Chief, Documents  
 US Naval Academy/Aerospace Engr. Dept.  
 Weapons System Evaluation Group/Director  
 White Sands Missile Range/Tech. Library